Title
CAR Pooling: High throughput screening of CAR T cells identifies diverse immune signaling domains for next-generation immunotherapies

Author
Azimi, Camillia

Publication Date
2022

Peer reviewed|Thesis/dissertation

CAR Pooling: High throughput screening of CAR T cells identifies diverse immune signaling domains for next-generation immunotherapies

by

Camillia Azimi

DISSERTATION

Submitted in partial satisfaction of the requirements for degree of

DOCTOR OF PHILOSOPHY

in

Biomedical Sciences

in the

GRADUATE DIVISION

of the

UNIVERSITY OF CALIFORNIA, SAN FRANCISCO

Approved:

DocuSigned by: Alexander Marson — Alexander Marson

7F25CDCE383C4A8...

Chair

DocuSigned by: Kole Roybal — Kole Roybal

4EC38987D948B...

DocuSigned by: Qizhi Tang — Qizhi Tang

DocuSigned by: Arthur Weiss — Arthur Weiss

A45915AB27B74F5...

Committee Members

Dedication

This dissertation is dedicated to women. Those who have raised me, those who have grown with me, and those who have inspired me. You have been indispensable.

And to Mladen, without whom my life would be incomplete.

Acknowledgements

To Mladen, you are a true partner and the best husband I could ever ask for. Thank you for everything you have brought me these last 11 years. You have made it possible for me to survive my PhD while still feeling balanced, happy, and whole.

To my parents, Mardelle and Hadi Azimi, for coming to this country and/or escaping your boundaries through education, and emphasizing that it always comes first. You both have given me the ability and opportunity to pursue science in a way that many never have.

To my cousins, Arta and Nika, for being true beacons of light in the world and filling my days with joy.

To my friends—especially Kim, Katelynn, and Bria—for being such huge believers and always reminding me who I am.

To BMS Wine Night—Lindsey, Denise, Casey, and Tara—for being the central pillar upon which my PhD was able to stand.

To Michele Ardolino, David Raulet, Olivia Majer, Greg Barton, Kevin Corbett, and the many others whose training and wisdom have helped make me the scientist I am today and establish the foundation I needed in graduate school.

To Kole and the Roybal lab, for creating a space full of creativity and some of the hardest workers I know to have spent the last five years with. It has been invaluable.

To my thesis committee, Alex Marson, Qhizi Tang, and Arthur Weiss for your indispensable expertise and input throughout this work.

Contributions

This thesis work was performed under the direct supervision of Dr. Kole Roybal with guidance from Dr. Alex Marson and Dr. Jeff Bluestone. It was also done in partnership with Dr. Daniel Goodman. Thesis committee members Dr. Qhizi Tang and Dr. Arthur Weiss provided invaluable expertise and input throughout this work.

Chapter 1 is a review on synthetic immunology from Current Opinions in Immunology written by myself, Kole Roybal, Jeff Bluestone, and Qhizi Tang.

> Azimi CS, Tang Q, Roybal KT, Bluestone JA. NextGen cell-based immunotherapies in cancer and other immune disorders. Curr Opin Immunol. 2019 Aug;59:79-87. doi: 10.1016/j.coi.2019.03.007. Epub 2019 May 6. PMID: 31071513.

Chapter 2 is a manuscript accepted at Science Translational Medicine and adapted from the biorxiv. See reference below.

> Daniel B. Goodman*, Camillia S. Azimi*, Kendall Kearns, et al. Pooled screening of CAR T cells identifies non-native signaling domains for next-generation immunotherapies [Internet]. 2021 July page 2021.07.11.451980. Available from: https://doi.org/10.1101/2021.07.11.451980
>
> * These authors contributed equally to this work

CSA, JAB, DBG, AM, and KTR conceptualized the study. CSA, DBG, KK, and KTR developed the methodology. DBG, KG, KK, and NP built and developed the software. CSA, DBG, KK, and EP partook in the investigations for the pooled screens. CSA and KK partook in the investigations for the arrayed screens. CSA, JE, JG, KK, BS, AT, and VV partook in the investigations for the in vivo experiments. DBG, BH, DL, and JY partook in the investigations for the scRNAseq and CITEseq. CSA, JAB, DBG, AM, and KTR wrote the manuscript.

Abstract

CAR Pooling:

High throughput screening of CAR T cells identifies diverse immune signaling domains for next-generation immunotherapies

Camillia Azimi

Chimeric antigen receptors (CARs) repurpose natural signaling components to retarget T cells to refractory cancers but have shown limited efficacy in persistent, recurrent malignancies. Here, we introduce “CAR Pooling”, a multiplexed approach to rapidly identify CAR designs with clinical potential. Forty CARs with signaling domains derived from a range of immune cell lineages were evaluated in pooled assays for their ability to stimulate critical T cell effector functions during repetitive stimulation that mimics long-term tumor antigen exposure. Several domains were identified from the tumor necrosis factor (TNF) receptor family that have been primarily associated with B cells. CD40 enhanced proliferation, whereas B-cell activating factor receptor (BAFF-R) and transmembrane activator and CAML interactor (TACI) promoted cytotoxicity. These functions were enhanced relative to clinical benchmarks after prolonged antigen stimulation, and fell into distinct states of memory, cytotoxicity, and metabolism. BAFF-R CAR T cells were enriched for a highly cytotoxic transcriptional signature previously associated with positive clinical outcomes. Additionally, we observed that replacing the 4-1BB intracellular signaling domain with the BAFF-R signaling domain in a clinically validated B-cell maturation antigen (BCMA)-specific CAR resulted in enhanced activity in a xenotransplant model of multiple myeloma. Together, these results show that “CAR Pooling” is a general approach for rapid exploration of CAR architecture and activity to improve the efficacy of CAR T cell therapies.

Table of Contents

List of Figures

List of Tables

List of Abbreviations

AA – Amino Acids

ACT – adoptive cell therapy

ALPPL2 – Alkaline phosphatase, placental-like 2

AP-1 – activator protein 1

AUC – area under the curve

BAFF-R – B-cell activating factor receptor

BCMA – B Cell Maturation Antigen

BiTE – bi-specific T-cell engagers

CAR – Chimeric Antigen Receptor

CITE-seq – cellular indexing of transcriptomes and epitopes by Sequencing

CRISPR – clustered regularly interspaced short palindromic repeats

CRS – cytokine release syndrome

CTV – CellTrace Violet

Exh – exhuastion

FACS – fluorescence activated cell sorting

FBS–fetal bovine serum

GFP – green fluorescent protein

GITR – glucocorticoid-induced TNFR-related protein

GvHD – graft-versus-host disease

Grb2 – growth factor receptor-bound protein 2

HIF1a – hypoxia inducible factor 1 subunit alpha

ICDs – intracellular domains

IFN-γ – interferon gamma

IgSF – immunoglobulin superfamily

IL-2 – Interleukin-2

iPS – induced Pluripotent Stem

IRF – increased relative frequency

ITAMs – immunoreceptor tyrosine-based activation motifs

LAG3 – lymphocyte activating 3

Lck – lymphocyte-specific protein tyrosine kinase

KLRG1 – killer cell lectin like receptor G1

MFI – mean fluorescence intensity

MHC – major histocompatibility complex

NFAT – nuclear factor of activated T cells

NFκB – nuclear factor kappa B

NGS – next-generation sequencing

NK – natural killer cells

NSG – NOD-scid IL2Rgammanull

PBMC – peripheral blood mononuclear cell

PBS – Phosphate-buffered saline

PCA – principal component analysis

PD1 – programmed cell death protein 1

PI3K – phosphatidylinositol-3-kinase

synNotch – synthetic Notch receptors

SCENITH – single-cell energetic metabolism profiling

scRNA-seq – single-cell RNA sequencing

RM – repeated measures

TACI – transmembrane activator and CAML interactor

TCR – T cell Receptor

TF – transcription factor

TGF-b – transforming growth factor b

TILs – tumor-infiltrating lymphocytes

TIM – T cell/transmembrane, immunoglobulin, and mucin

TIM3 – T-cell immunoglobulin mucin-3

TMD – TransMembrane Domain

TME – tumor microenvironment

TNF – tumor necrosis factor

TNFRSF – TNF receptor super family

TRAF – TNF receptor associated factor

TREM – triggering receptors expressed on myeloid cells

Tregs – regulatory T cells

UMAP – uniform manifold approximation and projection

Unt – untransduced

WNN – Weighted-nearest neighbor

VSTs – viral-specific T cells

Chapter 1

NextGen cell-based immunotherapies in cancer and other immune disorders

Material for this chapter comes from the following published work:

Azimi CS, Tang Q, Roybal KT, Bluestone JA. NextGen cell-based immunotherapies in cancer and other immune disorders. Curr Opin Immunol. 2019 Aug;59:79-87. doi: 10.1016/j.coi.2019.03.007. Epub 2019 May 6. PMID: 31071513.

1.1 Abstract

T lymphocyte and other cell therapies have the potential to transform how we treat cancers and other diseases that have few therapeutic options. Here, we review the current progress in engineered T cell therapies and look to the future of what will establish cell therapy as the next pillar of medicine. The tools of synthetic biology along with fundamental knowledge in cell biology and immunology have enabled the development of approaches to engineer cells with enhanced capacity to recognize and treat disease safely and effectively. This along with new modes of engineering cells with CRISPR and strategies to make universal 'off-the-shelf' cell therapies will provide more rapid, flexible, and cheaper translation to the clinic.

1.2 Introduction

It has been over 50 years since the first bone marrow transplant was used successfully to reconstitute the entire blood system to cure cancer [1]. This singular success transformed the field of hematology-oncology and paved the way for a cell therapy revolution including the implementation of antigen-specific T cell therapies to treat a variety of tumors such as melanoma, renal, lung, and multiple other solid tumors [2]. In a secondary wave of innovation, new in vitro techniques to efficiently expand neoantigen-specific T cells from tumor tissue have shown efficacy in treating a number of tumors. Recently, the third revolution, enabled by the use of genetic engineering to modify cells with exceptional specificity and almost unlimited flexibility, is poised to dramatically advance modern medicine. Target-specific Chimeric Antigen-specific Receptors (CAR), which combine cell surface tumor antigen specificity of monoclonal antibodies with the signaling machinery of T cells, have led to the development of two FDA-approved cell-based drugs, Yescarta™ and Kymriah™. These novel genetically engineered therapeutics have yielded extraordinary cures of CD19+ lym- phomas and for the treatment of multiple blood cancers and myeloma on the horizon. But many challenges in the field remain unresolved including: side effects resulting from cytokine release syndrome (CRS); difficulty in harnessing the technology for solid tumors; and issues of tumor antigen escape, adoptive T cell durability, stability, and exhaustion. In this perspective, we will summarize the advances and opportunities in the field of human adoptive cell therapy (ACT), emphasizing the breath of opportunities using various cell subsets, gene engineering and creative gene editing approaches in TCRab cells, although there are ongoing research efforts to develop engineered NK, macrophage and TCRgd cells as well. Novel synthetic biology approaches will be highlighted that introduce payloads and multi-antigen specificities, regulate receptors and alter epigenetic landscapes that impact T cell functionality,

durability, and efficacy in a hostile microenvironment in the cancer, autoimmunity and organ transplant settings. Finally, we peek into the future when highly regulated, universal ACT are developed, not just from T cells but induced Pluripotent Stem (iPS) cells, to treat an array of immune-mediated and other inflammation-associated diseases.

1.3 Generation of antigen-specific T cells

The adaptive immune system has evolved to detect small often single-amino acid changes in a foreign protein. For T cells, this is accomplished through the T cell receptor complex (TCR) designed to recognize small peptides presented by major histocompatibility complex (MHC) class I and II. In contrast, B cells use two-chain antibodies to recognize epitopes created by tertiary protein structures. Modern ACT for cancer has hijacked individual receptors to expand and, in many cases, engineer antigen-specific T cells. Specific TCRab chains have been isolated from disease-reactive T cells and introduced into function effector cells to mediate the relevant immunity, be it cytotoxicity (for cancer and infectious diseases) or suppression (in autoimmunity and transplantation). The TCRs have the advantage of recognizing peptides derived from the entire proteome and have evolved high sensitivity to a small number of MHC–peptide complexes on an antigen-presenting cell [3,4]. In contrast, antibodies recognize epitopes expressed on whole proteins, either soluble or on the surface of cells. CARs utilize the antibody recognition structure, fused to costimulatory and TCR signaling domains, to direct T cells to cell surface-displayed whole proteins. CARs are generally less sensitive than TCRs and sometimes exhibit on-target, off-tissue activities. These two modes of targeting and activating T cell therapies are the basis for much of the current approaches to antigen-specific ACT (Fig. 1.1).

1.4 TCR versus CAR ACT

Two major strategies have been deployed to treat cancer with T cells with tumor-specific TCRs. One is to isolate, expand, and reinfuse tumor-infiltrating lymphocytes (TILs) from excised tumors. This strategy uses the power of a polyclonal tumor-specific T cell population that can lead to a multi-pronged attack. A second strategy is to sequence the TCRs of TILs and engineer selected

receptors into patient-derived T cells for ACT. Unlike TIL therapy, which often has a mixed population that includes many irrelevant T cells thus limiting efficacy, engineered TCR therapies can generate uniformly functional T cells. These neoantigen-specific T cells, which target unique tumor mutations have limited off-target effects [5,6] and, in some cases, the TCRs target shared tumor antigens, often of embryonic origin [7], making the therapeutic strategy even more broadly applicable. The use of antigen-specific TCRs are also being exploited for regulatory T cells (Tregs) therapies as well to treat organ transplant rejection and potentially, autoimmunity [8]. Highly selective TCR-based T cell therapies will continue to evolve and may be superior to CARs in certain therapeutic settings due to the unique properties of the receptor and available targetable antigens.

The efficacy of CARs can be seen in the first two FDA-approved CAR T cell therapies in which both tisagenlecleucel and axicabtagene ciloleucel recognize an extracellularly expressed protein (CD19) to eliminate certain lymphomas. In contrast to TCRs that are capable of being activated by a single peptide-MHC complex [9], CARs require a minimum of $200–10000 target molecules to activate [10,11]. The low sensitivity of CARs can be overcome by high-density ligands such that CARs can drive potent anti-tumor T cell responses. However, in some cases, the cells cause toxicity via on-target off-tumor specificity or induction of CRS [12,13]. Despite these flaws, the high affinity, lack of MHC restriction, and modular architecture for rapid engineering CARs have made them a focal point in ACT. Next-generation CARs, reviewed below, have been engineered to address critical problems within therapeutic applications such as antigen escape, T cell exhaustion, and the need for universal ‘off-the-shelf’ CARs.

CARs and TCRs are now being engineered to detect new classes of antigens. For example, TCR-like CARs have been generated that detect intracellular neoantigens in the context of MHC [14]. In addition, both TCRs and CARs are being developed against phosphorylated and citrullinated proteins, fusion proteins, alternative splice variants, and mutations in driver antigens such as KRAS [15,16]. Therefore, investigators at the NCI and companies, such as PACT Pharma, are gearing up to conquer personalized ACT by identifying and generating receptors against neoantigens (especially truncal mutations) [17–19]. In these studies, it will be essential to make sure that these receptors do not have toxic off-tumor effects [20,21]. In the case of TCRs, mispairing with the endogenous chains can lead to receptors with unknown specificity [22], which can be avoided with single-chain alpha-beta TCRs, cysteine bridges and other genetic modifications [23,24]. Lastly, despite the signaling and engineering advantages, TCR therapies are intrinsically HLA-restricted. While this is not a problem in personalized medicine, shared tumor antigens will only be targetable by TCRs within patients of similar genetic backgrounds or on less polymorphic HLA molecules such as HLA-E or HLA-G.

1.5 Tackling the challenge of solid tumors

There is growing evidence that controlling T cell activation, specificity, receptor signaling dynamics, and cell communication systems (e.g. cytokines and chemokines) will be essential in the successful adaptation of CARs to treat solid tumors. Many investigators have turned toward engineered regulatory mechanisms to control each aspect of CAR-T cell function.

As the field has progressed, CAR T cell therapy has challenged researchers and clinicians with the threat of CRS and T cell exhaustion. Regulating CAR T cell activity can be as simple as controlling the longevity of CAR expression. One of the easiest ways to accomplish this is to transiently express the CAR via electroporation of mRNA [25,26]. However, once the CAR expression is lost,

there is no way to regain activity and multiple doses will likely be required. Therefore, more sophisticated control of CAR expression dynamics would be ideal. With advances in the use of CRISPR in T cells, groups have achieved high-efficiency integration of CARs into the TCRa locus (TRAC), where CAR expression is controlled by endogenous regulatory elements [27]. This is beneficial because it reduces the complexity of T cell engineering and mimics the dynamics of TCR expression upon antigen stimulation. The natural regulation of CAR expression, which likely controls the timing and duration of signaling, can reduce exhaustion and improve therapeutic efficacy (Fig. 1.2) [28,29].

1.6 Controlling CAR signaling and activation.

Aside from modulating CAR expression, several groups have begun engineering solutions to CRS and T cell exhaustion by directly engineering CAR signaling domains. Feucht et al. set out to promote long-term T cell proliferation and persistence by mutation of the CD3z immunoreceptor tyrosine-based activation motifs thus dampening CAR signaling [30]. The company TCR2 has designed a chimeric scFv–TCR complex that may improve T cell responses due to more natural TCR activation [31]. While many labs have focused on TCR signaling, others enhanced CAR T cell activation and differentiation by integrating cytokine JAK-STAT signaling domains, such that T cells strongly proliferate and are less dependent on their microenvironment (Fig. 1.3) [32,33]. There have also been extensive characterizations of the two clinically utilized costimulatory domains, 4-1BB and CD28, that has shown stark differences in signaling speed (with CD28 being faster), signaling strength (with CD28 being stronger), and signaling persistance (with 4-1BB lasting longer), all of which have an effect on the long-term efficacy within patients. Although the modularity of CARs is conducive to innovative engineering, it remains unknown how to alter CAR signaling to produce ideal clinical results.

Beyond engineering signaling domains into CARs to shape the T cell response, others have developed new strategies to gate the activity of CARs such that they are activated in a context-dependent manner. Desnoyers et al. engineered a system of 'receptor masking' where CAR-target engagement is blocked by a probody: an scFv whose binding is dynamically controlled by matrix metalloproteinases commonly found in the tumor microenvironment (TME) [34]. Roybal et al. developed a novel synthetic receptor system called synthetic Notch receptors (synNotch) which, unlike CARs, translate ligand-binding to release of a receptor-tethered tran- scription factor that regulates a user-defined transcriptional circuit [35,36]. SynNotch receptors can reliably control the expression of CARs such that the CAR is only expressed in the TME, confining T cell activity to the disease site (Fig. 1.3). An added feature of SynNotch/CAR circuits is combinatorial antigen recognition, which improves the specificity of ACTs. Wu et al. and later Raj et al. took a different approach by controlling CAR activity with small molecule drugs making the strength and duration of CAR activation titratable [37,38]. This synthetic regulation of CARs via their external cues designated a new way of thinking about CAR dynamics and reducing on-target off-tumor toxicities; however, it did not address the growing complication of antigen escape. To address this issue, designs revolving around the dynamic control of CAR specificity and activation once in vivo has resulted in solutions such as the convertible CARs of Xyphos, Calibr, and Unum or more recently the SUPRA CAR system [39–42,43]. These regulation platforms highlight a dynamic, rapidly expanding field of in vivo dynamic CAR regulation. (Fig. 1.3).

1.7 Controlling the T cell and cellular environments.

Investigators have begun to realize how the nature of the T cell type that is modified with the TCR or CAR can control cell fate. For instance, groups have expressed CARs or TCRs in viral-specific

T cells (VSTs) and suggest this better exploits the proliferative capability of the T cell with vaccination during treatment [44]. Others have used subsets of purified central memory cells as vaccine studies have suggested that this cell type is more efficient at longterm immunity [45–47]. Conversely, others have focused on modifying the TME, rather than the T cell itself, to alter T cell function. Many of the suppressive mechanisms of the TME (e.g. metabolic control, suppressive cytokines and infiltrating cell types) are now being targeted with ACT to improve the efficacy of the T cell response in the inhospitable environment. Many labs have focused on how CAR T cells can synthetically control the effects of immunosuppressive cytokines such as TGFb or IL-4. New CAR T cells that sequester immunosuppressive cytokines, activate within their presence, block their signaling, or secrete orthogonal cytokines that confine communication to the engineered T cells are being developed to reduce the impact of the TME [48,49,50,51,52]. Recently, multiple versions of antibodies, including nanobodies, have been used to target growth factors to attenuate tumor aggressiveness [53–56], in the form of titratable bispecifics [57–61]. These include the use of bi-specific T-cell engagers (BiTE) that combine specificities for cytokines, cell surface target antigens and checkpoint inhibitors to maximize cell-based therapies [62–66]. CAR-T cells paired with synNotch and granzyme-B systems could soon be used to deliver these therapeutics and attenuate the suppressive capabilities of the TME [36,67,68] (Fig. 1.4).

1.8 Cell therapy for the masses — universal ACT

Cell therapies have successfully avoided issues of graft-versus-host disease (GvHD) because the current therapies utilize autologous T cells [69,70]. While this is an FDA-approved pipeline, the treatment could be simplified through the use of ‘off-the-shelf’ universal cells— therapeutics in which patients would receive allogeneic cells that evade detection by the recipient immune system. Many groups have focused on editing out the TCR to prevent GvHD [71,72] while others,

have selectively deleted HLA class I and class II molecules to avoid recognition by host T cells and, thus, prevent rejection by the adaptive immune system of the host. These modifications in combination with CAR engineering may allow allogeneic universal CAR T cells to eradicate tumor cells with similar efficacy to autologous CAR T cells. This approach has been successful clinically in two patients with pediatric B-ALL [71,73].

In fact, there is an incredible rate of progress in genome editing and cellular engineering technologies leading to new approaches to rapidly generate universal T cells for cell therapies. T cells have been reprogrammed into an embryonic-like state to enable unlimited proliferation and production of iPS T cells [74,75]. Clarke et al. recently generated FT819 [76], an iPS cell line containing the standard CD19 CAR and a bi-allelic disruption of the TRAC locus [76]. Cooper et al. utilized CRISPR/Cas9 to create UCART7, a universal CAR T cell therapy targeting CD7+ T cells with both CD7 and its TRAC locus knocked out, making it fratricide and GvHD resistant [77]. While these approaches need to be further tested in the lab and clinic, they mark a critical step toward true universal T cell therapies that could be cost-effective, ready for immediate use, and compatible with a wider patient population, particularly those with few therapeutic options.

1.9 Conclusion

ACT has now been established as another pillar of medicine along with small molecule drugs and biologics. The promise of cell therapy goes beyond cancer, or even immune diseases such as autoimmunity and organ transplantation. In fact, under the right conditions, 'off-the-shelf' T cells, engineered with novel receptors, may be applied to many applications from tissue repair and regeneration to the elimination of senescent cells in degenerative diseases such as dementias and heart disease. To get there, the use of novel gene editing and deliberate synthetic biology approaches, described above, will be key and the ability to engineer both enhanced therapeutic functionality and control systems into cells will increase safety and efficacy. Additionally, the incorporation of synthetic solutions to central problems such as CAR T cell exhaustion will be central to ensuring their persistence both in the patient and in the clinic. It should also be noted that the current limitations of cost of goods will need to be addressed using novel manufacturing approaches, virus-free introduction of gene edits and receptors, and better closed automated systems for cell expansion. In addition to the cost of goods, reducing the burden of labor for designing novel receptors will need to become a priority as faster iteration reduces cost of novel therapeutics. This is an exciting time in immunology, synthetic biology, and systems biology as we can now envision the wide-range of tools that will be developed to control cells. We are at an inflection point in cell-based immunotherapies, but the field must be thorough in testing this transformative form of therapy to make sure the safety profile matches the therapeutic need.

Funding and disclosures

KTR is funded by the Parker Institute for Cancer Immunotherapy, the UCSF Helen Diller Family Comprehensive Cancer Center, Chan Zuckerberg Biohub, a NIH Director's New Innovator Award

(DP2 CA239143), Cancer Research UK, Kleberg Foundation, and Emerson Collective. JAB is funded by the Parker Institute for Cancer Immunotherapy, N.I.H., JDRF, Larry L. Hillblom Foundation and the Helmsley Charitable Trust. General support is provided for the JAB lab by the Sean N. Parker Autoimmune Research Laboratory. QT is funded by NIAID, NIDDK, JDRF, and the Helmsley Charitable Trust.

KTR is an inventor on patents for synthetic Notch receptors (WO2016138034A1, PRV/2016/62/333,106) and receives licensing fees and royalties. The patents were licensed by Cell Design labs and are now part of Gilead. He was a founding scientist/consultant and stock-holder in Cell Design Labs now a Gilead Company. KTR holds stock in Gilead. KTR is also a consultant and stockholder in Xyphos. and a consultant for Nurix and Third Rock Ventures.

JAB is a consultant for Juno, a Celgene company; a stockholder and member of the Board of Directors on Rheos Medicines, a stockholder and member of the Scientific Advisory Boards of Pfizer Center for Therapeutic Innovation, Vir Therapeutics, Arcus Biotherapeutics, Quentis Therapeutics, Solid Biosciences, and Celsius Therapeutics. JAB owns stock in MacroGenics Inc., Vir Therapeutics, Arcus Biotherapeutics, Quentis Therapeutics, Solid Biosciences, Celsius Therapeutics and Kadmon Holdings.

CA has no disclosures to report.

1.10 Figures for Chapter 1

Figure 1.1

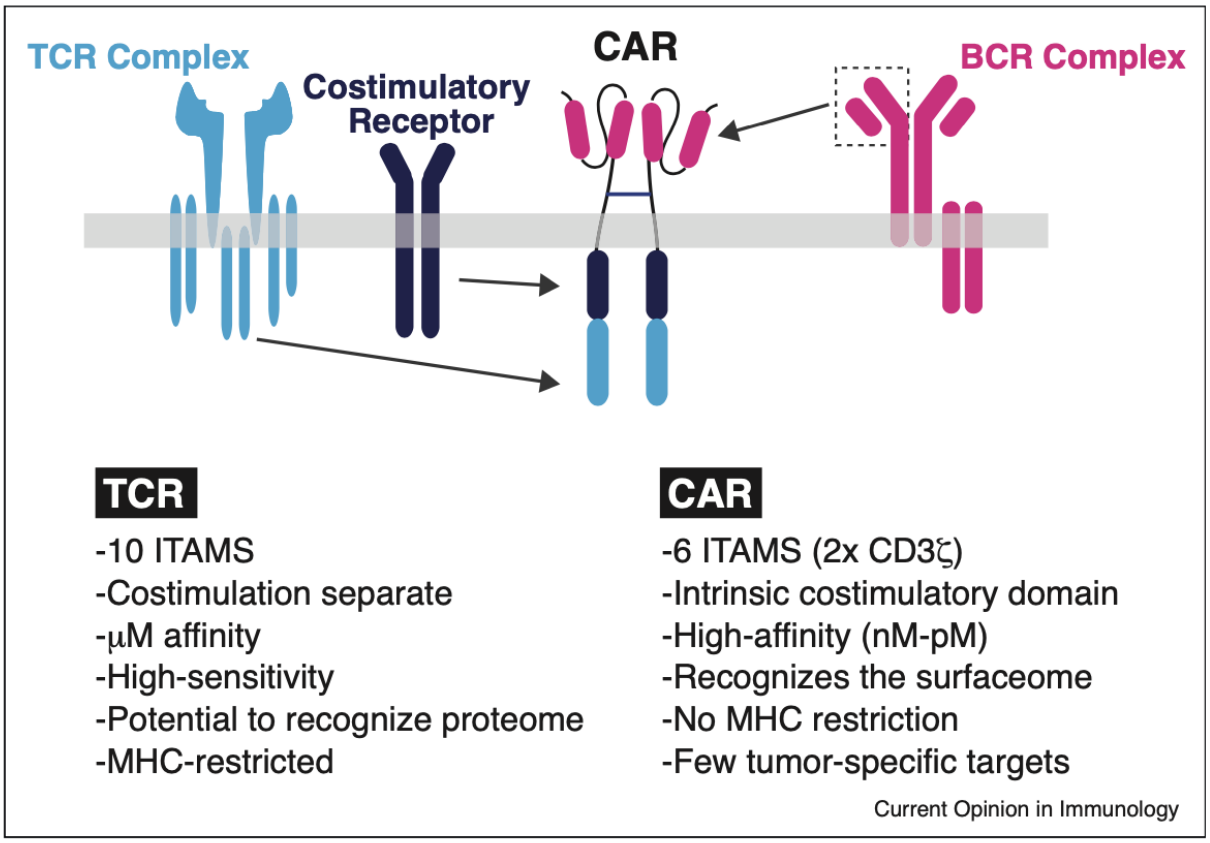

Figure 1.1. CAR versus TCR. A comparison of T cell receptors (TCRs) and chimeric antigen receptors (CARs) T cell therapy. CARs are composed of a BCR-like monoclonal antibody-based scFv binding domain and an intracellular signaling domain composed of an ITAM containing domain such as CD3ζ and a costimulatory signaling domain.

Figure 1.2

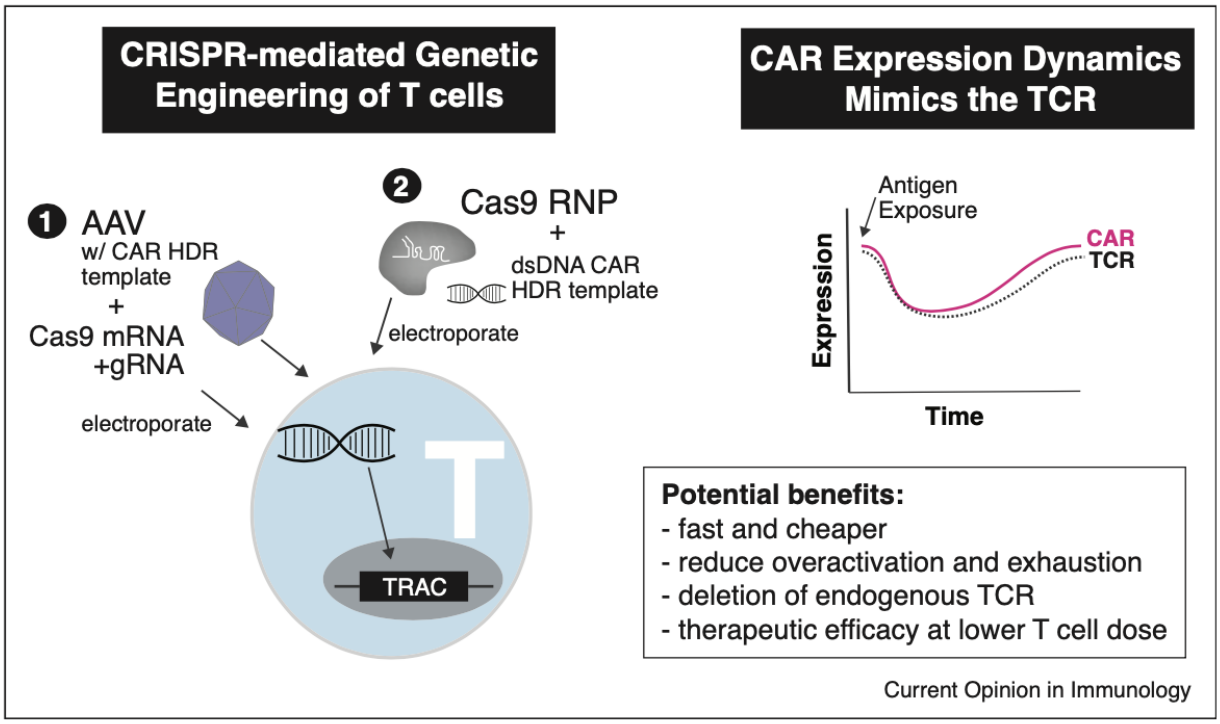

Figure 1.2. Targeted Insertion of CARs with CRISPR. The entities 1) and 2) demonstrate two recent methods for utilizing CRISPR to genetically engineer T cells for ACT. Insertion of the engineered receptor into the TRAC locus results in a TCR-like expression pattern in response to antigen exposure. These approaches provide a flexible platform to engineer cell therapies with implications beyond CARs.

Figure 1.3

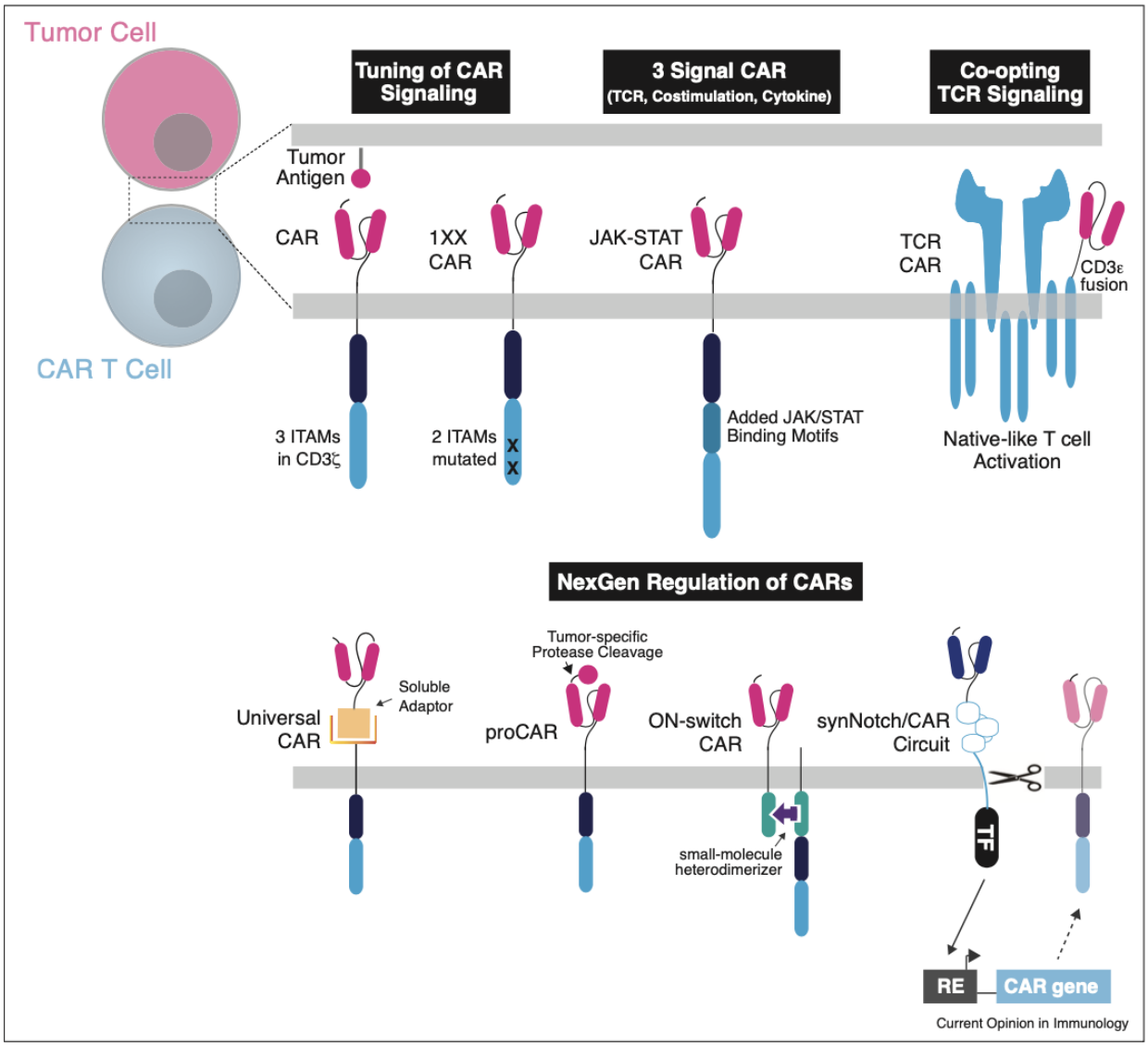

Figure 1.3. Next-generation CARs for ACT. Overcoming the challenges of CRS and T cell exhaustion with receptor signaling and regulatory modalities. The top panel is a comparison of the most recent CAR designs with altered signaling. From left to right: the classical CAR, the 1XX CAR (with only a singular N terminal CD3ζ ITAM), the JAK-STAT CAR (with additional cytokine signaling domains), and the TCR2 CAR (an scFv CD3ε fusion). The bottom panel is a comparison of the recent CAR designs that allow for dynamic in vivo regulation. From left to right: the Universal CAR (with swappable binding elements that allow for titratable and convertible specificity), the proCAR (scFv can only engage with its target only when certain TME-specific proteases are present), the ON-switch CAR (signaling controlled by a small molecule), and the synNotch/CAR circuits (context-specific CAR expression and multi-antigen recognition capabilities).

Figure 1.4

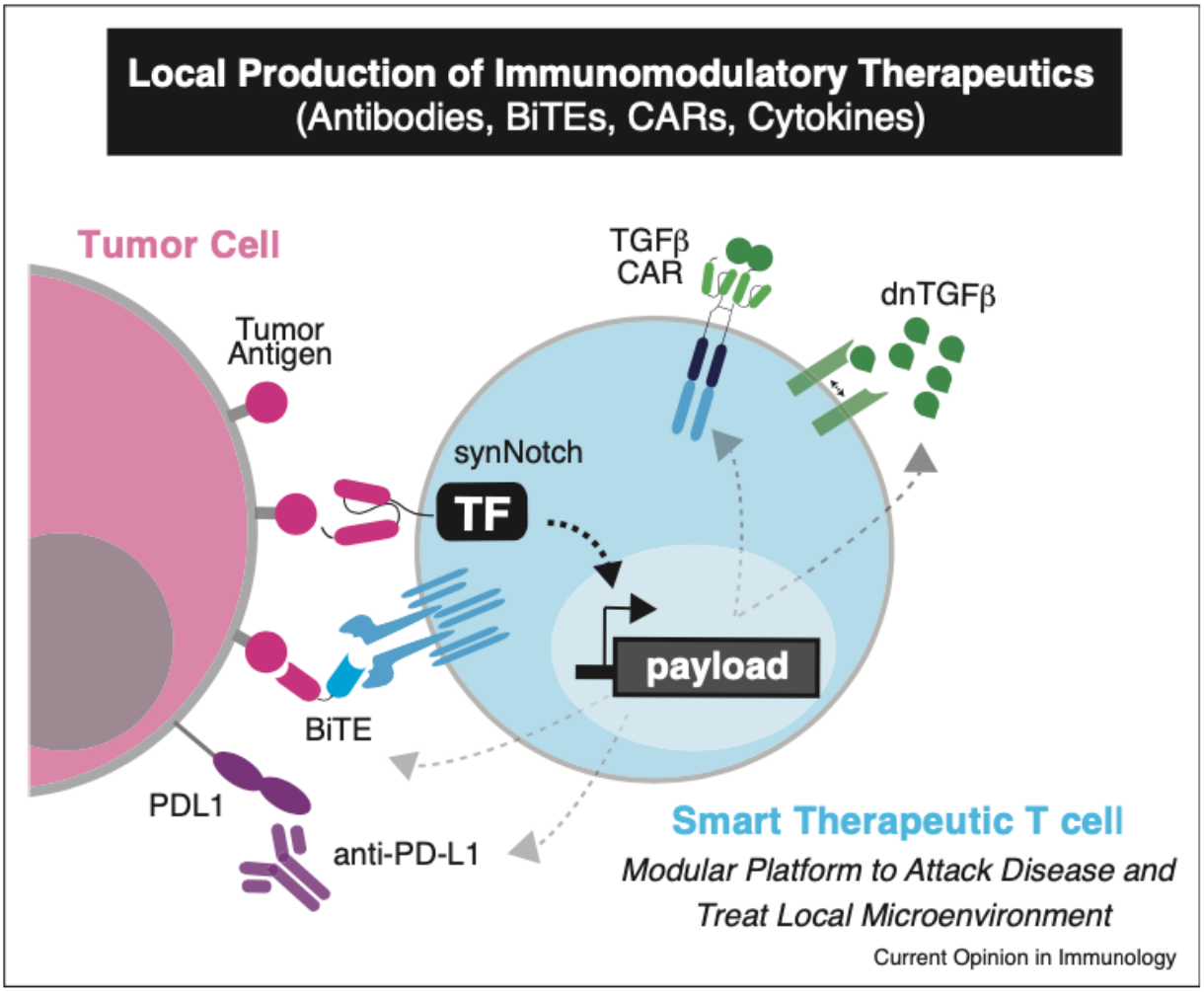

Figure 1.4. Custom regulation of therapeutic immune cells. The expansive capabilities of locally delivered payload therapeutics to alter the targeted microenvironment. Payload delivery systems such as the synNotch can transcriptionally regulate the expression of natural or non-natural therapeutics that can alter the surrounding microenvironment. Targeted delivery of antibody-based BiTEs and immunotherapies as well as biologics that sequester immunosuppressive cytokines or block their signaling capabilities on the CAR T cell can drastically affect the cell therapy's persistence, proliferation, and continued activation.

1.11 References

1. Copelan EA: Hematopoietic stem-cell transplantation. N Engl J Med 2006, 354:1813-1826.
2. Rosenberg SA, Spiess P, Lafreniere R: A new approach to the adoptive immunotherapy of cancer with tumor-infiltrating lymphocytes. Science 1986, 233:1318-1321.
3. Huang J, Brameshuber M, Zeng X, Xie J, Li Q-J: A single peptide-major histocompatibility complex ligand triggers digital cytokine secretion in CD4+ T cells. Immunity 2014, 39 http://dx. doi.org/10.1016/j.immuni.2013.08.036.A.
4. Sykulev Y, Joo M, Vturina I, Tsomides TJ, Eisen HN: Evidence that a single peptide–MHC complex on a target cell can elicit a cytolytic T cell response. Immunity 1996, 4:565-571.
5. Cameron BJ, Gerry AB, Dukes J, Harper JV, Bianchi FC, Grand F et al.: Identification of a titin-derived HLA-A1–presented peptide as a cross-reactive target for engineered MAGE A3– directed T cells. Sci Transl Med 2013, 5 http://dx.doi.org/ 10.1126/scitranslmed.3006034.
6. Linette GP, Stadtmauer EA, Maus MV, Rapoport AP, Levine BL, Emery L et al.: Cardiovascular toxicity and titin cross-reactivity of affinity-enhanced T cells in myeloma and melanoma. Blood 2013, 122:863-871.
7. Ping Y, Liu C, Zhang Y: T-cell receptor-engineered T cells for cancer treatment: current status and future directions. Protein Cell 2018, 9:254-266.
8. Levine AG, Hemmers S, Baptista AP, Schizas M, Faire MB, Moltedo B et al.: Suppression of lethal autoimmunity by regulatory T cells with a single TCR specificity. J Exp Med 2017, 214:609-622.

9. Huang J, Brameshuber M, Zeng X, Xie J, Li Q-J, Chien Y-H et al.: A single peptide-major histocompatibility complex ligand triggers digital cytokine secretion in CD4+ T cells. Immunity 2013, 39:846-857.
10. Watanabe K, Terakura S, Martens AC, van Meerten T, Uchiyama S, Imai M et al.: Target antigen density governs the efficacy of anti–CD20-CD28-CD3 z chimeric antigen receptor–modified effector CD8+ T cells. J Immunol 2015, 194:911-920.
11. Majzner RG, Mackall CL: Tumor antigen escape from CAR T-cell therapy. Cancer Discov 2018, 8:1219-1226.
12. Gauthier J, Turtle CJ: Insights into cytokine release syndrome and neurotoxicity after CD19-specific CAR-T cell therapy. Curr Res Transl Med 2018, 66:50-52.
13. Lee DW, Santomasso BD, Locke FL, Ghobadi A, Turtle CJ, Brudno JN et al.: ASBMT consensus grading for cytokine release syndrome and neurologic toxicity associated with immune effector cells. Biol Blood Marrow Transplant 2018, 25:625-638 http://dx.doi.org/10.1016/j.bbmt.2018.12.758.
14. Maus MV, Plotkin J, Jakka G, Stewart-Jones G, Rivie` re I, Merghoub T et al.: An MHC-restricted antibody-based chimeric antigen receptor requires TCR-like affinity to maintain antigen specificity. Mol Ther Oncolytics 2016, 3:1-9.
15. Tran E, Robbins PF, Lu Y-C, Prickett TD, Gartner JJ, Jia L et al.: T-cell transfer therapy targeting mutant KRAS in cancer. N Engl J Med 2016, 375:2255-2262.
16. Gee MH, Han A, Lofgren SM, Beausang JF, Mendoza JL, Birnbaum ME et al.: Antigen identification for orphan T cell receptors expressed on tumor-infiltrating lymphocytes. Cell 2018, 172:549-563.e16.

17. Matsuda T, Leisegang M, Park J-H, Ren L, Kato T, Ikeda Y et al.: Induction of neoantigen-specific cytotoxic T cells and construction of T-cell receptor – engineered T cells for ovarian cancer. Clin Cancer Res 2018:5357-5368.
18. Lee C-H, Yelensky R, Jooss K, Chan TA: Update on tumor neoantigens and their utility: why it is good to be different. Trends Immunol 2018, 39:536-548.
19. Schumacher TN, Schreiber RD: Neoantigens in cancer immunotherapy. Science 2015, 348.
20. Linette GP, Stadtmauer EA, Maus MV, Rapoport AP, Levine BL, Emery L et al.: Cardiovascular toxicity and titin cross-reactivity of affinity-enhanced T cells in myeloma and melanoma. Blood 2019, 122:863-872.
21. Morgan RA, Chinnasamy N, Abate-daga D, Gros A, Robbins PF et al.: Cancer regression and neurological toxicity following anti-MAGE-A3 TCR gene therapy. J Immunother 2013, 36:133- 151.
22. Shao H, Zhang W, Hu Q, Wu F, Shen H, Huang S: TCR mispairing in genetically modified T cells was detected by fluorescence resonance energy transfer. Mol Biol Rep 2010, 37:3951-3956.
23. Bethune MT, Gee MH, Bunse M, Lee MS, Gschweng EH, Pagadala MS et al.: Domain-swapped t cell receptors improve the safety of TCR gene therapy. eLife 2016, 5:1-24.
24. Dossett ML, Wolfl M, Ho WY, Voss R-HH, Fowler C, Greenberg PD et al.: Facilitating matched pairing and expression of TCR chains introduced into human T cells. Blood 2007, 109:2331- 2338.
25. Zhang Z, Qiu S, Zhang X, Chen W: Optimized DNA electroporation for primary human T cell engineering. BMC Biotechnol 2018, 18:4.

26. Zhao Y, Moon E, Carpenito C, Paulos CM, Liu X, Brennan AL et al.: Multiple injections of electroporated autologous T cells expressing a chimeric antigen receptor mediate regression of human disseminated tumor. Cancer Res 2010, 70:9053-9061.

27. Eyquem J, Mansilla-soto J, Giavridis T, Hamieh M, Cunanan KM, Odak A et al.: Targeting a CAR to the TRAC locus with CRISPR/Cas9 enhances tumour rejection. Nature 2017, 543:113-117.

28. Macleod DT, Antony J, Martin AJ, Moser RJ, Hekele A, Wetzel KJ et al.: Integration of a CD19 CAR into the TCR alpha chain locus streamlines production of allogeneic gene-edited CAR T cells. Mol Ther 2017, 25:949-961.

29. Roth TL, Puig-Saus C, Yu R, Shifrut E, Carnevale J, Li PJ et al.: Reprogramming human T cell function and specificity with non-viral genome targeting. Nature 2019, 559:405-409.

30. Feucht J, Sun J, Eyquem J, Ho Y-J, Zhao Z, Leibold J et al.: Calibration of CAR activation potential directs alternative T cell fates and therapeutic potency. Nat Med 2019, 25 http://dx.doi.org/10.1038/s41591-018-0290-5.

31. Helsen CW, Hammill JA, Lau VWC, Mwawasi KA, Afsahi A, Bezverbnaya K et al.: The chimeric TAC receptor co-opts the T cell receptor yielding robust anti-tumor activity without toxicity. Nat Commun 2018, 9:3049.

32. Kagoya Y, Tanaka S, Guo T, Anczurowski M, Wang C-H, Saso K et al.: A novel chimeric antigen receptor containing a JAK–STAT signaling domain mediates superior antitumor effects. Nat Med 2018, 24:352.

33. Chmielewski M, Abken H: TRUCKs with IL-18 payload: toward shaping the immune landscape for a more efficacious CAR T cell therapy of solid cancer. Adv Cell Gene Ther 2018, 1:e7.

34. Desnoyers LR, Vasiljeva O, Richardson JH, Yang A, Menendez EEM, Liang TW et al.: Tumor-specific activation of an EGFR-targeting probody enhances therapeutic index. Sci Trans Med 2013, 5.

35. Roybal KT: Refining cell therapy. Science 2018, 359:1112-1113.

36. Roybal KT, Williams JZ, Morsut L, Rupp LJ, Kolinko I, Choe JH et al.: Engineering T cells with customized therapeutic response programs using synthetic notch receptors. Cell 2016, 167:419-432.e16.

37. Raj D, Yang M-H, Rodgers D, Hampton EN, Begum J, Mustafa A et al.: Switchable CAR-T cells mediate remission in metastatic pancreatic ductal adenocarcinoma. Pancreas 2018:1-13.

38. Wu C-Y, Roybal KT, Puchner EM, Onuffer J, Lim WA: Remote control of therapeutic T cells through a small molecule-gated chimeric receptor. Science 2015, 350:aab4077 http://dx.doi.org/ 10.1126/science.aab4077.

39. Technology - Xyphos. In: Xyphos [Internet]. [cited 2 Feb 2019]. Available: https://xyphosinc.com/technology/convertiblecar/.

40. Rodgers DT, Mazagova M, Hampton EN, Cao Y, Ramadoss NS, Hardy IR et al.: Switch-mediated activation and retargeting of CAR-T cells for B-cell malignancies. Proc Natl Acad Sci U S A 2016, 113:E459-68.

41. Antibody-Coupled T-cell Receptor (ACTR) Technology | Unum Therapeutic. In: Unum Therapeutics | Clinical-Stage Biopharmaceutical Company [Internet]. [cited 2 Feb 2019]. Available: https://www.unumrx.com/technology.
42. Viaud S, Ma JSY, Hardy IR, Hampton EN, Benish B, Sherwood L et al.: Switchable control over in vivo CAR T expansion, B cell depletion, and induction of memory. Proc Natl Acad Sci U S A 2018, 115:E10898-E10906.
43. Cho JH, Collins JJ, Wong WW: Universal chimeric antigen receptors for multiplexed and logical control of T cell responses. Cell 2018, 173:1426-1438.e11.
44. Omer B: Chimeric antigen receptor signaling domains differentially regulate proliferation and native T cell receptor function in virus-specific T. Front Med 2018, 5:1-13.
45. Fraietta JA, Lacey SF, Orlando EJ, Pruteanu-Malinici I, Gohil M, Lundh S et al.: Determinants of response and resistance to CD19 chimeric antigen receptor (CAR) T cell therapy of chronic lymphocytic leukemia. Nat Med 2018, 24:563-571.
46. Golubovskaya V, Wu L: Different subsets of T cells, memory, effector functions, and CAR-T immunotherapy. Cancers 2016, 8 http://dx.doi.org/10.3390/cancers8030036.
47. Morgan MA, Schambach A: Engineering CAR-T cells for improved function against solid tumors. Front Immunol 2018, 9:2493.
48. Sukumaran S, Watanabe N, Bajgain P, Raja K, Mohammed S, Fisher WE et al.: Enhancing the potency and specificity of engineered T cells for cancer treatment. Cancer Discov 2018, 8:972-987.
49. Sockolosky JT, Trotta E, Parisi G, Picton L, Su LL, Le AC et al.: Selective targeting of engineered T cells using orthogonal IL-2 cytokine-receptor complexes. Science 2018, 359:1037-1042.

50. Kim SK, Barron L, Hinck CS, Petrunak EM, Cano KE, Thangirala A et al.: An engineered transforming growth factor b (TGF-b) monomer that functions as a dominant negative to block TGF-b signaling. J Biol Chem 2017, 292:7173-7188.
51. Kloss CC, Lee J, Zhang A, Chen F, Melenhorst JJ, Lacey SF et al.: Dominant-negative TGF-b receptor enhances PSMA-targeted human CAR T cell proliferation and augments prostate cancer eradication. Mol Ther 2018, 26:1855-1866.
52. Chang ZL, Lorenzini MH, Chen X, Tran U, Bangayan NJ, Chen YY: Rewiring T-cell responses to soluble factors with chimeric antigen receptors. Nat Chem Biol 2018, 14:317-324.
53. Kazemi-Lomedasht F, Behdani M, Bagheri KP, Habibi-Anbouhi M, Abolhassani M, Arezumand R et al.: Inhibition of angiogenesis in human endothelial cell using VEGF specific nanobody. Mol Immunol 2015, 65:58-67.
54. Omidfar K, Amjad Zanjani FS, Hagh AG, Azizi MD, Rasouli SJ, Kashanian S: Efficient growth inhibition of EGFR over-expressing tumor cells by an anti-EGFR nanobody. Mol Biol Rep 2013, 40:6737-6745.
55. Vosjan MJWD, Vercammen J, Kolkman JA, Stigter van Walsum M, Revets H, van Dongen GAMS: Nanobodies targeting the hepatocyte growth factor: potential new drugs for molecular cancer therapy. Mol Cancer Ther 2012, 11:1017-1025.
56. Zhu Y, Bassoff N, Reinshagen C, Bhere D, Nowicki MO, Lawler SE et al.: Bi-specific molecule against EGFR and death receptors simultaneously targets proliferation and death pathways in tumors. Sci Rep 2017, 7:1-11.
57. Bargou R, Leo E, Zugmaier G, Klinger M, Goebeler M, Knop S et al.: Tumor regression in cancer of a T cell-engaging antibody. Science 2008, 3:974-978.

58. Huston JS, Mudgett-Hunter M, Tai M-S, McCartney J, Warren F, Haeer E, Oppermann H: [3] Protein engineering of single-chain Fv analogs and fusion proteins. Methods Enzymol 1991, 203:46- 48.

59. Kantarjian H, Stein A, Go¨kbuget N, Fielding AK, Schuh AC, Ribera J-M et al.: Blinatumomab versus chemotherapy for advanced acute lymphoblastic leukemia. N Engl J Med 2017, 376:836-847.

60. Topp MS, Kufer P, Go¨kbuget N, Goebeler M, Klinger M, Neumann S et al.: Targeted therapy with the T-cell-engaging antibody blinatumomab of chemotherapy-refractory minimal residual disease in B-lineage acute lymphoblastic leukemia patients results in high response rate and prolonged leukemia-free survival. J Clin Oncol 2011, 29:2493-2498.

61. Wolf E, Hofmeister R, Kufer P, Schlereth B, Baeuerle PA: BiTEs: bispecific antibody constructs with unique anti-tumor activity. Drug Discov Today 2005, 10:1237-1244.

62. Sun X, Yan X, Zhuo W, Gu J, Zuo K, Liu W et al.: PD-l1 nanobody competitively inhibits the formation of the PD-1/PD-l1 complex: Comparative molecular dynamics simulations. Int J Mol Sci 2018, 19 http://dx.doi.org/10.3390/ijms19071984.

63. Zhang F, Wei H, Wang X, Bai Y, Wang P, Wu J et al.: Structural basis of a novel PD-L1 nanobody for immune checkpoint blockade. Cell Discov 2017, 3:1-12.

64. Rafiq S, Yeku OO, Jackson HJ, Purdon TJ, van Leeuwen DG, Drakes DJ et al.: Targeted delivery of a PD-1-blocking scFv by CAR-T cells enhances anti-tumor efficacy in vivo. Nat Biotechnol 2018, 36:847-856.

65. Blanchetot C, Verzijl D, Mujic-Delic A, Bosch L, Rem L, Leurs R et al.: Neutralizing nanobodies targeting diverse chemokines effectively inhibit chemokine function. J Biol Chem 2013, 288:25173-25182.

66. Danquah W, Catherine MS, Rissiek B, Pinto C, Arnau SP, Amadi M et al.: Nanobodies that block gating of the P2X7 ion channel ameliorate inflammation. Sci Transl Med 2016, 8 http://dx.doi. org/10.1126/scitranslmed.aaf8463.

67. Morsut L, Roybal KTKT, Xiong X, Gordley RM, Coyle SM, Thomson M et al.: Engineering customized cell sensing and response behaviors using synthetic notch receptors. Cell 2016, 164:780-791.

68. Woodsworth DJ, Dreolini L, Abraham L, Holt RA: Targeted cell-to-cell delivery of protein payloads via the granzyme-perforin pathway. Mol Ther Methods Clin Dev 2017, 7:132-145.

69. Brentjens RJ, Davila ML, Riviere I, Park J, Wang X, Cowell LG et al.: CD19-targeted T cells rapidly induce molecular remissions in adults with chemotherapy-refractory acute lymphoblastic leukemia. Sci Transl Med 2013, 5:177ra.

70. Kochenderfer JN, Dudley ME, Kassim SH, Somerville RPT, Carpenter RO, Stetler-Stevenson M et al.: Chemotherapy-refractory diffuse large B-cell lymphoma and indolent B-cell malignancies can be effectively treated with autologous T cells expressing an anti-CD19 chimeric antigen receptor. J Clin Oncol 2015, 33:540-549.

71. Qasim W, Zhan H, Samarasinghe S, Adams S, Amrolia P, Stafford S et al.: Molecular remission of infant B-ALL after infusion of universal TALEN gene-edited CAR T cells. Sci Transl Med 2017, 9 http://dx.doi.org/10.1126/scitranslmed.aaj2013.

72. Torikai H, Reik A, Liu PQ, Zhou Y, Zhang L, Maiti S et al.: A foundation for universal T-cell based immunotherapy: T cells engineered to express a CD19-specific chimeric-antigen-receptor and eliminate expression of endogenous TCR. Blood 2012, 119:5697-5705.

73. Poirot L, Philip B, Schiffer-Mannioui C, Le Clerre D, Chion-Sotinel I, Derniame S et al.: Multiplex genome-edited t-cell manufacturing platform for "Off-the-Shelf" adoptive T-cell immunotherapies. Cancer Res 2015, 75:3853-3864.

74. Nishimura T, Kaneko S, Kawana-Tachikawa A, Tajima Y, Goto H, Zhu D et al.: Generation of rejuvenated antigen-specific T cells by reprogramming to pluripotency and redifferentiation. Cell Stem Cell 2013, 12:114-126.

75. Themeli M, Kloss CC, Ciriello G, Fedorov VD, Perna F, Gonen M et al.: Generation of tumor-targeted human T lymphocytes from induced pluripotent stem cells for cancer therapy. Nat Biotechnol 2013, 31:928-933.

76. Clarke RL, van der Stegen S, Lee T, Mansilla-Soto J, Chang C-W, Sasaki J et al.: Abstract LB-108: generation of off-the-shelf TCR-less CAR-targeted cytotoxic T cells from renewable pluripotent cells for cancer immunotherapy. Cancer Res 2018, 78 LB–108–LB–108.

77. Cooper ML, Choi J, Staser K, Ritchey JK, Devenport JM, Eckardt K et al.: An "off-the-shelf" fratricide-resistant CAR-T for the treatment of T cell hematologic malignancies. Leukemia 2018, 3. 32:1970-1983.

Chapter 2

CAR Pooling: High throughput screening of CAR T cells identifies diverse immune signaling domains for next-generation immunotherapies

2.1 Abstract

Chimeric antigen receptors (CARs) repurpose natural signaling components to retarget T cells to refractory cancers but have shown limited efficacy in persistent, recurrent malignancies. Here, we introduce “CAR Pooling”, a multiplexed approach to rapidly identify CAR designs with clinical potential. Forty CARs with signaling domains derived from a range of immune cell lineages were evaluated in pooled assays for their ability to stimulate critical T cell effector functions during repetitive stimulation that mimics long-term tumor antigen exposure. Several domains were identified from the tumor necrosis factor (TNF) receptor family that have been primarily associated with B cells. CD40 enhanced proliferation, whereas B-cell activating factor receptor (BAFF-R) and transmembrane activator and CAML interactor (TACI) promoted cytotoxicity. These functions were enhanced relative to clinical benchmarks after prolonged antigen stimulation, and fell into distinct states of memory, cytotoxicity, and metabolism. BAFF-R CAR T cells were enriched for a highly cytotoxic transcriptional signature previously associated with positive clinical outcomes. Additionally, we observed that replacing the 4-1BB intracellular signaling domain with the BAFF-R signaling domain in a clinically validated B-cell maturation antigen (BCMA)-specific CAR resulted in enhanced activity in a xenotransplant model of multiple myeloma. Together, these results show that “CAR Pooling” is a general approach for rapid exploration of CAR architecture and activity to improve the efficacy of CAR T cell therapies.

2.2 Introduction

Adoptive cell therapy using engineered chimeric antigen receptor (CAR) T cells has revolutionized the treatment of B-cell leukemias and lymphomas(1, 2). CAR T cells currently in the clinic use either a 4-1BB or CD28 intracellular costimulatory domain, which come from natural, well-studied T cell costimulatory receptors. Costimulation is a critical component of immune activation, and CARs lacking the "signal 2" from a costimulatory domain quickly become anergic upon stimulation(3). CARs containing 4-1BB and CD28 intracellular domains are used in second generation CAR T cells, which elicit more robust and sustained T cell activation than the original CD3ζ-only CARs. Although both CD28-and 4-1BB-CAR T cells are effective therapeutics, there are substantial differences in their synapse development, cytotoxicity, metabolic state, and clinical performance(4–7). Additionally, preclinical and clinical studies show that T cells expressing CD28 CARs are initially faster to proliferate and kill tumor cells, but suffer from reduced long-term engraftment and heightened exhaustion after prolonged activation(8–12).

There is considerable diversity in costimulatory domains, and evidence for both quantitative and qualitative differences in costimulatory signaling in the context of a CAR(7). 4-1BB and CD28 utilize two separate signaling pathways [tumor necrosis factor (TNF) receptor associated factor (TRAF) and phosphatidylinositol-3-kinase (PI3K)/lymphocyte-specific protein tyrosine kinase (Lck)/growth factor receptor-bound protein 2 (Grb2), respectively], however these pathways converge upon conserved signaling intermediates, suggesting that costimulatory domains from other immune cells may also be able to signal in T cells(13–15). Other studies have individually characterized additional T cell costimulatory domains within CARs or searched for mutant

domains with enhanced properties(16–20). However, the scale of these searches has been limited to selected domains, focused on receptors with known functions in T cells.

Pooled screens are a powerful tool for probing T cell biology, including using clustered regularly interspaced short palindromic repeats (CRISPR) knockouts and switch receptors(21, 22), but have only recently been applied to CAR engineering. Pooled assays offer increased throughput and direct comparison of cells from the same blood donor tested in identical conditions. Screening of large numbers of domains to assess their effects on multiple cell-intrinsic T cell phenotypes would help identify optimal CAR designs for clinical applications. Although pooled measurement can be applied to many aspects of CAR architecture, signaling domains-which are small, have minimal secondary structure, consist of short and modular signaling motifs(23)-lend themselves to pooled characterization using large synthetic DNA libraries(24). Signaling domains identified from these screens can then be more deeply characterized for potential clinical translation.

The lack of persistence and long-term efficacy in patients is a central problem for current CAR T therapies, in both solid cancers and hematological tumors such as multiple myeloma(25–27). To answer this clinical need, we assembled a signaling domain library consisting of both inhibitory and stimulatory domains from a range of innate and adaptive immune cells to assess their propensity to resist exhaustion within the CAR architecture(3). We then performed a suite of pooled assays in primary human CD4 or CD8 T cells containing this CAR library using a repetitive stimulation assay we developed to mimic the protracted stress and exhaustion of chronic antigen exposure on T cells in difficult-to-eliminate tumors. The dataset produced from

these assays represents a systematic survey of the CAR T cell costimulation landscape. We identified a set of potent costimulatory domains from the TNF receptor family – CD40, B-cell activating factor receptor (BAFF-R), and transmembrane activator and CAML interactor (TACI) – that drove T cells to exhibit enhanced proliferation and cytotoxicity in vitro, despite the domains being primarily associated with the B cell lineage. We also identified killer cell lectin like receptor G1 (KLRG1), an inhibitory domain, that silenced CD3ζ activation and kept CAR T cells in a naive transcriptional state. Additionally, single-cell RNA and surface protein expression profiles among these candidates showed that CAR T cells using the signaling domain of BAFF-R were enriched for a highly cytotoxic transcriptional signature, which has been associated with enhanced CAR T engraftment and improved response against melanoma in clinical studies(28, 29). BAFF-R-based CAR T cells, as compared to benchmark 4-1BB- and CD28-based CAR T cells, exhibited equivalent efficacy in a mouse model of mesothelioma and superior efficacy in a model of multiple myeloma.

2.3 CAR Pooling allows for screening of a pooled library of CARs with diverse costimulatory domains.

Innate and adaptive immune cells use a set of specialized receptors to sense their extracellular environment and elicit critical cellular functions. To transduce these signals, these receptors often use modular linear signaling motifs within their intracellular domains, which bind to downstream signaling proteins. These motifs and signaling partners are often highly conserved across the immune system(3, 23), and we hypothesized that some of these unexplored signaling domains and motifs could engage distinct and beneficial T cell signaling in the context of a CAR. To test this, we developed a method for high-throughput, pooled screening of CAR signaling libraries within

primary human T cells, which we call “CAR Pooling”. To generate the CAR Pooling library, we mined 40 costimulatory and coinhibitory receptor intracellular domains from different protein families and functional classes associated with several immune cell types, including natural killer (NK) cells, B cells, and other innate immune cells (Fig. 2.1A and B, table S1). We synthesized and cloned the domains into a second-generation CAR scaffold and lentivirally transduced the CAR into independent CD4 and CD8 primary human T cell cultures from matched donors (Fig. 2.1C). CAR-positive T cells were sorted for a defined range of CAR expression using a 2A-green fluorescent protein (GFP) marker and rested before proceeding with tumor cell stimulation (Fig. 2.1C).

To mimic the exhaustion conditions encountered in patients with a high tumor burden, we performed repetitive, long-term in vitro stimulations of the CAR T cells over 24 to 33 days, with CD19+ or CD19- K562 cells added 1:1 to the T cell culture every three days (Fig. 2.1D). K562 cells were irradiated prior to their addition to reduce their proliferative capacity and prevent rapid depletion of the media. CD28 and 4-1BB CAR T cells in this assay became increasingly exhausted (Fig. 2.1E, fig. 2.8A and B). Additionally, a CAR containing only the CD3ζ domain appeared to have an anergic phenotype by day 15 and did not survive after day 24, indicating that the effect of costimulation, which is critical to durable responses in vivo, is at least partially captured by this model(7, 30–32).

To efficiently characterize the CAR Pooling library across multiple assays and time points, we employed FlowSeq, a pooled measurement that quantitatively measures any cell-based fluorescent readout across a genetically-diverse population of cells(33). We used FlowSeq to measure different

markers of T cell function, such as activation (CD69), cytokine production [interferon (IFN)-γ and interleukin (IL)-2], and proliferation using CellTrace Violet (CTV) dye. For each pooled assay, cells were sorted and separately sequenced to compare the functional differences among the domains (Fig. 2.1D and F; Fig. 2.2A and B). This multiplexed approach allowed us to compare differential CAR T activity between CD4 and CD8 T cell types, and between early and late stages of antigen stimulation and expansion.

Despite donor variability, the domain ranking across replicates for all assays was consistent and highly correlated (Kruskal-Wallis $H > 110$; $p < 1e\text{-}10$) (fig. 2.8C). We found no correlation among the library domains between either initial domain abundance or length and early or late relative expansion (fig. 2.8D). Given these measurements, we determined that CAR Pooling is a generally reproducible and robust platform for these multiplexed assays.

2.4 Multidimensional comparison of signaling domains across repetitive expansion identifies new potent costimulatory domains.

Antigen-induced proliferation, cytokine secretion, and activation varied across CAR T cells expressing different costimulatory domains (Fig. 2.2A, fig. 2.9A, B, and C), and the canonical CD28 and 4-1BB domains were among those that promoted the most cytokine secretion and proliferation (average rank 4 and 5, respectively; Mann-Whitney U, $p < 9.6e\text{-}8$, across all assays). However, other domains consistently appeared among the top-performers, including BAFF-R and TACI (average ranks 1 and 2, respectively).

Antigen-independent proliferation also varied considerably among the domains. Although overall proliferation was universally lower without antigen, domains that promoted strong

proliferation upon antigen-exposure also tended to exhibit enhanced proliferation in antigen-negative co-culture (Spearman's $\rho = 0.63\text{-}0.75$, $p = 1.3\text{x}10\text{-}5$), indicating a strong correlation between antigen-dependent proliferation and increased basal proliferation (fig. 2.9B). Among the top-performing domains, CD28 and TACI exhibited the highest degree of non-specific proliferation, whereas CD40 had the lowest (fig. 2.9B).

We measured IL-2 and IFN-γ production (Fig. 2.2B, fig. 2.9C) and CD69 expression (fig. 2.9D in both CD4 and CD8 T cells. Ranking of CARs from least to most cytokine production in log2 fold change, IL-2 and IFN-γ secretion was similar in multiple cultures of CD4 and CD8 T cells (yellow, orange) across three human donors (Fig. 2.2B, fig. 2.9C).

The lack of long-term CAR T cell persistence is often cited as a major reason for antigen-positive relapse in patients (34). Multiple aspects of cell dynamics underlie CAR T cell persistence, including a cell's lifespan during and after stimulation. Cell proliferation (CTV) is thus an incomplete representation of CAR T efficacy. To better capture persistence, we also measured change in the relative frequency of a domain over time, termed "relative expansion". We compared amplicon sequencing of the library immediately before stimulation and subsequently after the first, sixth, and eighth stimulations (days 3 or 4, 14 or 16, and 24, respectively, for CD4 T cells and CD8 T cells) (Fig. 2.2C). Many of the domains that preferentially expanded after the first stimulation were subsequently diminished after further stimulations, indicating that initial proliferation did not correlate well with long-term proliferative capacity and persistence (fig. 2.9E). We also saw some domains differentially enriched in either CD4 or CD8 T cells (Fig. 2.2D). Most domains promoted a greater expansion

overall in CD8 T cells, with the notable exceptions of CD30, CD40, and 4-1BB, where, after 24 days of stimulation, CD4 T cells expanded over two-fold more than CD8 T cells. As noted by previous studies, these results imply that using different costimulatory domains in CD4 versus CD8 T cells may improve overall CAR T therapeutic efficacy (17).

2.5 Scoring CARs across pooled measurements identifies signaling domains with distinct stimulatory activity.

To summarize the relative performance of all domains over the repetitive stimulation assays, hierarchical clustering was performed (Fig. 2.3A). A subset of CAR T cells containing CD28, 4-1BB, and several additional domains clustered into a potent costimulatory group, demonstrating enhanced T cell functions relative to the average domain in the library (Fig. 2.3A). This group was highly enriched for domains belonging to the TNF receptor family. CD40 and CD30 were most similar to 4-1BB, demonstrating substantial overall expansion and late-stage proliferation in both CD4 and CD8 T cells. In contrast, BAFF-R, CD28, and TACI showed moderately enhanced expansion and late-stage proliferation but promoted substantial cytokine production, with CD28 and TACI producing high IL-2. Overall, the eight most potent CAR costimulatory domains were distributed along a spectrum of late-stage proliferators to high-cytokine producers, suggesting that there may be inherent tradeoffs between these two aspects of CAR T activity. As members of the TNF receptor family spanned the stimulatory spectrum, we highlighted BAFF-R (light green), TACI (dark green), CD40 (light purple), and CD30 (dark purple).

Some domains, such as KLRG1 and NKR-P1A, consistently demonstrated the lowest initial proliferation, activation, and cytokine production in both CD4 and CD8 T cells (Fig. 2.3A). These

are also of interest because inhibitory signaling could be used to halt, dampen, or dynamically modulate T cell functions (35). For this reason we added KLRG1, a potential inhibitory domain (pink), in our subsequent investigations.

To further compare overall library performance, a principal component analysis (PCA) was performed across all measurements with and without antigen stimulation (Fig. 2.3B, fig. 2.10A and B). The PCA showed that domains are spread across a diverse signaling landscape, with principal component (PC) 1 being associated with early proliferation, cytokine secretion, CD69 activation, and more tonic signaling; in contrast, PC2 was associated with long-term expansion in CD8 T cells, less cytokine secretion, less early proliferation, and relatively less tonic signaling (fig. 2.10A). PC2 was also correlated with domain size, suggesting that increasing the distance between the membrane and CD3ζ reduces the strength of early activation and tonic signaling (fig. 2.10B). This is supported by recent work showing that altering the position of CD3ζ immunoreceptor tyrosine-based activation motifs (ITAMs) modulates differentiation and memory formation(36–39). There was no discernable clustering based on cell-type specific expression or protein family structure, aside from the aforementioned enrichment of TNF family members in the stimulatory group (Fig. 2.3B). Additionally, there were only minor differences in cell surface expression for each of the highlighted CARs measured using an N-terminal myc tag normalized for transduction through the co-expressed T2A GFP reporter (fig. 2.10C).

CAR T cells that used BAFF-R, TACI, CD40, or CD30 also enhanced persistence in the pooled library, demonstrated by the dynamics of their relative expansion through day 24 (Fig. 2.3C). In addition, CD30 and CD40 showed the most and least antigen-independent expansion, respectively

(fig. 2.10D). Lastly, as our highlighted domains all belong to the TNF receptor family, and thus all use TRAF signaling (40), we surveyed their literature-annotated TRAF binding sites and post-translational modifications (41) to assess shared signaling characteristics (fig. 2.10E). They can associate with a diverse set of TRAFs, with no discernible shared motif or partner across the 5 domains (42–45).

2.6 A subset of signaling domains differentially affects proliferation, long-term expansion, and late-stage metabolism.

To further assess the five selected CARs in CD4 and CD8 T cells and to confirm their efficacy outside of the pooled assays, an extended in vitro repetitive stimulation assay was performed on each individually. 4-1BB, CD28, and a CD3ζ first-generation CAR were included as benchmarks due to their clinical relevance and characterization within the literature (6, 46). Proliferation was measured weekly using CTV over 33 days of repetitive antigen stimulation in two primary human donors (Fig. 2.4A to C, fig. 2.11A and B). Representative measurements for a single donor are shown alongside quantifications of the average change in mean fluorescence intensity (MFI) of the CTV stain (Fig. 2.4B and C). These arrayed stimulations resulted in relative proliferations similar to those observed in the pooled screen, with CD28 demonstrating less proliferation in CD4 T cells at later time points, CD40 generating strong proliferation in CD4 T cells, 4-1BB and BAFF-R demonstrating stronger late-stage proliferation through day 33, and KLRG1 displaying dramatically less cell division overall. Lastly, contrary to our pooled data, CD30 drove an initial burst of proliferation, primarily in CD4 T cells, but this was not sustained in later weeks. Overall, we found a high degree of correlation between our pooled and arrayed proliferation screens.

In addition to measuring proliferation by CTV dilution, we counted the number of T cells in culture every 3 days prior to restimulation with additional K562 tumor cells using flow cytometry and cell-counting beads. We used these counts to calculate the overall cumulative expansion of each CAR. Like the relative expansion measurements in our pooled screen, this considers both proliferation and resistance to cell death. In CD4 T cells from both donors, 4-1BB promoted a higher degree of cumulative expansion and persistence than CD28, in line with the clinical findings that 4-1BB CAR T cells are better long-term proliferators in vivo and are more resistant to exhaustion than CD28 CAR T cells (Fig. 2.4D) (4). However, we found that over 33 days, CD4 CAR T cells with CD40 costimulation doubled at an average of 1.8x the rate of those with 4-1BB or CD28 across both donors (Repeated Measures ANOVA, p=3.3x10-3), indicating, as in our pooled experiment, a heightened propensity for proliferation, resistance to cell death, or both during prolonged antigen stimulation.

A recent study found a strong association between enhanced mitochondrial metabolism and long-term proliferation (6). Therefore, we used single-cell energetic metabolism profiling (SCENITH), which uses oligomycin to inhibit mitochondrial oxidative phosphorylation (47) to determine its relative contribution to the overall metabolic output of each CAR T variant after 21 days in culture (fig. 2.11C). As expected, the CD3ζ-only CAR T cells demonstrated a low degree of mitochondrial metabolism, indicating an increased dependence on glycolysis. 4-1BB and CD28 CAR T cells were biased towards mitochondrial or glycolytic metabolism respectively, as previously noted in the literature (6). BAFF-R CAR T cells exhibited even higher mitochondrial

dependence than 4-1BB after 21 days, in line with its long-term persistence in culture after repeated stimulations.

2.7 T cells expressing BAFF-R and TACI CARs retain markers linked to persistence and demonstrate delayed exhaustion.

To determine the relationship between cell state and expansion of these CAR variants, we measured the expression of several exhaustion (programmed cell death protein 1 (PD1), lymphocyte activating 3 (LAG3), T-cell immunoglobulin mucin-3 (TIM3), CD39) and differentiation markers (CD62L, CD45RO, CD45RA, CD27, CCR7) throughout 33 days of repetitive stimulation (Fig. 2.4E, fig. 2.11D and E). BAFF-R CAR T cells exhibited slower upregulation of multiple exhaustion markers than 4-1BB and CD28, as shown by its overall lower number of markers on days 6 and 15 in both CD4 T cells and CD8 T cells (Fig. 2.4F, fig. 2.11D, E, and F). Additionally, although the CAR T cells showed relatively similar differentiation over time, both BAFF-R and TACI CD8 CAR T cells showed sustained CD27 expression over time, in contrast to CD28 and 4-1BB, where CD27 expression progressively decreased (fig. 2.4G and 2.11G). We did not observe this trend in CD4 T cells (fig. 2.11G). CD27 has been linked to CD8 T cell survival after extensive proliferation, and resistance to terminal effector differentiation and contraction(48–51). Finally, as seen in our proliferation assays, expression of exhaustion and differentiation markers by KLRG1 CAR T cells were most similar to those in untransduced T cells, suggesting that a larger fraction of KLRG1 CAR T cells remain in a naive-like memory state (fig. 2.11D to H).

2.8 Cytokine secretion and in vitro toxicity differ across signaling domains.

In addition to proliferation and persistence, we sought to measure differences in CAR T cell anti-tumor activity by cytokine secretion and cytotoxicity. We measured cytokine production in CD4 T cells in two human donors using intracellular flow cytometry after 1, 2, 3, 6 and 9 repeated stimulations in culture (Fig. 2.5A to B, fig. 2.12A). Most CAR T cells exhibited maximal cytokine production on day 4. Although comparisons can be made at early time points, none of the CAR T cells, including those containing the CD28 and 4-1BB costimulatory domains, produced substantial amounts of IFN-γ, IL-2, or TNF-α, as measured by intracellular staining after 3 or more in vitro stimulations (fig. 2.12A).

We next sought to assess the persistence of each CAR T cell's cytotoxic capability in culture after intervals of repetitive antigen stimulation. To directly measure cytotoxicity in vitro, we used Incucyte live-cell imaging, which allows for long-term imaging of fluorescently labeled cancer and T cell co-cultures inside of an incubator. At multiple timepoints after the repeated antigen stimulations, we sorted either CD4 or CD8 T cells from the co-culture using fluorescence activated cell sorting (FACS) and let them rest overnight (Fig. 2.5A). The next day, we combined the sorted T cells with red-fluorescent K562 cancer cells and performed time-lapse live-cell microscopy to observe cell killing (Fig. 2.5C and D). We then quantified the percentage of cancer cells killed at 80 hours (CD4 T cells) or 32 hours (CD8 T cells) after each stimulation (Fig. 2.5C).

Although we observed differences in the cytotoxic capacity between the two donors, BAFF-R- and TACI-expressing showed superior cytotoxicity relative to other CAR T cells (Fig. 2.5C and

D, fig. 2.12B). This was especially pronounced after multiple rounds of antigen stimulation within CD4 T cells. This enhanced cytotoxicity was statistically significant within both donors in CD4 T cells and CD8 T cells when comparing BAFF-R activity to CD28, CD40, CD30, KLRG1 and CD3ζ-only CAR T cells, and when comparing TACI to CD28, KLRG1, and CD3ζ-only CAR T cells (FDR < 0.05 by Wilcoxon Signed-rank test, Fig. 2.5E). We repeated these assays with two additional donors in CD4 T cells, comparing the top four domains (CD28, 4-1BB, BAFF-R, TACI), which further confirmed significantly enhanced CD4 cytotoxicity for BAFF-R versus the other 3 domains (FDR < 0.05, Wilcoxon Signed-rank test) (fig. 2.12C to E).

Additionally, we saw that KLRG1 had drastically reduced cytotoxicity, often only killing between 0 and 20% of K562 tumor cells, compared to the CD3ζ-only CAR, which killed approximately 75% of tumor cells at each timepoint (Fig. 2.5C to E). This was significant compared to the cytotoxic capabilities of all other CAR T cells (FDR < 0.0001, Fig. 2.5E). Combined with the proliferation, exhaustion, and differentiation data, this supports the hypothesis that KLRG1 significantly dampens the CD3ζ domain's function within a CAR T cell.

2.9 Transcriptional reporters indicate differences in early signaling dynamics among the signaling domains.

Although most of our analyses indicated distinctions in CAR T cell phenotypes after prolonged periods of stimulation in vitro, we sought to determine if there were early differences in signaling upon the initial activation of each CAR that could help to understand the mechanisms behind these phenotypic differences. We transduced each of the CARs into three reporter Jurkat T cell systems that individually measured the transcriptional activity of activator protein 1 (AP-1), nuclear factor

of activated T cells (NFAT), and nuclear factor kappa B (NFκB)(52). We then co-cultured these purified CAR-positive Jurkat reporters with CD19+ or CD19- K562 cancer cells for 8, 24, or 48 hours and measured their activity using flow cytometry (Fig. 2.5F, fig. 2.12F and G). We observed differences in basal and antigen-responsive transcription factor (TF) activity across the CARs, particularly in NFκB activity. Cells expressing BAFF-R, TACI, and CD30 CARs showed both accelerated dynamics and a higher total percentage of cells with NFκB activity (Fig. 2.5F), a TF that is closely associated with TNF receptor signaling (53, 54). These three CARs also upregulate AP-1 activity within the first 8 hours, two-fold more rapidly than any other costimulatory domain, whereas CD28 and 4-1BB CAR T cells expressed higher AP-1 without any antigen-based stimulation (fig. 2.12F). In addition to increased AP-1 signaling, NFAT reporter induction was more rapid and sustained in BAFF-R and TACI (fig. 2.12G). As expected, KLRG1 CAR T cells had reduced activity for all three TF reporters as compared to CD3ζ-only CAR T and untransduced T cells. Lastly, we also saw reduced basal AP-1 activity from CD40, which correlates with its lack of tonic signaling (fig. 2.12F). We did not include CD30 in any further analyses due to its high degree of tonic signaling and exhaustion marker expression in the arrayed in vitro experiments.

2.10 Single-cell RNA-seq and CITE-seq characterize functional differences between CAR costimulatory domains.

The marked differences between the CARs in the transcriptional reporter assay suggested that a deep and unbiased look into early transcriptomic signatures could explain their long-term functional differences in cytotoxicity, proliferation, and exhaustion which we observed throughout our repetitive stimulation co-culture. Previous studies have used single-cell RNA sequencing (scRNA-seq) to compare CARs containing CD28 and 4-1BB domains, identifying differences in signaling, metabolism, and differentiation (55). To achieve a comprehensive understanding of the

phenotypic landscape of CAR T cells incorporating these new signaling domains, we evaluated single cell RNA expression and employed a cellular indexing of transcriptomes and epitopes by Sequencing (CITE-seq) antibody panel of 75 proteins (56) in order to map the unbiased transcriptome measurements onto well-studied T cell surface markers. We separately transduced each CAR, except for CD30, into bulk CD3 T cells from two peripheral blood mononuclear cell (PBMC) donors and performed 10x Chromium 3' v3 scRNA-seq after two days in culture, either with or without stimulation provided by irradiated CD19+ K562s. (Fig. 2.6A).

We used a weighted-nearest neighbor graph-based clustering approach to combine both the CITE-seq and scRNA-seq data across 79,892 cells, followed by uniform manifold approximation and projection (UMAP) dimensionality reduction(57). This combined protein and RNA embedding separated the cells into well-defined CD4 and CD8 lobes (left and right), with resting cells at the outer edges and stimulated CD4 and CD8 cells in the center bottom, in distinct but adjacent regions (Fig. 2.6A, fig. 2.13A), suggesting that CD4 and CD8 CAR T cells converge towards a more similar activated phenotype after CAR stimulation. Additionally, although the cells were grouped into 8 CD4 clusters and 9 CD8 clusters (Fig. 2.6A and B), we noticed a pronounced mirroring of transcriptional programs across 5 pairs of clusters between CD4 T cells and CD8 T cells (Naive/CD62L, Memory, Cytotoxic, OXPHOS, and Glycolytic), and thus describe these clusters with matching labels (fig. S6B). Resting CAR T cells were found almost entirely in naive-like (Naive/CD62L and Naive/CD7) and memory clusters, whereas stimulated cells fell into three main clusters with differing cytotoxic and metabolic transcriptional and surface protein signatures (discussed below), as well as a few other clusters with phenotypes in between naive-like and fully activated (Fig. 2.6A to C, fig. 2.13C).

2.11 Activated CAR T cells fall into 3 distinct clusters shared between CD4 and CD8 T cells.

In both CD4 and CD8 T cells, activated CAR T cells segregated into 3 distinct clusters we named Glycolytic, OXPHOS, and Cytotoxic, which differ in the transcription of several important metabolic genes and signaling pathways (Fig. 2.6B to D, fig. 2.13D). Cells in the Glycolytic cluster differentially upregulated transcription of genes involved in aerobic glycolysis (ARG2, PGK1, LDHA), the hypoxia inducible factor 1 subunit alpha (HIF1a) pathway (SLC2A3, ENO1, ALDOC), mitochondrial autophagy (BNIP3), protein markers involved in costimulation and T cell activation (IL2RA, CD69), and inhibitory receptors (PD1, CTLA4) (Fig. 2.6B and D, fig. 2.13E). Cells in the OXPHOS cluster upregulated genes involved in oxidative phosphorylation and arginine metabolism (SRM, C1QBP, ATP5MC3, MT-CO3), as well as the Myc, MTOR, and PI3K pathways (Fig. 2.6D). The third activated cluster, which we named Cytotoxic, had a strong inflammatory transcription signature, including high IFNG expression and expression of multiple granzymes and cytotoxic molecules including GZMB, GZMK, GZMH, NKG7, and PRF1. The Cytotoxic cluster was also enriched for transcripts associated with NFκB signaling, including BIRC3. Both CD4 and CD8 Cytotoxic cells also abundantly expressed both RNA and protein for major histocompatibility complex (MHC) class II and CD74, an MHC class II chaperone, as well as RNA and protein for a variety of integrins and chemokine receptors including ITGB2 (CD29), ITGA2 (CD49b), ITGA4 (CD49d), CXCR3, and CCR5. The Cytotoxic cluster was more like Glycolytic than OXPHOS but shows distinct and overall lower expression of various inhibitory and activation protein markers, including IL2RA, OX40, 4-1BB, PD1, and glucocorticoid-induced TNFR-related protein (GITR); the Cytotoxic cluster also exhibited high expression of memory markers, including CD95 and CD45RO (Fig. 2.6C).

Having identified a variety of activation states and transcriptional signatures across CAR clusters, we next sought to identify those which were preferentially promoted by specific costimulatory domains (Fig. 2.6E, fig. 2.13A,C, and E). Although all 5 costimulatory domains were present in the three most activated clusters, CAR T cells that contained the CD28 and 4-1BB costimulatory domain were enriched in the CD4 and CD8 Glycolytic and OXPHOS clusters, whereas the BAFF-R CAR T cells were particularly enriched in the Cytotoxic clusters. BAFF-R was also the most enriched CAR in the Memory cluster after stimulation, which indicated that a larger proportion of CAR T cells containing this domain remained in a less activated and less differentiated state after CAR stimulation. This divergence in BAFF-R versus CD28 and 4-1BB enrichment was observed in both donors (fig. 2.13E).

2.12 The cytotoxic cluster matches signatures of improved clinical response and CAR engraftment.

Neither mouse xenografts nor in vitro assays can fully recapitulate human in vivo biology and predict clinical outcomes of adoptive cellular therapies, but the unbiased and high-dimensional data acquired from single cell sequencing offers an opportunity to identify transcriptional signatures that correlate with positive clinical outcomes in patients. We found that the Cytotoxic cluster closely matches gene signatures associated with tumor infiltrating lymphocyte (TIL) and CAR efficacy identified in two recent studies. A study of clonal kinetics in patients undergoing CAR T immunotherapy identified a gene signature enriched in CAR T clones that preferentially expanded (IRF, increased relative frequency) in patients 1 to 2 weeks after infusion(28). We found that this IRF gene signature showed a distinct and significant overlap with gene expression in the CD4 and CD8 Cytotoxic clusters ($p = 1x10\text{-}9$), and that the BAFF-R CAR was enriched for this CAR expansion signature (Fig. 2.6F). A second set of studies by Nicolet and colleagues identified

a T cell transcriptional signature that resulted in enhanced IFN-γ secretion and increased survival in patients with melanoma (29, 58). Their studies associated this cytotoxic gene signature with the integrin CD29. In the Cytotoxic cluster, particularly in BAFF-R CAR T cells, we see an overlap with this CD29 gene signature (Fig. 2.6F). We additionally see within both the Cytotoxic cluster and the BAFF-R CAR T cells an upregulation in RNA and protein expression of both CD29 and CD49d, which together form the heterodimeric VLA-2 integrin complex that is associated with more potent effector memory T cell responses (fig. 2.13D and F) (59, 60).

In addition to the increased expression of MHC genes and integrins, the Cytotoxic and Memory clusters also transcribed several receptors more typical of NK cells, including KLRB1, which encodes CD161. CD161 is expressed by a subset of T cells with characteristic tissue homing(61) and increased cytotoxicity (62), and recent work has shown that CD8+CD161+ T cells define a potent effector memory subset with enhanced CAR T cell efficacy (63). To explore this further, we turned to a recent study which identified a continuous gene expression gradient of lymphocyte innateness from T cells to NK cells(64). This innate lymphocyte gene expression program largely overlapped with the transcripts enriched in our Cytotoxicity and Memory clusters, transcripts enriched in the activated BAFF-R CAR T cells, and the clinical CAR T cell engraftment and CD29 and IFN-γ transcriptional signatures we identified from recent literature (fig. 2.13G). The unexpected overlap among these disparate data suggested a linkage between innate-like gene expression and beneficial cytotoxic CAR phenotypes. Overall, we showed that the CAR signaling domains we identified using CAR Pooling promote altered T cell states, including ones associated with beneficial anti-tumor responses.

2.13 BAFF-R CAR T cells demonstrate enhanced in vivo efficacy.

To validate our observations in vivo, we tested the CAR T cells in two established tumor models known for their persistence and resistance to treatment. The first was an established epithelioid mesothelioma solid tumor model (M28), which is known to produce durable tumors that require CAR T cell persistence rather than rapid initial proliferation(52). We exogenously expressed CD19 on M28 cells and sorted for cells with CD19 expression comparable to K562 cells utilized in screening experiments. We injected NOD-scid IL2Rgammanull (NSG) mice with 4x106 M28 cells and 7 days later treated them with 6x106 anti-CD19 CAR T cells. The TRAC locus of the CAR T cells was knocked-out using CRISPR to reduce potential graft-versus-host disease (GVHD) due to the long-term timescale of these experiments. To compare the rejection dynamics and ensure CARs targeting the exogenous CD19 antigen were similar to the previously established CARs targeting the endogenous ALPPL2 antigen, we set up a side-by-side in vivo experiment utilizing either anti-ALPPL2 4-1BB or anti-CD19 4-1BB CAR treatments. We saw no differences in tumor growth or rejection dynamics between CAR T cell treatments targeting the two antigens (fig. 2.14A and B).

Having confirmed similar tumor rejection between CAR T cells targeting the engineered and natural ligands, we compared the different CAR costimulatory domains head-to-head in the M28 CD19 model (Fig. 2.7A). We were unable to distinguish a difference between —4-1BB and CD28 CAR T cells at the time points shown here, despite the large amount of evidence from human studies that 4-1BB has increased long-term killing and persistence. Both 4-1BB and CD28, as well as the TACI and BAFF-R CAR treatments, exhibited similar tumor clearance and remission over 50 days. Additionally, CD40 demonstrated markedly diminished in vivo efficacy as compared to

4-1BB, CD28, TACI, and BAFF-R. This is likely related to CD40's moderate in vitro cytokine production and cytotoxicity (Fig. 2.5B to E). Lastly, CAR T cells expressing KLRG1 mirrored the results from the in vitro cytotoxicity assay and showed markedly increased tumor burden compared to all other CAR T cells, including the CD3ζ-only CAR, while showing modest efficacy compared to untransduced T cells (Fig. 2.7B). The in vivo M28 data included are representative of 5 repeated experiments in two human donors (fig. 2.14C).

We also assessed CAR T activity in a multiple myeloma tumor model (MM1S) at a low "stress test" T cell dose. Multiple myeloma is a slow, incurable disease in which relapse is often a central clinical challenge. CAR T cells targeting BCMA are proving to be a transformative treatment against multiple myeloma (27). These primarily use 4-1BB costimulation, and although there have been substantial responses in patients treated with these CAR T cells, frequent relapse remains an issue (27). Thus, we engineered a clinical benchmark anti-BCMA 4-1BB CAR and replaced the costimulatory domain with the BAFF-R intracellular domain to determine if it could improve in vivo efficacy. We integrated the CAR into the TRAC locus using ssDNA non-viral integration (65) and injected 2x105 CAR T cells intravenously into mice that received 0.5 to 1x106 MM1S cells 21 days prior (0.5x106 for Donor 1 and 1x106 for Donor 2) (fig. 2.14D). We then measured tumors using bioluminescence for over 30 days. In data from two independent donors, the anti-BCMA BAFF-R CAR showed significantly improved control of MM1S cancer compared to 4-1BB ($p = 0.017$; t-test based on the normalized total cancer radiance AUC) (Fig. 2.7C). Anti-BCMA BAFF-R CAR T cell treatment significantly enhanced mouse survival over 100 days compared to the 4-1BB CAR 100 days post tumor cell injection (Mantel Cox test, $p<0.05$; Fig. 2.7D). Little variation was found in survival curves for a second human donor (fig. 2.14E).

Swapping the costimulatory domain from 4-1BB to CD28 resulted in no enhancement of cancer control or survival (fig. 2.14E and F). Collectively, we show that BAFF-R-based CARs exhibit promise for clinical indications, as they show enhanced survival and tumor clearance in a mouse model of multiple myeloma and most closely phenocopy a transcriptional signature for enhanced T cell fitness and persistence that was independently identified within two human patient studies.

2.14 Discussion

Costimulation is essential for long-term T cell proliferation, differentiation, survival, and is known to enhance CAR T cell efficacy. A wide variety of known signaling domains beyond the canonical T cell costimulatory domains 4-1BB and CD28, have yet to be tested in CARs, and the extent to which signaling domains from other cell types can act upon T cells is poorly understood. Here, we identified several novel CAR signaling domains through pooled library screens in primary human T cells that enhance persistence or cytotoxicity over those used in the current generation of FDA-approved CARs. By screening 40 domains, we show the breadth of the signaling landscape within primary human CAR T cells. We observed that many of the most potent costimulatory domains measured belong to the TNF receptor family, which includes 4-1BB. 4-1BB signaling is known to increase T cell persistence and late stage proliferation relative to CD28*(7)*, and our screen shows that this property extends to several other members of the TNF receptor family, especially CD40 and BAFF-R. Based on the results of our pooled screens, we selected CARs containing 4 new costimulatory domains from the TNF receptor family, as well as a novel inhibitory CAR, and performed comprehensive characterization of their proliferation, persistence, differentiation, exhaustion, cytokine production, and cytotoxicity *in vitro* over several weeks of repetitive antigen stimulations. Characterizing these domains separately in CD4s and CD8s allowed us to identify

effects specific to each cell type. We found that the BAFF-R and TACI signaling domains had heightened cytotoxicity, CD40 had heightened persistence in CD4s, and KLRG1 can dampen ITAM-based signaling, preventing many hallmark features of T cell activation and differentiation.

To identify differences in gene expression elicited by our curated set of costimulatory domains, we explored each CAR's transcriptomic profile and surface protein expression via scRNAseq and CITE-Seq both before and after antigen exposure. We observed significant differences in gene and protein expression between the CARs, based on their representation in clusters mapped to states of differentiation, activation, cytotoxicity, and metabolism, and also observed a distinctive mirroring of these clusters across the CD4-CD8 axis. Activated CAR T cells fell into three clusters which differed in their expression of key metabolic and cytotoxic genes. We named these activated clusters Glycolytic, OXPHOS, and Cytotoxic. The Cytotoxic cluster was significantly enriched for CARs containing the BAFF-R costimulatory domain, which also showed strong anti-tumor and proliferative performance in our prior *in vitro* assays. We found significant overlap between this Cytotoxic cluster and gene signatures from several other recent studies of 4-1BB CAR infusion products and TIL efficacy in cancer patients, suggesting that this signature correlates with higher engraftment, persistence, and tumor rejection. Compared to 4-1BB, BAFF-R CAR-T cells are approximately two-fold enriched (3x in CD4s, 1.5x in CD8s) for this gene signature, suggesting that a BAFF-R CAR infusion product would have a much larger fraction of cells in this hyper-effective state, potentially resulting in improved patient outcomes.

Finally, we compared CAR-T performance in two *in vivo* models and found that our prior *in vitro* characterization and scRNAseq/CITE-Seq signature analysis successfully identified CARs with

enhanced *in vivo* anti-tumor activity. In the xenograft model of epithelioid mesothelioma, BAFF-R- and TACI-based CARs demonstrated equivalent tumor clearance to clinical benchmarks containing 4-1BB or CD28. In multiple myeloma, we observed significantly enhanced tumor clearance and mouse survival upon anti-BCMA BAFF-R CAR T cell treatment with low stress-test doses, pointing to the potential for clinical development of BAFF-R-based CARs in multiple myeloma. Given high rates of multiple myeloma relapse due to limited CAR persistence, an expanded set of CAR architectures with enhanced functions could improve clinical outcomes. *(27)*.

Caveats and future improvements to CAR Pooling - arrayed validation, in vivo screening, going beyond 'screening for hits'

Although 'CAR Pooling' allows us to compare large numbers of signaling domains directly and efficientlys, discrepancies can arise between the performance of domains in a pooled versus an arrayed setting. For instance, we observed robust long-term expansion of CD30 in the pooled screens but more rapid exhaustion and tonic signaling in the follow-up arrayed screen. We additionally observed high IL2 production with TACI CARs within the pooled screens but more moderate IL2 production within the follow-up arrayed screen. This could be due to the more diverse set of paracrine signals and cytokines produced by neighboring CAR T cells in the pooled screens. Subsequent arrayed testing of CARs can thus be critical to rule out complex paracrine effects from a mixed cellular pool. We also observed differences between *in vitro* and *in vivo* performance, such as the lack of *in vivo* anti-tumor efficacy for CD40. To address such discrepancies, future CAR Pooling assays could also be performed directly *in vivo.* Measurements

associated with cytotoxicity (cytokine production, granzymes, or CD107a) could also be performed *ex vivo* after intratumoral expansion of the library.

Although we are primarily concerned here with identifying improved costimulatory domains, it is important to note that the novel KLRG1 CAR is not simply a negative control but a potential tool to control CAR activity, and could be useful for reducing cytokine release syndrome, abrogating on-target off-tumor activation, and even generating post-translational oscillations in CAR activity that would mimic natural TCR signaling dynamics. Pooled screens can thus be employed not simply to find the optimal costimulatory domain 'hits', but rather as a discovery tool to understand how different receptor signals alter T cell biology and how these signals can be modulated to manipulate T cell function beyond optimizing a single chimeric antigen receptor.

CAR Pooling combined with rapid design and synthesis of altered or non-natural synthetic signaling domains – a potential path to access new CAR T cell biology

Much of the existing literature tends to compare CARs one-dimensionally as more or less effective overall, while we instead observed that individual CARs often excelled within specific assays or when expressed in different T cell types. This multidimensionality of costimulation was somewhat unexpected, reinforcing that what is usually referred to as a monolithic 'signal 2' is instead a variety of heterogeneous pathways, sometimes in opposition, which have the potential to be individually tuned to optimize different aspects of T cell function. This also suggests that future engineering could isolate individual signaling motifs to enhance specific T cell phenotypes and create synthetic combinatorial domains which are optimized for specific scFvs, tumor types, or to

better combat the functional deficiencies seen in CARs for solid tumors. Finally, in addition to engineering better therapeutics, future high-throughput studies will help to elucidate the 'design rules' for synthetic receptors and signaling motifs, generate powerful new tools to manipulate T cells for basic immunology research, and lead us to a greater understanding of T cell differentiation, development, and immune-related disease.

2.16 Materials and Methods

Study design

The aim of this study was to develop a new multiplexed system for comparing many genetic CAR architectures, and to identify and characterize new costimulatory domains for improving CAR efficacy during a repetitive/chronic antigen challenge. We started by generating a library of second-generation CAR-Ts using 40 different signaling domains. This library was measured using several parallel multiplexed screens in a repetitive *in vitro* stimulation model. For the pooled screens, two or three donors were used, and CD4 and CD8 cells were transduced separately for each. Measurements were removed for an individual construct/replicate if fewer than 500 cells were sorted for that construct. Seven of these domains were chosen, and two separate donors were used to validate and further characterize them. All donor PBMCs were collected from healthy donors. For all *in vivo* experiments, mice were assigned to treatments randomly and the researchers were blinded until after data collection.

Library Construction

Costimulatory intracellular domains (ICDs) were synthesized by Integrated DNA Technologies, amplified, and individually cloned of the C-terminal portion of a CAR construct (CD3z-2A-GFP) and sequence-verified. Each domain was mini-prepped separately and pooled at 1:1 molar ratio. A fragment containing an SFFV promoter and N-terminal portion of the CAR up until the costimulatory domain was inserted in front of the pooled ICD plasmid library using Golden Gate Assembly and electroporation. This was then digested and inserted via restriction cloning and electroporation into a pHR-SIN lentiviral backbone. We ensured at least 1000x coverage at each electroporation step.

Lentivirus Production/Concentration and Cell Lines

To produce lentivirus, Lenti-X 293T cells (Takara Bio) were transfected with a transgene expression vector and the viral packaging plasmids pCMVdR8.91 and pMD2.G using TransIT-Lenti Transfection Reagent (Mirus Bio LLC). K562 tumor cells were originally obtained from American Type Culture Collection (ATCC), CCL-243. M28 tumor cells were originally obtained from B. Gerwin's laboratory at the National Cancer Institute. Both M28 and K562 cell lines were transduced to exogenously express CD19 using lentiviral transduction and flow cytometry sorting to obtain a pure population with CD19 expression within a one log maximum width. Lentiviral concentration was performed 72 hours after Lenti-X 293T cell transfection through collection and filtration of the viral supernatant. Per 20mL of viral supernatant we added 4.58mL 50% PEG 8000 (final concentration 8%) and 2mL of 4M NaCl (final concentration 0.3M) for 6-8 hours. We

pelleted the virus by spinning down cells at 3500rpm for 20 minutes at 4C, decanted, and resuspended the pellet in 200uL PBS. We then snap froze aliquots on dry ice for storage in a -80C freezer.

In Vitro T cell Production

Blood samples in the form of leukopaks were obtained from healthy male and female volunteers through STEMCELL Technologies. For *in vitro* experiments, T cells were isolated from PBMCs via a CD4 or CD8 negative selection kit and frozen. For *in vivo* experiments, T cells were isolated from PBMCs via a CD3 negative selection kit and frozen. We stimulated the T cells 24 hours after thawing with 25uL of CD3/CD28 beads (Thermo Fisher Dynabeads) per $1x10^6$ T cells (1:1 ratio). Concentrated lentivirus was added 48 hours after thawing to reach a transduction rate of under 15% for the pooled library experiments, between 30-50% for the arrayed screens, and between 65-90% for the *in vivo* experiments (see below for in vivo). Virus was removed within 18 hours of addition and cells were expanded. Five days after thawing, the CD3/CD28 Dynabeads were removed via magnetic separation and cells were sorted for GFP expression at least half a log higher than the negative population and spanning no more than a log in MFI. Cells were plated at $0.5x10^6$ cells/mL and split every three days to this density until 10-14 days after thawing. All references to T cell media indicates usage of X-VIVO 15 + 5% hAb serum + 10mM NAC neutralized with 1N NaOH + 0.5% pen/strep + 1X beta-mercaptoethanol.

Repeat In Vitro Stimulations with K562s

For the pooled experiments, we started stimulation with tumor cells on day 10 and for the arrayed experiments we started stimulation with tumor cells on day 14. To stimulate the T cells we combined them 1:1 with irradiated K562s (see next method) that either expressed or did not express surface human CD19 and plated at a density of $5x10^5$ K562s/mL and $5x10^5$ T cells/mL. Every three days we spun, resuspended, and counted the cultures using flow cytometry to split the T cells and add more irradiated K562s.

We counted the T cells by adding an aliquot of the resuspended culture to CountBright beads and calculating the number of T cells through analysis on the BD X-50 Flow Cytometer and Flowjo. The cultures were restimulated with the addition of a new bolus of irradiated K562s 1:1 to total T cells in each culture. They were replated at the density of $5x10^5$ T cells/mL. This was repeated for a total of 3-33 days.

K562 Irradiation

Live K562 cells (ATCC® CCL-243™) were grown up in T182 flasks until confluent. Cells were resuspended to $10x10^6$/mL on ice and irradiated using a Cesium-137 irradiator for 20 minutes (~200 rad/min) in a 50mL falcon for a total dose of approximately 4,000 Rads. Cells were then aliquoted and frozen in IMDM media containing 10% DMSO and 10% FBS in liquid nitrogen until needed in the protocol.

CellTrace Violet (CTV) dye

T cells were taken from culture, resuspended, and washed with PBS. We resuspended the culture to $1x10^6$ cells/mL of a 5μM solution of CellTrace Violet (CTV) in PBS and incubated at room temperature for twenty minutes in the dark. We then added 5mL of T cell media on top for every $1x10^6$ cells that were stained and incubated another 10 minutes in the dark. Then, cells were pelleted via centrifugation at 500g for 5 minutes and resuspended and plated in T cell media at $1x10^6$ cells/mL. To stimulate proliferation, we plated an equal amount of K562s relative to the total number of T cells in each well, with or without CD19 expression, as described above. We assessed the proliferation 3 days after stimulation for CD4s via flow cytometry. For CD8 T cells, we restimulated T cells with an additional dose of irradiated K562s day 3 after the initial stimulation and stained for flow cytometry on day 4 after the initial stimulation. To determine proliferation after prolonged co-culture, rather than restaining, we kept a proportion of the cells separate in culture and stained on day 9 (CTV2), day 18 (CTV3), or day 27 (CTV4) post-initial stimulation. Therefore all CTV stained populations were seeing the CTV dye for the first time. We assayed proliferation on day 16 (CTV2), day 24 (CTV3), or day 33 (CTV4) via flow cytometry.

CD69 Activation Staining

To determine the degree of activation of each CAR we stimulated antigen-naive T cells with irradiated K562s, either with or without CD19 expression, in a 1:1 ratio. 24 hours after we plated the co-culture we centrifuged the cells at 500g for 5 minutes, washed twice into flow buffer (PBS + 2% FBS), and stained with anti CD69 antibodies at 4°C for 20 minutes. We washed the cells twice with flow buffer (PBS + 2% FBS) and ran on a flow cytometer.

Cytokine Staining

To determine the degree of cytokine production upon activation of each CAR, we stimulated antigen-naive T cells with irradiated K562s, either with or without CD19 expression, in a 1:1 ratio. 3 days after, we replated the co-culture with a secondary bolus of K562s (see the above method). We then added 2x Brefeldin A 12 hours later for an additional 6 hours. We centrifuged the cells at 500g for 5 minutes, washed twice into flow buffer (PBS + 2% FBS), stained with anti-CD4 or -CD8 antibodies at 4C for 20 minutes. We washed the cells twice with flow buffer and added 100uL of fixative (50uL of flow buffer + 50 uL of Invitrogen IC fix) to each well. We incubated at room temperature for 1 hour in the dark. After fixation we spun the cells at 600g for 5 minutes and resuspended in Cytolast for continued staining the next day. To permeabilize the cells we added 200uL of 1x Permeabilization buffer to each well, immediately spun at 600g for 5 minutes, and stained for intracellular antigens with anti-IL-2, -TNFα, and -IFNγ antibodies diluted in perm buffer. We stained in 50uL at room temperature for 30 minutes in the dark. We then washed twice with Permeabilization buffer and ran it on a flow cytometer.

Incucyte Killing Assays

50 µL 5 µg/mL of fibronectin was dispensed to each utilized well of a 96-well plate. Plate was incubated for 60 minutes at room temperature, and fibronectin was removed, followed by another 60 minute incubation at room temperature. Both CAR T cells and live K562 target cells (either expressing mKate and CD19 or only mKate) were spun down and resuspend in Jurkat media + 30 U/mL IL-2; Jurkat media (RPMI-1640 medium + 10% FBS + 1% PenStrep + 1X Glutamax) has less fluorescence than media based on X-VIVO-15. Cells were counted and diluted to $2.5x10^5$/mL each, and 100 µL of each (T cell and Targets) was added to each well for a final assay volume of

200 µL. Each condition was done in duplicate so long as sufficient cells were available. We allowed plates to settle at room temperature for 30 minutes before beginning the incucyte assay. Images were taken every 60 minutes using the Incucyte software over the course of the experiments (see relevant Figures for total assay times, which varied between conditions).

DNA Extraction/Sequencing

After fluorescence activated cell sorting assays, after in vitro growth with target cells, or after transduction as a library abundance baseline measure, T cells containing the CAR library were spun down into pellets, supernatant removed, and frozen at -80°C. Subsequently, genomic DNA was prepared from cells using either the Machery-Nagel Nucleospin Tissue XS column, Machery-Nagel Nucleospin column, or the Nucleospin 96 Tissue extraction plate. Manufacturer protocols were followed except for the addition of 10 µg polyadenylated RNA to each sample to increase yield.

After gDNA prep, Picogreen and a plate-based fluorescence reader were used to quantify the extracted genomic DNA. Initial PCR amplification of the costimulatory domain region from the different samples (PCR1) were done in 3 batches with differing numbers of cycles (12, 16 or 22 cycles) depending on the genomic DNA concentration. PCRs were performed with Takara ExTAQ to allow for maximum template concentration to be used in the PCR reaction. Reactions were done in 70 µL with between 200 and 1000 ng of DNA used as template depending on the batch as described above.

For the subsequent PCR to add Illumina barcodes and adapters to the products (PCR2), all products from PCR1 were diluted 15x and 25 μL of template was used in a 50 μL reaction with Takara ExTAQ. Different forward and reverse primers were used for each sample for PCR2 to add unique custom Illumina I5 and I7 barcode sequences to each sample.

Finally, PCR2 products were again quantified using Picogreen in a plate-based fluorescence reader. These products were pooled at 1:1 molar ratio, diluted, loaded, and run on a MiniSeq 2x150 cycle cartridge using the standard manufacturer protocols.

Sequencing Analysis

After demultiplexing, CAR costimulatory domain sequences in FASTQ format for each sample were adapter-trimmed, sorted, deduplicated, and aligned using custom python scripts and BWA-mem. These alignments were then converted into count tables and analyzed using DESeq2 and custom R scripts (https://github.com/dbgoodman/tcsl-lenti).

Statistical methods for Fig 3A heatmap

Each metric along the Y axis of Figure 3A was converted into a set of z-scores within each donor, replicate, and T cell subset and checked for adherence to normality via Anderson-Darling and visually using Q-Q plots. Z-scores were then combined across donors and replicates using Stouffer's method and then a one-sample *z*-test was performed on each domain and FDR-corrected using the Benjamini-Hochberg procedure. All relevant code is available in our GitHub repository, (https://github.com/dbgoodman/tcsl-lenti).

Calculations for In Vitro Cumulative Expansion Over Repeat Stimulation

Each culture of CAR T cells was produced as described above in "*In Vitro* T cell Production." T cells were then stimulated 1:1 with irradiated K562 cells as described and counted every three days using CountBright beads at a ratio of 1:20 in volume of beads to cells. This mixture was then run on an X-50 Fortessa and analyzed for the number of CAR positive T cells in culture (analyzed using the T2A-GFP).

M28 In Vivo Injections

Four days prior to tumor injection, M28 CD19+ tumor cells (generation explained above) were split and $0.75x10^6$ cells were plated in one T182 flask for every 2.5 mice for propogation. On day 0, we tripsonized M28 CD19+ cells, counted and resuspended them in RPMI at $40x10^6$ cells/mL. We injected NOD-*scid* IL2Rgamma^{null} (NSG) mice with $4x10^6$ M28 cells subcutaneously on the right flank and measured the initial tumor growth via caliper 6 days later. On the 10th day after thawing the T cells (following the protocol for T cell production above), and a total of 7 days after we tumor injection, we injected $6x10^6$ GFP positive anti-CD19 CAR T cells via tail vein. Tumors were measured via caliper every 3-7 days for a total of 30-50 days.

In vivo T cell production: ALPPL2 vs CD19

Using PBMCs from either leukopaks or TRIMA residuals, T cells were isolated via a CD3 negative selection kit and frozen. We then produced T cells as described above using 30uL concentrated

virus per 1x10^6 T cells to reach a transduction rate between 65-90% as assessed by flow cytometry. T cells were injected as described above within the M28 In Vivo Injections section.

In vivo T cell production: M28 TRAC-KO

The following describes the T cell production utilized when knocking out the TRAC locus for TCR downregulation and prolonged in vivo timelines. We stimulated bulk CD3+ T cells isolated from human PBMCs 4 hours after thawing with 25uL of CD3/CD28 beads (Thermo Fisher Dynabeads) per 1x10^6 T cells (1:1 ratio). 24 hours after stimulation, concentrated lentivirus was added to the T cells at 30uL per 1x10^6 T cells. 48 hours after stimulation, the lentivirus was washed off and Dynabeads were removed via magnetic separation. Cells were replated at 1x10^6 cells/mL. After an additional 24 hours we electroporated Cas9 and guide RNP to knock out the TRAC locus with approximately 98-99% efficiency as assessed via flow cytometry. Cells were plated at 1x10^6 cells/mL and split every three days to this density until 10 days after thawing.

MM1S In Vivo Tumor Injections

We used 8- to 12-week-old NOD.Cg-Prkdc^{scid}Il2rg^{tm1Wjl}/SzJ (NSG) (RRID:IMSR_JAX:005557) male mice (in-house breeding), under a protocol approved by the UCSF Institutional Animal Care and Use Committee. Mice were inoculated with 0.5x10^6-1x10^6 MM1S-luciferase$^+$ cells by tail vein injection (0.5x10^6 for donor 1, 1x10^6 for donor 2). Three weeks after, mice were randomized post BLI tumor radiance measurements and 200,000 BCMA targeting CAR T cells were injected. Bioluminsence was measured with the Xenogen IVIS Imaging System (Xenogen) ~10-12 minutes after injecting 200uL of luciferin IP and analyzed utilizing the Living Image software.

In vivo T cell production: MM1S TRAC Knockin

Long single-stranded DNA was manufactured at large scale by Genscript Biotech via a proprietary process (PCT/CN2019/128948) exactly as described by the Marson lab*(65)*. Bulk T cells were isolated from PBMCs as described above and stimulated 4 hours later 1:1 with CD3/CD28 Dynabeads. 48 hours after stimulation, Dynabeads were removed via magnetic separation and cells were electroporated with Cas9 and guide RNP to knock out the TRAC locus with approximately 98-99% efficiency as assessed via flow cytometry. Immediately after the electroporation, long ssDNA was added to integrate the CAR into the TRAC locus. Cells were plated at $1x10^6$ cells/mL and split every three days to this density until 10 days after thawing. 200,000 cells were then injected intravenously 21 days after MM1S injection.

scRNAseq: T Cell Purification and Transduction

Experiments for each donor were performed separately on different days. CD3 T cells were purified from PBMCs extracted from either leukopacks or TRIMA residuals, as described in more detail above. CARs were then lentivirally transduced into bulk CD3s, using the same methods as previously described, and five days after transduction, T cells were FACS-sorted based on GFP marker expression based on a range of a one log away from the mean expression across all constructs. Untransduced T cells were not sorted.

scRNAseq: T Cell Stimulation and 10x Prep

Five days after sorting (total of 10 days after transduction), $2x10^6$ cells were plated with either $2x10^6$ irradiated CD19+ K562 cells (described above) or replated in fresh media without K562 cells, at a density of $1x10^6$ T cells/mL, for a total of 18 conditions per T cell donor: 6 second-generation CARs (excluding CD30), a CD3ζ-only CAR, and untransduced T cells, both with and without K562 co-culture. For the second donor, a CD3/CD28 Dynabead-stimulation condition was also performed with untransduced cells, following instructions from the manufacturer. A K562-only control sample was also generated for both donors. After co-culture for 48 hours, cells in each condition were individually counted and stained CD3, DRAQ7, and with unique combinations of two TotalSeq-B hashtag antibodies (Biolegend) following the manufacturer's instructions. After staining, the cells were pooled at approximately equal ratios based on counts taken prior to staining. The pooled cells were then sorted based on FSC/SSC, CD3, GFP, and DRAQ-7-negative gates to remove dead cells and irradiated K562s. Finally, the sorted cells were stained using the BD Bioscience ABseq antibody panel and loaded and processed via the standard Chromium V3 3' sequencing pipeline. Two lanes were loaded per donor at 60,000 cells per lane. Cells were able to be loaded at this high density because doublets could be identified based on HTO barcode collisions between samples. One 200-cycle Novaseq S4 lane of Illumina sequencing was performed per donor (approximately 6e9 reads in total).

scRNAseq: Data Loading and Cleaning

UMI counts were generated using CellRanger v5.0.1 using the standard settings and imported into Seurat v4, R v4.0.4, Rstudio v1.4. Barcode combinations were deconvolved using custom scripts and potential doublets were identified and removed based on barcode collisions

(https://github.com/dbgoodman/tcsl-lenti). CD4 and CD8 cells were identified based on RNA and ADT expression of CD4/CD8, and double-positive cells were removed from consideration. Cells whose UMIs came from mitochondrial genes greater than 25% of the time were removed. A total of 79,892 cells remained after removing potential doublets and cells enriched for mitochondrial RNA.

scRNAseq: Multidonor and Multimodal Data Integration and Clustering

Generation of UMAP embedding on both RNAseq and CITE-Seq data was performed using Seurat v4's SCTransform and FindMultiModalNeighbors functions. Regression was done on cell cycle genes (Seurat's *cc.genes*). Then, FindClusters was used to generate initial clusters with algorithm 3, cluster resolution 1.3. For initial data exploration purposes, this UMAP embedding and clustering procedure was performed separately for activated CD4s, activated CD8s, all CD4s, all CD8s, and finally with all cells (the latter generating the embedding shown in Fig. 2.6A). Initial clusters were identified, then categorized and consolidated into the final clusters in Fig. 2.6A, based on curation of the most differentially expressed genes and proteins, an extensive search of the literature, using the VISION tool, GSEA and mSigDB, and by hierarchical clustering of average gene expression across clusters.

Materials

A table of all reagents with source and catalog number are listed in the Supplementary Information under the heading 'Table of Materials'.

Statistical Analysis

All relevant code used for statistical modeling, summarization, and visualization is available in our GitHub repository, (https://github.com/dbgoodman/tcsl-lenti). In all cases, multiple testing corrections were performed using the Benjamini–Hochberg procedure.

For figures 2C, 3C, 4D, repeated-measures mixed effects linear models were constructed in R using the *nlme* package to assess statistical significance for relative expansion over time across the CAR signaling domains across different donors, time-points, and between CD4 and CD8 subsets, where applicable. Model selection was performed using AIC/BIC and an AR1 correlation structure was chosen. For Figure 2C, CD4 and CD8 subsets were considered separately, while for Figure 3C, they were combined. A similar model was fit to the CD40/CD28/4-1BB arrayed expansion comparison in Figure 4D.

For figures 1E, 4F, 4G, S4F, repeated-measures ANOVA models were constructed in R using the *aov* function to assess statistical significance. Donor and (and CD4/CD8 T cell subsets, where applicable) were used as error strata (e.g. aov(measure ~ car * day + Error(donor)) .

2.17 Figures

Figure 2.1

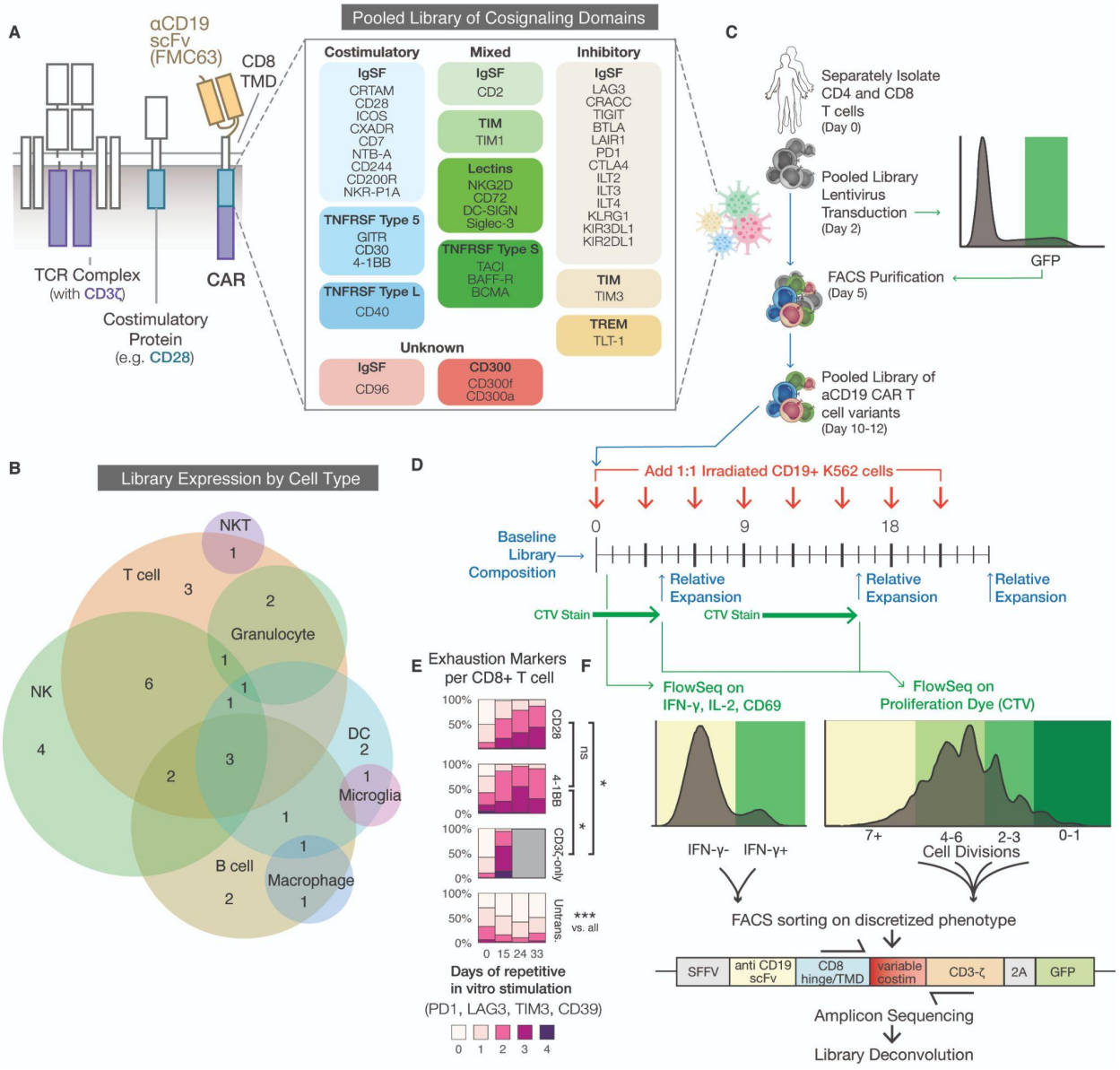

Fig. 2.1. Generation and screening of a pooled library of CARs with diverse signaling domains.

(A) Our CARs combine an αCD19 ScFv (FMC63), a CD8 hinge and transmembrane domain (TMD), an intracellular signaling domain, and a CD3ζ domain (left). Forty domains from across the human proteome were codon-optimized, synthesized, pooled into a plasmid library, and packaged to generate lentivirus (right). These spanned protein families such as immunoglobulin superfamily (IgSF), T cell/transmembrane, immunoglobulin, and mucin (TIM), TNF receptor super family (TNFRSF), and triggering receptors expressed on myeloid cells (TREM). (B) A Venn diagram showing natural expression of library members across immune cell types. Expression patterns are listed in table S1. NK, natural killer cell; NKT, natural killer T cell; DC, dendritic cell. (C) Primary human CD4 and CD8 T cells were separately isolated from PBMCs for two human donors and lentivirally transduced with the library. The cells were FACS purified using T2A-GFP fluorescence within one log of mean expression to reduce variability. (D) The pooled library was repeatedly stimulated 1:1 with CD19+ or CD19- irradiated K562 tumor cells to quantify antigen specific activation (CD69), cytokine production (IFN-γ, IL-2), and proliferation (CTV: CellTrace Violet). The library was also sequenced at the specified timepoints to measure relative expansion of individual constructs. (E) Percentage of CD8+ T cells expressing different numbers of exhaustion markers (PD1, TIM3, LAG3, CD39) after a repeat stimulation assay with CD19+ irradiated K562 tumor cells. T cells expressing CD28, 4-1BB, or CD3ζ-only CARs are compared to untransduced (Untrans.) cells. Grey boxes correspond to timepoints in which no live cells remained. Significance was assessed in CD8 T cells for 2 donors using a Repeated Measures ANOVA model. FDR-corrected $p < 0.05$:*, $p<0.001$:***; ns, not significant. The second donor and data for CD4+ T cells are shown in fig. S1 A and B. (F) We used FlowSeq, a FACS and next generation sequencing (NGS)-based pooled quantification workflow, to quantify enrichment by sorting the library into bins of fluorescent signal corresponding to a functional readout, as shown by the colored histograms. We then amplified the costimulatory domain by genomic DNA extraction and PCR, and performed amplicon sequencing on each bin to estimate the phenotype for each library member.

Figure 2.2

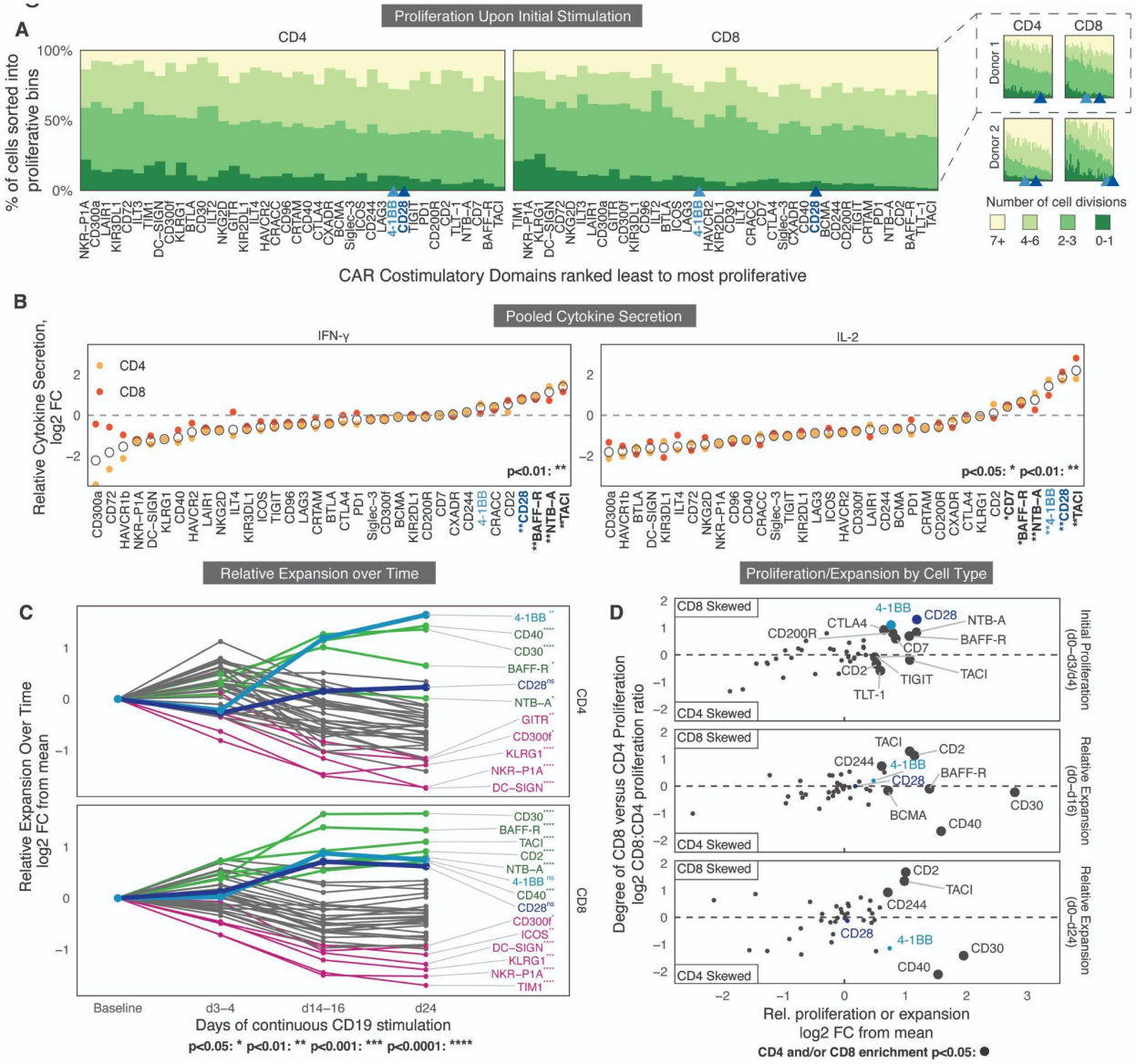
Proliferation Upon Initial Stimulation
A
CD4
CD8
% of cells sorted into proliferative bins
100%
50%
0%
Donor 1
Donor 2
Number of cell divisions
7+
4-6
2-3
0-1
CAR Costimulatory Domains ranked least to most proliferative
B
Pooled Cytokine Secretion
IFN-γ
IL-2
Relative Cytokine Secretion, log2 FC
p<0.01: **
p<0.05: * p<0.01: **
Relative Expansion over Time
Proliferation/Expansion by Cell Type
C
Relative Expansion Over Time log2 FC from mean
Baseline
d3–4
d14–16
d24
Days of continuous CD19 stimulation
p<0.05: * p<0.01: ** p<0.001: *** p<0.0001: ****
D
CD8 Skewed
CD4 Skewed
Degree of CD8 versus CD4 Proliferation log2 CD8:CD4 proliferation ratio
Initial Proliferation (d0–d3/d4)
Relative Expansion (d0–d16)
Relative Expansion (d0–d24)
Rel. proliferation or expansion log2 FC from mean
CD4 and/or CD8 enrichment p<0.05: ●

Fig. 2.2. Comparison of proliferation, expansion, and cytokine secretion identifies differences in costimulatory activity at different time scales and in different T cell types.
(A) FlowSeq measurement of proliferation are shown for CD4 (left) and CD8 (right) T cells containing different signaling domains, separately stimulated in vitro with irradiated CD19+ K562 tumor cells for 3 or 4 days (see Fig. 1D). Percentage of cells with different numbers of divisions were calculated from amplicon sequencing of sorted CTV bins. CARs are ranked from left to right by the average number of cell divisions in CD4 or CD8 cells from lowest (left) to highest (right). 4-1BB and CD28 CARs are highlighted in blue shades. On the right, two donors are shown separately along with 4-1BB and CD28 rank. (B) FlowSeq measurements of intracellular cytokine production are shown for CD4 (yellow) and CD8 (orange) T cells averaged across three independent donors, 18 hours after addition of CD19+ irradiated K562 cells. Mean of each domain is indicated by an open circle. Dashed lines indicate the cytokine production of the average library member, normalized for each donor and T cell subset. Significance was determined using a Wilcoxon rank-sum test. FC, fold-change. (C) Relative expansion over time is shown for CD4 and CD8 T cells, based on the average fold-change in library abundance from baseline before stimulation. Mean of 3 replicates from 2 donors are shown. The 6 domains with the most and least relative expansion are labeled in green and pink, respectively, with CD28 and 4-1BB labeled in blue shades. Significance is based on FDR-corrected p values derived from a linear mixed effects model (see Methods). (D) Comparison of CD4 versus CD8 proliferation and expansion after CD19+ K562 stimulation. Larger dots correspond to constructs that have significantly better performance in either CD4 T cells or CD8 T cells. The x-axis is the mean fold-change across CD4 and CD8 T cells, and the y-axis is the CD8:CD4 expansion ratio. Significance was determined using a Wald test. For all panels, FDR < 0.05:*, < 0.01:**, <0.001:***, <0.0001:****.

Figure 2.3

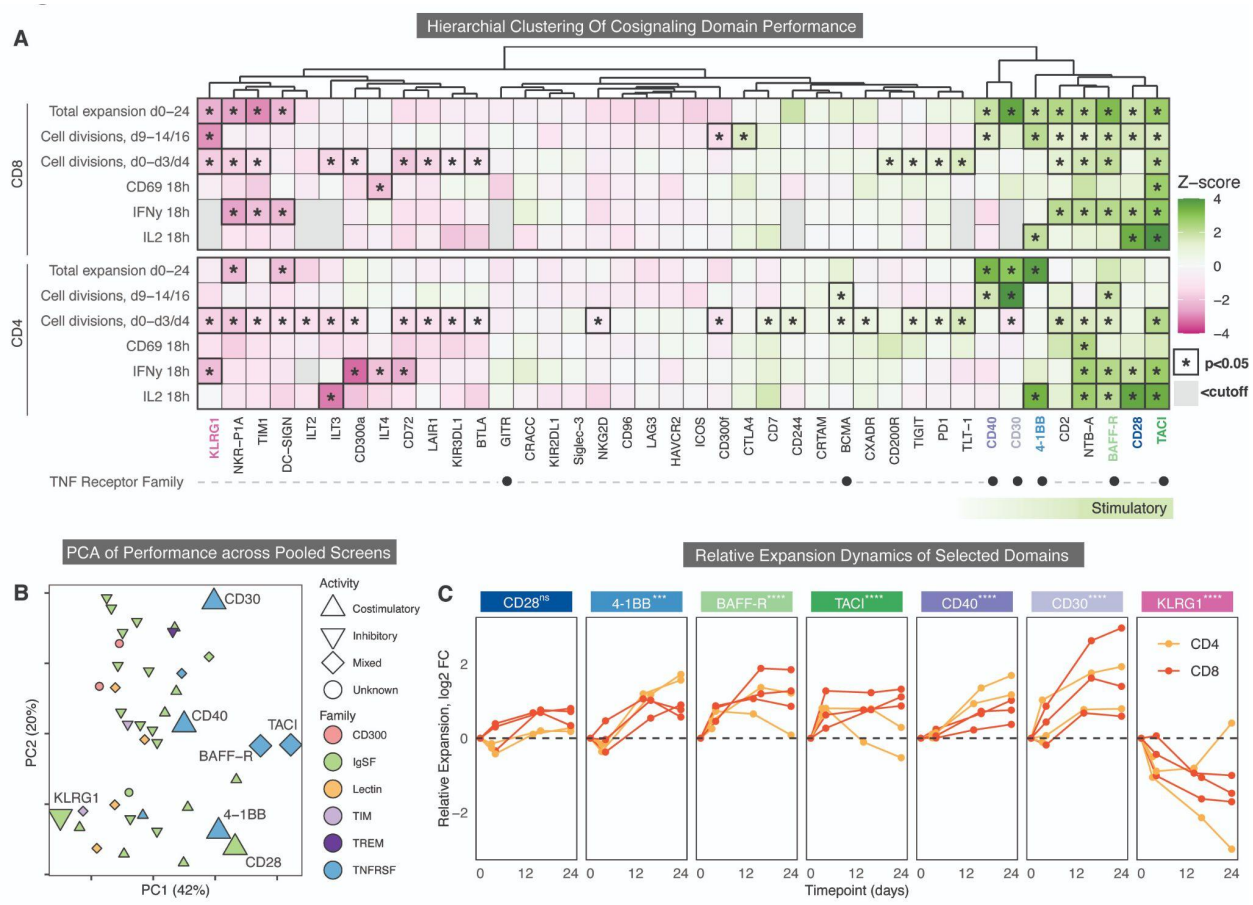

Fig. 2.3. Multidimensional comparison of signaling domains across multiple weeks of chronic antigen stimulation identifies a subset with potent stimulatory activity.

(A) Hierarchical clustering of the CAR signaling domain library in CD4 and CD8 T cells stimulated with CD19+ K562 tumor cells. All 40 domains were clustered based on their z-scores in each assay. 8 stimulatory domains were identified on the right (green bar). Gray boxes are excluded domains where < 500 cells were detected for the assay. TNF receptor family members are marked with black dots. KLRG1 (pink), CD40 (dark purple), CD30 (light purple), 4-1BB (light blue), BAFF-R (light green), CD28 (dark blue), and TACI (dark green) are highlighted. Significance is indicated by a black border and an asterisk(Wilcoxon rank-sum test, FDR < 0.05). (B) Principal components analysis (PCA) of pooled library screen cytokine, proliferation, expansion, and activation data is shown for CD4 T cells, CD8 T cells, CD19+ and CD19- stimulation conditions, and all donors and timepoints. Chosen CARs are larger, with shapes and color indicating known function and protein family. (C) Fold-change of the proportion of selected CARs within the library at each timepoint (x-axis) over 24 days of repeated stimulation with irradiated CD19+ K562 cells as compared to the average CAR in the pooled library. CARs were measured in CD4 and CD8 primary human T cells individually in 2 to 3 biological replicates.

Significant p values were derived from a linear mixed effects model; FDR < 0.05:*, < 0.01:**, <0.001:***, <0.0001:****.

Figure 2.4

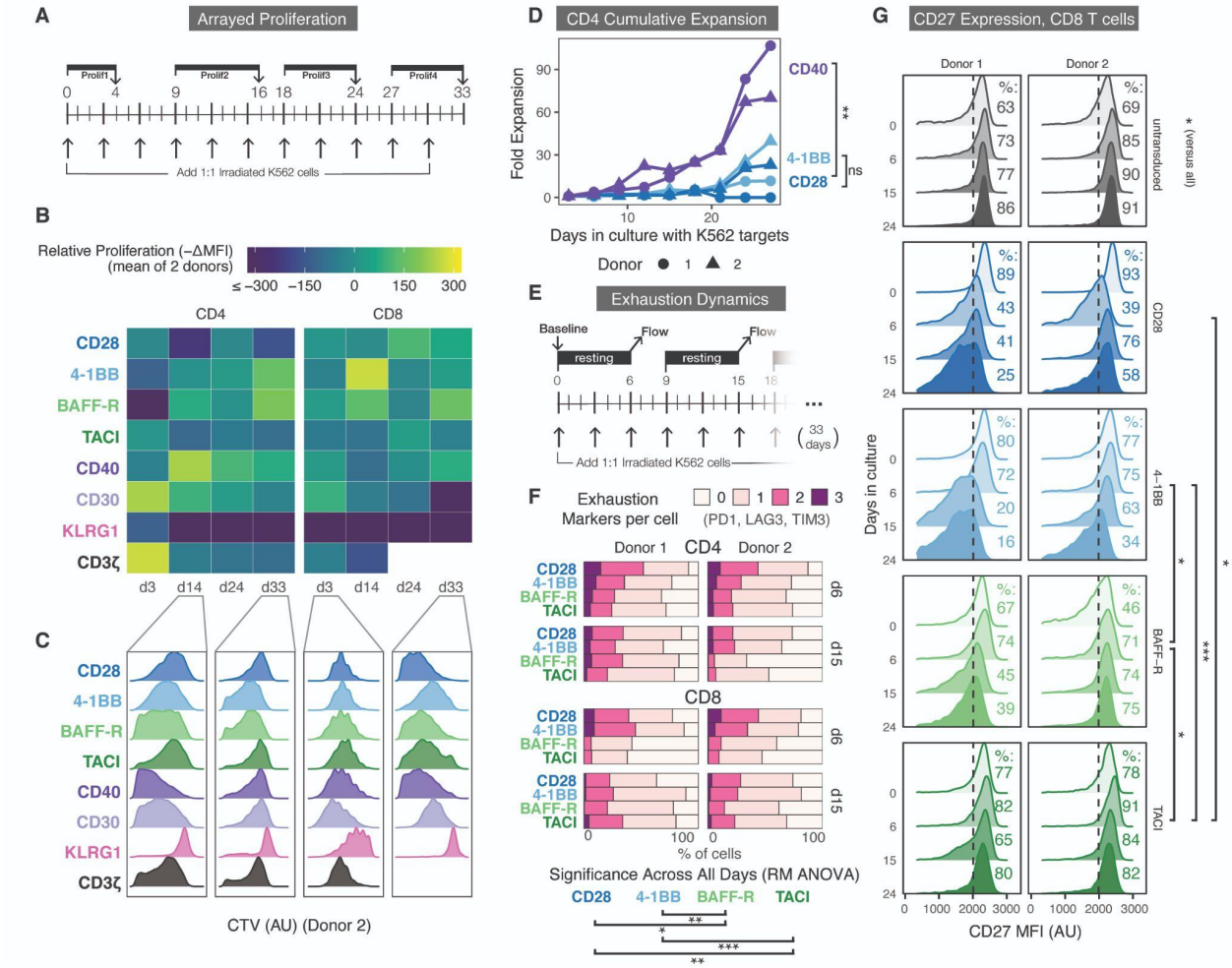

Fig. 2.4. Distinct signaling domains differentially affects proliferation, long-term expansion, markers of memory, and exhaustion.

(A) The timeline for arrayed proliferation assays in (B and C) is shown. Primary human CD4 and CD8 T cells were separately transduced with the 8 CARs in (B and C) and stimulated 1:1 with irradiated CD19+ or CD19- K562 cells every three days. Proliferation was assessed by CTV dilution every 9 days. (B) Relative proliferation of each CAR was quantified by the relative decrease in mean fluorescence intensity (MFI) (i.e. dilution of CTV dye) between two donors of CD4 or CD8 T cells. The color legend ranges from less proliferative (dark blue) to more proliferative (yellow). The x-axis indicates the day the cells were stained. White boxes are representative of CAR T cells that dropped out of culture. (C) Histograms of CTV staining of CD4 or CD8 CAR T cells in a representative donor on selected days are shown. Data summarized in (B). Both donors are shown in fig. S4A and B. AU, arbitrary units. (D) Quantification of the cumulative expansion of CD4 T cells engineered with either CD40 (purple), 4-1BB (light blue), or CD28 (dark blue) CARs and stimulated as described in (A). Co-cultures were measured every three days starting on day 3 by flow cytometry and counting beads. The y-axis measures cumulative fold-expansion every three days. (Significance was derived from a linear mixed effects model, for CD40 comparisons, all $p < .001$). (E) Cells were transduced and stimulated as described in (A). Every 9 days in culture, cells were rested for 6 days without additional stimulation and assessed for surface expression of PD1, LAG3, and TIM3. (F) Percentage of CAR T cells expressing 0 to 3 of the exhaustion markers PD1, TIM3, LAG3 after day 6 and day 15 as described in (E). All CARs, markers, and time points are shown in fig. S4D and E. (G) CD27 surface expression on CD8 CAR T cells was measured over 33 days, as in (E). Percentage of CD27-high cells is shown for each CAR and day on the right. All CARs and time points are shown in fig. S4G. Significance in (F and G) was assessed using a repeated measures (RM) ANOVA model, (FDR < 0.05:*, < 0.01:**, < 0.001:***, < 0.0001:****).

Figure 2.5

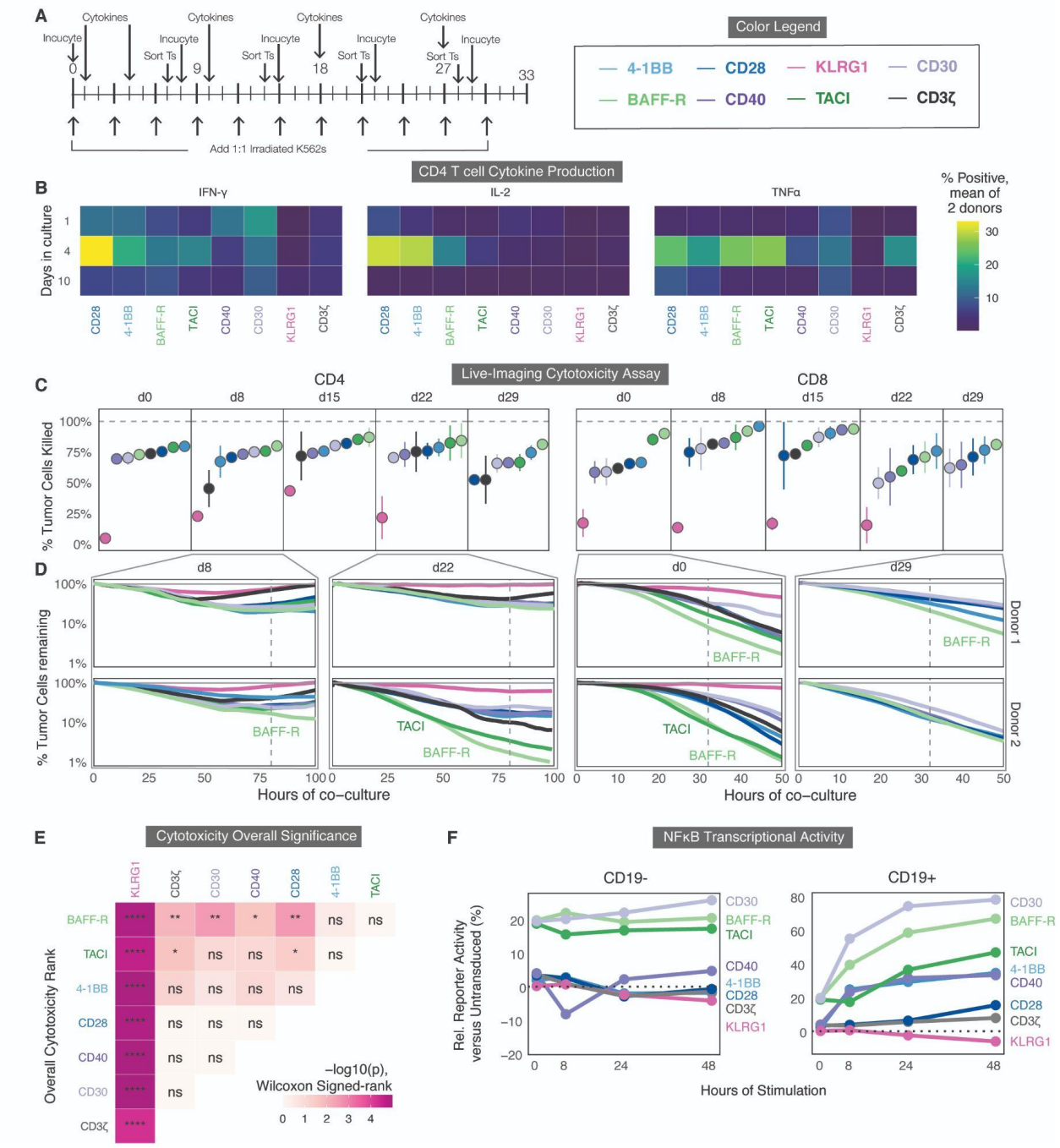
A
Cytokines
Incucyte
Sort Ts
0
9
18
27
33
Add 1:1 Irradiated K562s
Color Legend
4-1BB
CD28
KLRG1
CD30
BAFF-R
CD40
TACI
CD3ζ
B
CD4 T cell Cytokine Production
IFN-γ
IL-2
TNFα
Days in culture
% Positive, mean of 2 donors
C
Live-Imaging Cytotoxicity Assay
CD4
CD8
% Tumor Cells Killed
D
% Tumor Cells remaining
Donor 1
Donor 2
Hours of co−culture
E
Cytotoxicity Overall Significance
Overall Cytotoxicity Rank
−log10(p), Wilcoxon Signed-rank
F
NFκB Transcriptional Activity
CD19-
CD19+
Rel. Reporter Activity versus Untransduced (%)
Hours of Stimulation

Fig. 2.5. Comparison of signaling domains across measures of cytokine secretion, T cell signaling reporters, in vitro cytotoxicity, and in vivo solid tumor clearance.
(A) Timeline for in vitro cytotoxicity and cytokine production assays. CD4 or CD8 T cells were transduced and stimulated as in Fig. 4A. Once weekly, a portion were stained for cytokine production. (panel B). For cytotoxicity assays, a portion of T cells (Ts) were sorted from the same co-culture by FACS, rested overnight, then cultured 1:1 with mKate+ CD19+ K562 cells and imaged every 60 minutes by Incucyte for the next 3 to 5 days (C and D). The color legend is shown on the right. (B) Mean cytokine production by CD4 T cells at 1, 4, and 10 days, measured across two donors by intracellular cytokine staining. Percentage of cytokine-positive cells was averaged between two donors. (C) Cytotoxicity of CD4 or CD8 CAR T cells sorted at the indicated days was quantified at 80 and 32 of co-culture respectively, by calculating the percentage of tumor cells at each time point relative to no T cells. CARs are ranked from least to most cytotoxic for each day. (D) Representative plots of cytotoxicity are shown for two donors' CAR T cells sorted at day 8 and day 22 for CD4 T cells and day 0 and day 29 for CD8 T cells, plotting the percentage of mKate+ tumor cells remaining relative to a well with no T cells (gray). Vertical dashed lines indicate the time points analyzed in (C). (E) Overall significance is shown for the cytotoxicity of CD4 and CD8 T cells from two donors for all days indicated above. Data were analyzed using a Wilcoxon signed-rank test and FDR-corrected; $p<0.05$:*, $p<0.01$:**, $p<0.001$:***, $p<0.0001$:****; ns, not significant. (F) NFκB transcriptional activity was determined using a reporter Jurkat cell line transduced with each CAR and stimulated with either CD19- or CD19+ K562s. Samples were assessed by flow cytometry. The y-axis is relative (Rel.) to untransduced cells.

Figure 2.6

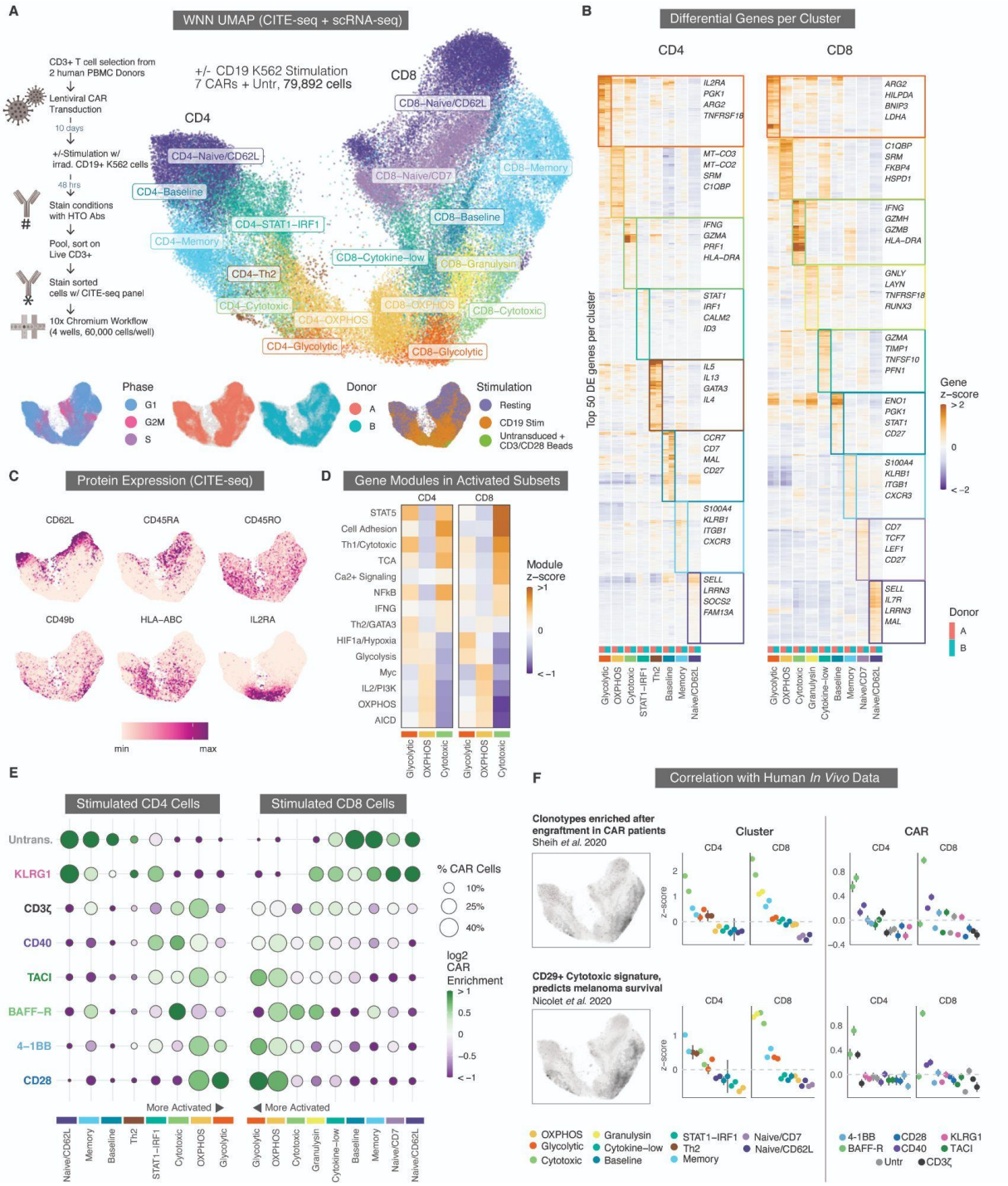
A
WNN UMAP (CITE-seq + scRNA-seq)
CD3+ T cell selection from 2 human PBMC Donors
Lentiviral CAR Transduction
10 days
+/-Stimulation w/ irrad. CD19+ K562 cells
48 hrs
Stain conditions with HTO Abs
Pool, sort on Live CD3+
Stain sorted cells w/ CITE-seq panel
10x Chromium Workflow (4 wells, 60,000 cells/well)
+/- CD19 K562 Stimulation
7 CARs + Untr, 79,892 cells
CD4
CD8
CD4–Naive/CD62L
CD4–Baseline
CD4–STAT1–IRF1
CD4–Memory
CD4–Th2
CD4–Cytotoxic
CD4–OXPHOS
CD4–Glycolytic
CD8–Naive/CD62L
CD8–Naive/CD7
CD8–Memory
CD8–Baseline
CD8–Cytokine–low
CD8–Granulysin
CD8–OXPHOS
CD8–Cytotoxic
CD8–Glycolytic
Phase
G1
G2M
S
Donor
A
B
Stimulation
Resting
CD19 Stim
Untransduced + CD3/CD28 Beads
B
Differential Genes per Cluster
CD4
CD8
Top 50 DE genes per cluster
IL2RA PGK1 ARG2 TNFRSF18
MT–CO3 MT–CO2 SRM C1QBP
IFNG GZMA PRF1 HLA–DRA
STAT1 IRF1 CALM2 ID3
IL5 IL13 GATA3 IL4
CCR7 CD7 MAL CD27
S100A4 KLRB1 ITGB1 CXCR3
SELL LRRN3 SOCS2 FAM13A
ARG2 HILPDA BNIP3 LDHA
C1QBP SRM FKBP4 HSPD1
IFNG GZMH GZMB HLA–DRA
GNLY LAYN TNFRSF18 RUNX3
GZMA TIMP1 TNFSF10 PFN1
ENO1 PGK1 STAT1 CD27
S100A4 KLRB1 ITGB1 CXCR3
CD7 TCF7 LEF1 CD27
SELL IL7R LRRN3 MAL
Gene z–score
>2
0
<–2
Donor
A
B
Glycolytic
OXPHOS
Cytotoxic
STAT1–IRF1
Th2
Baseline
Memory
Naive/CD62L
Granulysin
Cytokine–low
Naive/CD7
C
Protein Expression (CITE-seq)
CD62L
CD45RA
CD45RO
CD49b
HLA–ABC
IL2RA
min
max
D
Gene Modules in Activated Subsets
STAT5
Cell Adhesion
Th1/Cytotoxic
TCA
Ca2+ Signaling
NFkB
IFNG
Th2/GATA3
HIF1a/Hypoxia
Glycolysis
Myc
IL2/PI3K
OXPHOS
AICD
Module z–score
>1
0
<–1
E
Stimulated CD4 Cells
Stimulated CD8 Cells
Untrans.
KLRG1
CD3ζ
CD40
TACI
BAFF–R
4–1BB
CD28
% CAR Cells
10%
25%
40%
log2 CAR Enrichment
>1
0.5
0
–0.5
<–1
More Activated
F
Correlation with Human In Vivo Data
Clonotypes enriched after engraftment in CAR patients
Sheih et al. 2020
Cluster
CAR
CD29+ Cytotoxic signature, predicts melanoma survival
Nicolet et al. 2020
z–score
OXPHOS
Glycolytic
Cytotoxic
Granulysin
Cytokine–low
Baseline
STAT1–IRF1
Th2
Memory
Naive/CD7
Naive/CD62L
4–1BB
BAFF–R
CD28
CD40
KLRG1
TACI
Untr
CD3ζ

Fig. 2.6. Single-cell RNA-seq and CITE-seq characterize functional differences between CAR costimulatory domains.

(A) Weighted-nearest neighbor (WNN) Uniform Manifold Approximation and Projection (UMAP) embedding of scRNA-seq and CITE-seq data from stimulated and resting CAR T cells are shown for samples from two donors. UMAP separates into CD4 and CD8 lobes (left and right sides). Cells are colored by eight CD4 and nine CD8 phenotypic clusters. Bottom inset: Cells colored by cell cycle phase, donor identity, and stimulated versus resting cells. fig. S6A shows the UMAP faceted for each CAR and stimulation condition. (B) Heatmap of differentially expressed (DE) genes. For each cluster, the top 50 DE genes are ordered by hierarchical clustering of the pseudo-bulk expression z-scores for all clusters and donors. Genes in multiple clusters are only included for the cluster with the highest score. For each, four genes that are representative of the overall phenotype of the cluster are highlighted. (C) UMAP plots show relative CITE-seq expression for the surface expression of six markers associated with T cell differentiation and activation. HLA, human leukocyte antigen; IL2RA, IL-2 receptor subunit α. (D) Mean z-scores are shown for MSigDB gene modules associated with various aspects of T cell activation, metabolism, and signaling among the three major activated phenotypic clusters in CD4 and CD8 T cells. TCA, tricarboxylic acid cycle; HIF1a, hypoxia inducible factor 1 subunit alpha; OXPHOS, oxidative phosphorylation; AICD, activation-incudec cell death. (E) Enrichment of stimulated CAR T cells containing different signaling domains within each phenotypic cluster. The size of each dot corresponds to the percentage of stimulated CAR T cells in a cluster and with a costimulatory domain. The color of each dot corresponds to the log2 enrichment or depletion of that CAR relative to others. Clusters are arranged with the most activated at the center to correspond to the (A) UMAP. Similar plots for resting cells and a per-donor breakdown are in fig. S6C and E, respectively. (F) Correlation of T cell gene signatures indicative of enhanced CAR T engraftment (top) and melanoma survival (bottom) with phenotypic clusters in CD4 and CD8 CAR T cells (middle column) or with CARs containing different costimulatory domains (right column). Cluster and CAR colors match those in (E). The two dots per group correspond to two separate donors. Error bars indicate 99% confidence intervals for the z-scores.

Figure 2.7

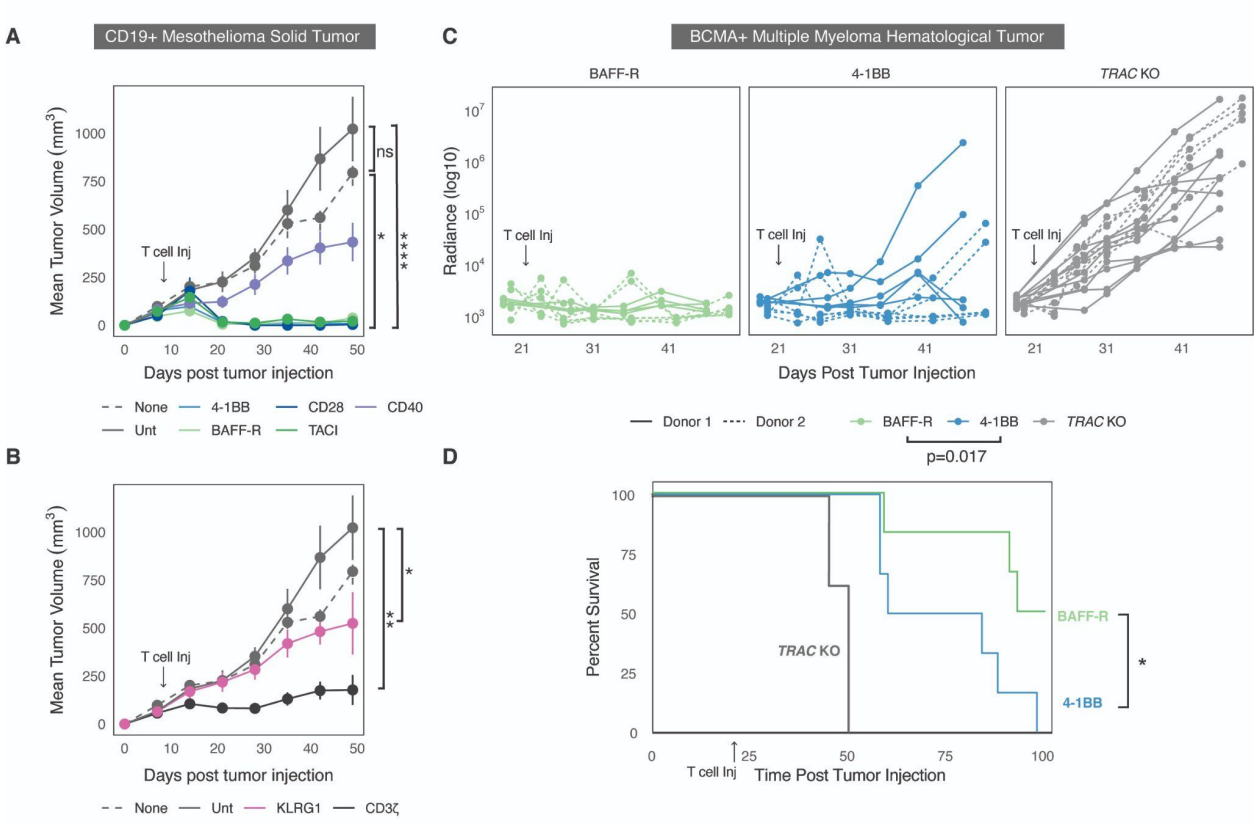

Fig. 2.7. BAFF-R demonstrates potent anti-tumor in vivo activity in solid and hematological cancers.

(A) Tumors were untreated, treated with untransduced T cells, or treated with engineered CAR T cells. Tumor size was monitored over 49 days post tumor injection. CAR T cells containing the potent costimulatory domains are shown, compared to untransduced T cells and no T cell controls. Data are representative of 5 in vivo experiments using 2 human donors. (B) Tumor size as in (A), showing a CD3ζ-only control and a KLRG1 inhibitory CAR, compared to untransduced T cells and no T cells. Error bars in (A and B) indicate tumor volume variability across mice with the same treatment. (C) MM1S cancer radiance after luciferin injection was plotted over time for individual mice across CAR T cells generated from two donors. Tumors were measured by BLI every 7 days for a total of over 30 days. This was repeated independently in two donors. For panels (A to C), statistical analysis was done by t test on the normalized tumor volume area under the curve (AUC). (D) Survival curves are shown mice with MM1S cancer using T cells from a representative donor; mice were followed past 100 days (Mantel Cox test). For all panels, $p<0.05$:*, $p<0.01$:**, $p<0.0001$:****; ns, not significant.

2.18 Supplemental Figures

Figure 2.8

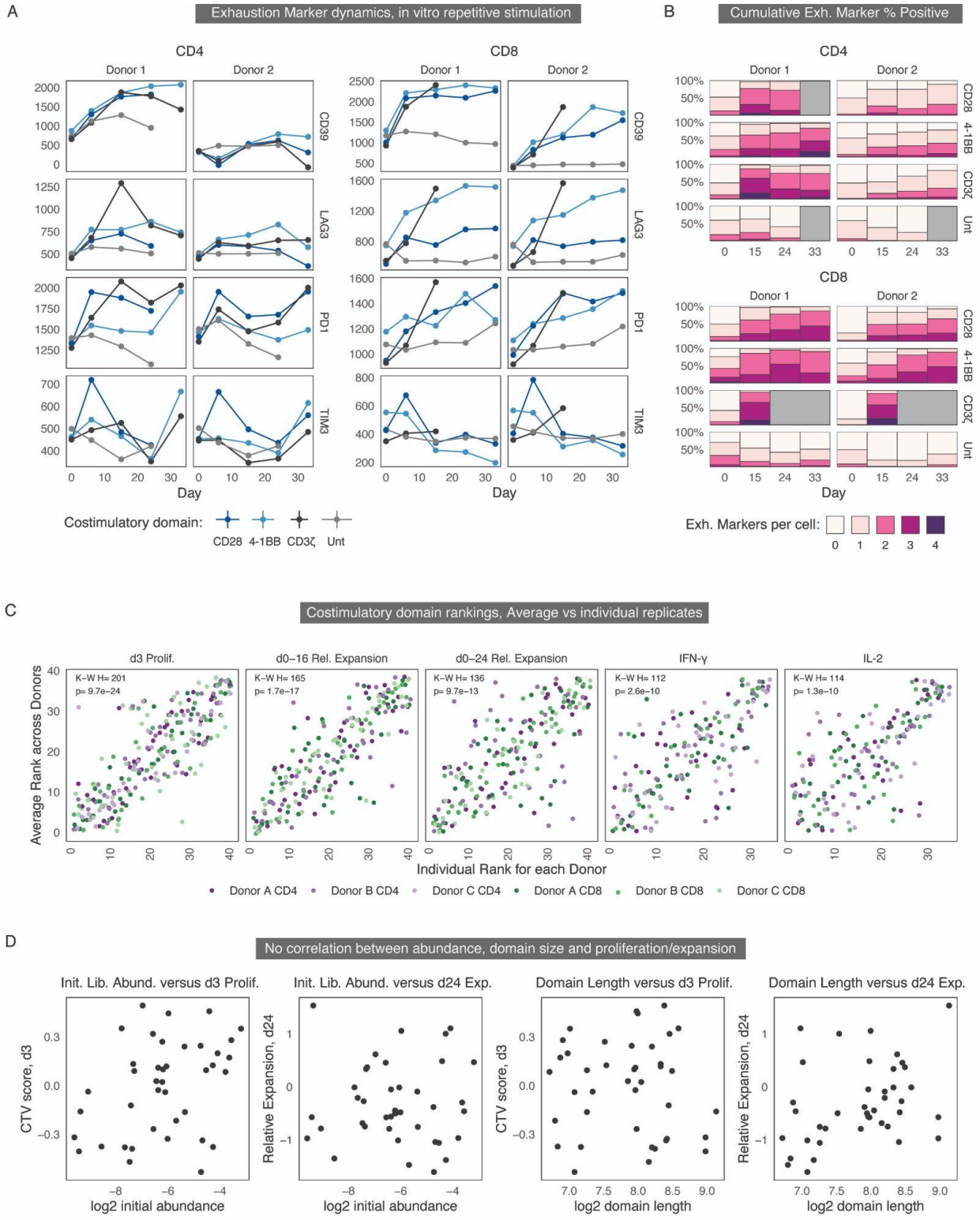

Fig. S1. Repetitive stimulation reproducibly induces exhaustion.
(A) Mean fluorescence intensity (MFI) for four cell surface markers of exhaustion (CD39, lymphocyte activating protein 3 (LAG3), programmed cell death protein 1 (PD1), T cell immunoglobulin domain and mucin domain 3 (TIM3)) in anti-CD19 chimeric antigen receptor (CAR) T cells generated from two donors measured after repeated stimulation with CD19-expressing irradiated K562 cells. CARs contained either 4-1BB or CD28 costimulation domains, no costimulatory domain (CD3ζ only), or were untransduced (Unt) T cells from the same donor as a control. (B) Aggregated measurements for panel (A) are shown, displayed as the percentage of cells expressing 0 to 4 exhaustion (Exh.) markers, for each donor, timepoint, and CAR. (C) Rank ordering of all 40 CARs within multiple assays is shown, with average rank for donor as well as CD4 and CD8 replicates plotted against the rank within the individual donors and T cell subsets. Proliferation (Prolif.), relative (Rel.) expansion, interferon (IFN)-γ production, and interleukin (IL)-2 production are shown. A Kruskal Wallis H test was performed for each assay, and the H statistic and p-value are shown. The upper right and lower left (lowest- and highest-ranked domains) are the most consistently ranked among individual replicates. (D) Initial library abundance (Init. Lib. Abund.) of each CAR (as a log2 fraction of the total read count) and domain length (log2 of the number of nucleotides) plotted versus either the Cell Trace Violet (CTV) score on day 3 (representing early proliferation) or the long-term expansion, log2-transformed and normalized to the average library member. None of these plots show any statistically significant correlation between either initial library abundance or costimulatory domain size and domain performance.

Figure 2.9

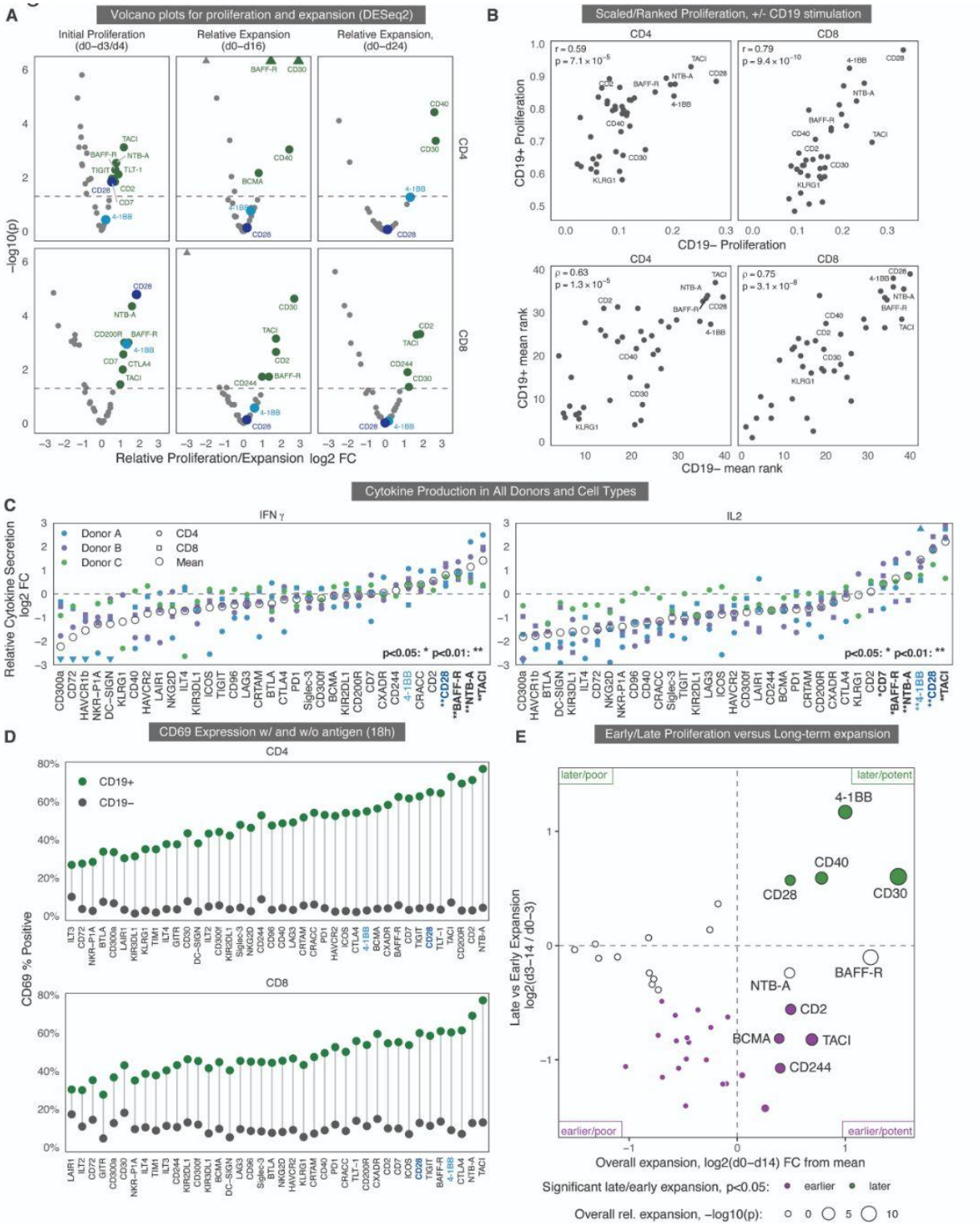
A
Volcano plots for proliferation and expansion (DESeq2)
Initial Proliferation (d0–d3/d4)
Relative Expansion (d0–d16)
Relative Expansion, (d0–d24)
CD4
CD8
−log10(p)
Relative Proliferation/Expansion log2 FC
B
Scaled/Ranked Proliferation, +/- CD19 stimulation
CD4
CD8
CD19+ Proliferation
CD19– Proliferation
CD19+ mean rank
CD19– mean rank
C
Cytokine Production in All Donors and Cell Types
IFN γ
IL2
Relative Cytokine Secretion log2 FC
Donor A
Donor B
Donor C
CD4
CD8
Mean
p<0.05: * p<0.01: **
D
CD69 Expression w/ and w/o antigen (18h)
CD4
CD8
CD69 % Positive
CD19+
CD19–
E
Early/Late Proliferation versus Long-term expansion
later/poor
later/potent
earlier/poor
earlier/potent
Late vs Early Expansion log2(d3–14 / d0–3)
Overall expansion, log2(d0–d14) FC from mean
Significant late/early expansion, p<0.05:
earlier
later
Overall rel. expansion, −log10(p):

Fig. 2.9. Additional data and statistical correlations for the differential activation, proliferation, and long-expansion in a library of CAR-T costimulatory domain variants.
(A) Volcano plots showing the relative proliferation or expansion (according to panel labels) of CD4 or CD8 T cells expressing CARs containing different costimulatory domains, during the repetitive stimulation assay with CD19+ K562 cells. The x-axis shows the calculated difference in log2-fold change (FC) in proliferation or expansion, and the y-axis shows the associated adjusted P-value, as calculated by the DESeq2 algorithm. (B) A comparison of CAR T cell proliferation from d0-d3 across the library with and without CD19 stimulation. The top plots show the scaled proliferation averaged over each replicate but retain the differences in relative proliferation between CD19- and CD19+ conditions, which were measured simultaneously in our FlowSeq CTV assay. The bottom plots show the mean CAR rankings separately for the CD19- and CD19+ conditions. The top-performing potent costimulatory CARs are labeled. On the top, the Y axis is truncated due to the higher relative proliferation in the CD19+ condition. (C) FlowSeq measurement of intracellular cytokine production are shown across library domains in CD4 and CD8 (circle, square) T cells across three independent human donors (blue, purple, green), 18 hours after the initial addition of CD19+/- irradiated K562 cells. Means of all conditions for each cytokine are indicated by an open circle. Domains labeled in bold with stars next to their name indicate significance using a Wilcoxon rank-sum test, FDR-corrected $p < 0.05$. (D) FlowSeq measurement of the percentage of CD69+ cells is shown for each CAR library domain in both CD4 and CD8 cells, 18 hours after the addition of irradiated K562 cells either with or without CD19 expression. Cells are ranked based on the difference in percentage of CD69+ cells between CD19+ and CD19- conditions. (E) A comparison of early versus late antigen-stimulated proliferation is shown. The x- axis measures overall expansion by day 14 or 16 (d14/16) with more potent CARs on the right and less potent CARs on the left. The y-axis measures the ratio of late proliferation (d3 to d14) versus early proliferation (d0 to d3). CARs above 0 on the y-axis are more expanded in the library at later time points, and CARs below 0 are more expanded earlier. Domains significantly enriched earlier versus later during the expansion were colored purple and green respectively. Significance of each domain's overall relative expansion indicated by size of circle (Wald test using DeSEQ2, -log10(p)).

Figure 2.10

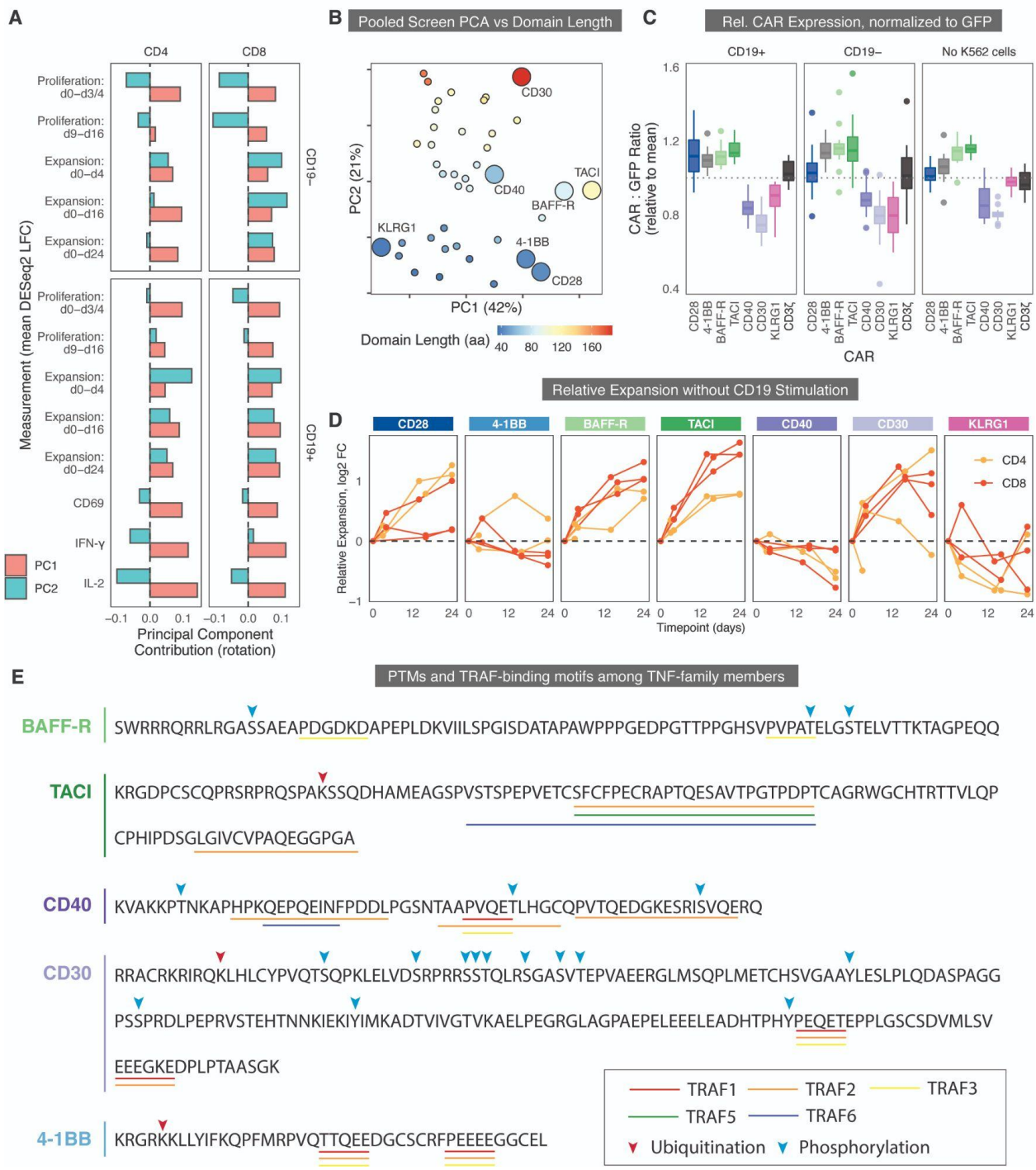
A
CD4
CD8
Proliferation: d0–d3/4
Proliferation: d9–d16
Expansion: d0–d4
Expansion: d0–d16
Expansion: d0–d24
CD69
IFN-γ
IL-2
CD19−
CD19+
PC1
PC2
Measurement (mean DESeq2 LFC)
Principal Component Contribution (rotation)
B
Pooled Screen PCA vs Domain Length
CD30
TACI
CD40
BAFF-R
KLRG1
4-1BB
CD28
PC2 (21%)
PC1 (42%)
Domain Length (aa)
C
Rel. CAR Expression, normalized to GFP
CD19+
CD19−
No K562 cells
CAR : GFP Ratio (relative to mean)
CAR
D
Relative Expansion without CD19 Stimulation
CD28
4-1BB
BAFF-R
TACI
CD40
CD30
KLRG1
CD4
CD8
Relative Expansion, log2 FC
Timepoint (days)
E
PTMs and TRAF-binding motifs among TNF-family members
BAFF-R
SWRRRQRRLRGASSAEAPDGDKDAPEPLDKVIILSPGISDATAPAWPPPGEDPGTTPPGHSVPVPATELGSTELVTTKTAGPEQQ
TACI
KRGDPCSCQPRSRPRQSPAKSSQDHAMEAGSPVSTSPEPVETCSFCFPECRAPTQESAVTPGTPDPTCAGRWGCHTRTTVLQP
CPHIPDSGLGIVCVPAQEGGPGA
CD40
KVAKKPTNKAPHPKQEPQEINFPDDLPGSNTAAPVQETLHGCQPVTQEDGKESRISVQERQ
CD30
RRACRKRIRQKLHLCYPVQTSQPKLELVDSRPRRSSTQLRSGASVTEPVAEERGLMSQPLMETCHSVGAAYLESLPLQDASPAGG
PSSPRDLPEPRVSTEHTNNKIEKIYIMKADTVIVGTVKAELPEGRGLAGPAEPELEEELEADHTPHYPEQETEPPLGSCSDVMLSV
EEEGKEDPLPTAASGK
4-1BB
KRGRKKLLYIFKQPFMRPVQTTQEEDGCSCRFPEEEEGGCEL
TRAF1
TRAF2
TRAF3
TRAF5
TRAF6
Ubiquitination
Phosphorylation

Fig. 2.10. Functional characterization of costimulatory landscape and analysis of the composition of the principal components of CAR performance across our library. (A) The bar plots show the relative contributions of different measurement types (in CD4 T cells and CD8 T cells, with and without antigenic stimulation) to each principal component (PC) of the PC analysis (PCA) plot in Fig. 3B and fig. S3B. Y axis indicates the mean log fold change (LFC) and the x-axis indicates the contribution of each PC. Contributions are grouped across donor replicates and separated out by different timepoints, proliferation (cell trace violet (CTV) FlowSeq), expansion (change in relative library abundance over time), intracellular cytokine FlowSeq, and activation (CD69 FlowSeq). PC1 (red) describes most of the variability in antigen-positive proliferation and expansion, and contributions to PC2 (blue) include early expansion (but not CTV-measured cell divisions), decreased CD4 cytokine secretion and reduced tonic signaling. (B) A recoloring of Fig. 3B is shown according to the amino acid length of each costimulatory domain, showing a slight correlation between domain length (blue to red is shortest to longest) and the second principal component, but not the first. (C) Ratio of surface CAR expression (using a myc tag and flow cytometry staining) to green fluorescent protein (GFP) fluorescence is shown for each CAR. All CAR variants were normalized to the mean within each time point, donor, and T cell type (CD4 or CD8). Expression with CD19+ K562 cells, CD19- K562 cells, and no target cells are shown separately. Box and whisker plots indicate median CAR:GFP ratio and variance as plotted by intequartile range, minimum, and maximum (excluding outliers plotted separately) for each measured CAR. (D) Relative expansion of library members CD28, 4-1BB, B cell activating factor receptor (BAFF-R), Transmembrane activator calcium modulator and cyclophilin ligand interactor (TACI), CD40, CD30, and killer cell lectin like receptor G1 (KLRG1) is shown over 24 days of repeated stimulation with irradiated CD19-K562 cells, as in Fig. 3C. Expansion was quantified by calculating the fold-change of the proportion of each CAR within the library at each timepoint (x-axis) as compared to baseline relative to the average CAR within the pooled library. The library was measured in CD4 and CD8 primary human T cells individually in 2 to 3 biological replicates. (E) Amino acid sequence and motif analysis of selected library members' belonging to the tumor necrosis factor (TNF) receptor family. TNF receptor associated factor (TRAF) binding sites indicated with colored lines under amino acid sequence. Phosphorylation and ubiquitination sites as annotated by Phosphosite are indicated with blue and red downward arrows, respectively.

Figure 2.11

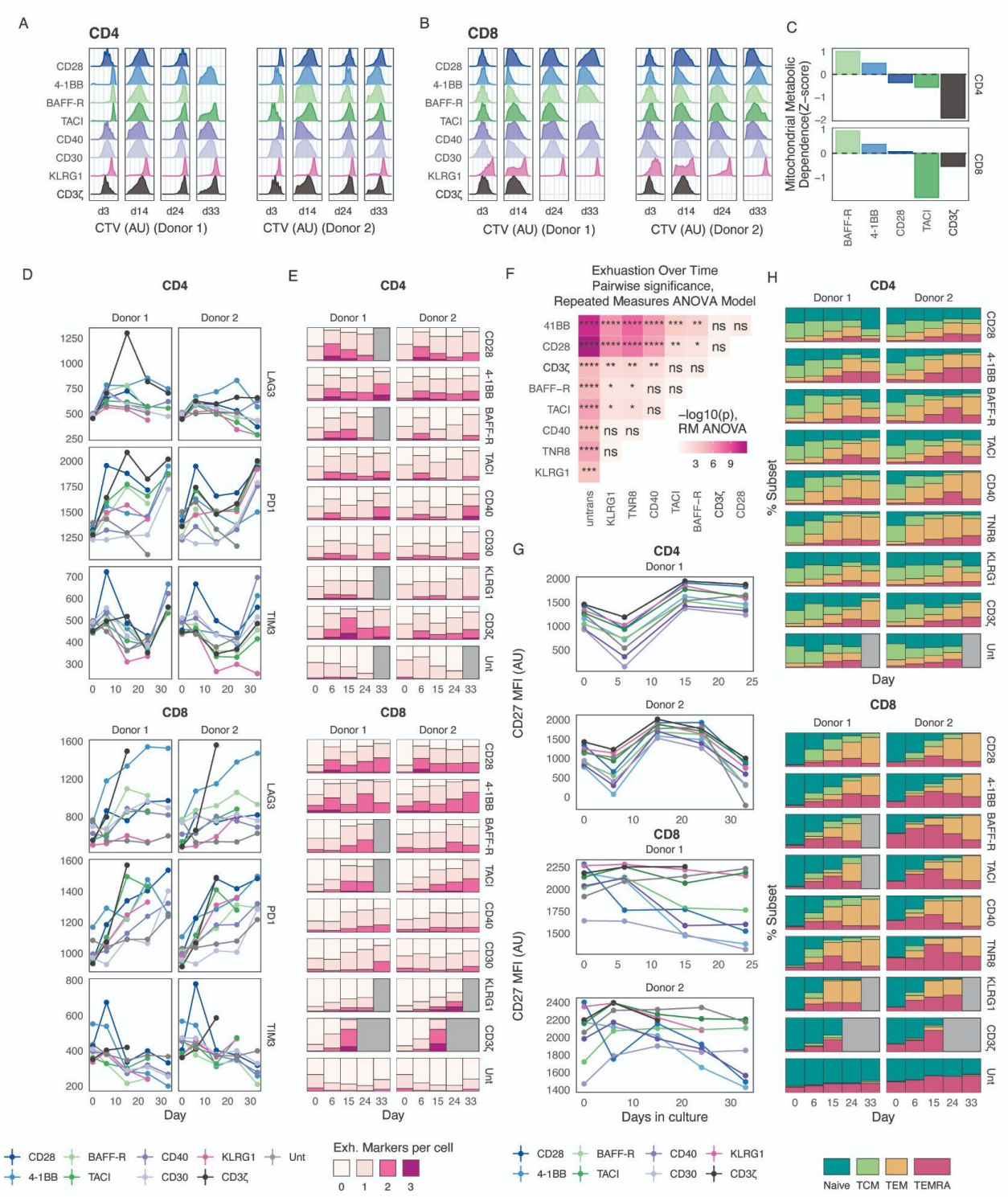
A
CD4
CD28
4-1BB
BAFF-R
TACI
CD40
CD30
KLRG1
CD3ζ
d3 d14 d24 d33
CTV (AU) (Donor 1)
CTV (AU) (Donor 2)
B
CD8
C
Mitochondrial Metabolic Dependence(Z−score)
CD4
CD8
BAFF-R 4-1BB CD28 TACI CD3ζ
D
CD4
Donor 1
Donor 2
LAG3
PD1
TIM3
CD8
Day
E
CD4
CD8
Unt
Day
F
Exhuastion Over Time
Pairwise significance,
Repeated Measures ANOVA Model
41BB
CD28
CD3ζ
BAFF−R
TACI
CD40
TNR8
KLRG1
untrans
−log10(p), RM ANOVA
G
CD4
CD8
CD27 MFI (AU)
Days in culture
H
CD4
CD8
% Subset
Day
CD28 4-1BB BAFF-R TACI CD40 CD30 KLRG1 CD3ζ
Exh. Markers per cell
0 1 2 3
Naive TCM TEM TEMRA

Fig. 2.11. Proliferation, exhaustion, and differentiation characteristics of CARs with chosen costimulatory domains, and metabolism of CARs with chosen costimulatory domains.
(A) CTV flow cytometry histograms are shown, as in Fig. 4C, for both donors, all time points, and CD4 T cells. AU, arbitrary units. (B) CTV cytometry histograms are shown, as in Fig. 4C, for both donors, all time points and CD8 T cells. (C) Normalized relative metabolic mitochondrial dependence for CD4 and CD8 T cells was measured among select CARs. This metric is based on measurement of protein synthesis using the simple method for complex immune-metabolic profiling (SCENITH) , which calculates the change in overall metabolic output with and without the addition of oligomycin, a mitochondrial inhibitor. (D) MFI for three cell surface markers of exhaustion (LAG3, PD1, and TIM3) is shown for anti-CD19 CAR T cells generated from two donors, measured after repeated stimulation with CD19+ irradiated K562 cells. (E) The proportion of CAR T cells expressing 0 to 3 of the exhaustion (Exh.) markers PD1, TIM3, and LAG3 after different numbers of days in culture is shown, as in Fig. 4F. (F) A table of significant differences in pairwise statistical tests based on a Repeated Measures ANOVA model is shown for mean exhaustion markers across different subtypes, donors, and days of measurement. FDR < 0.05:*, < 0.01:**, < 0.001:***, < 0.0001:****; ns, not significant. (G) MFI of CD27 was measured across all T cells, timepoints, and CAR T variants, as in Fig. 4G. (H) Differentiation of T cells at different timepoints throughout the repeated stimulation assay was evaluated. Differentiation subsets [Naive, Central Memory (TCM), Effector Memory (TEM), and Effector Memory RA-positive (TEMRA)] were calculated using surface expression of CD45RA and CD62L,.

Figure 2.12

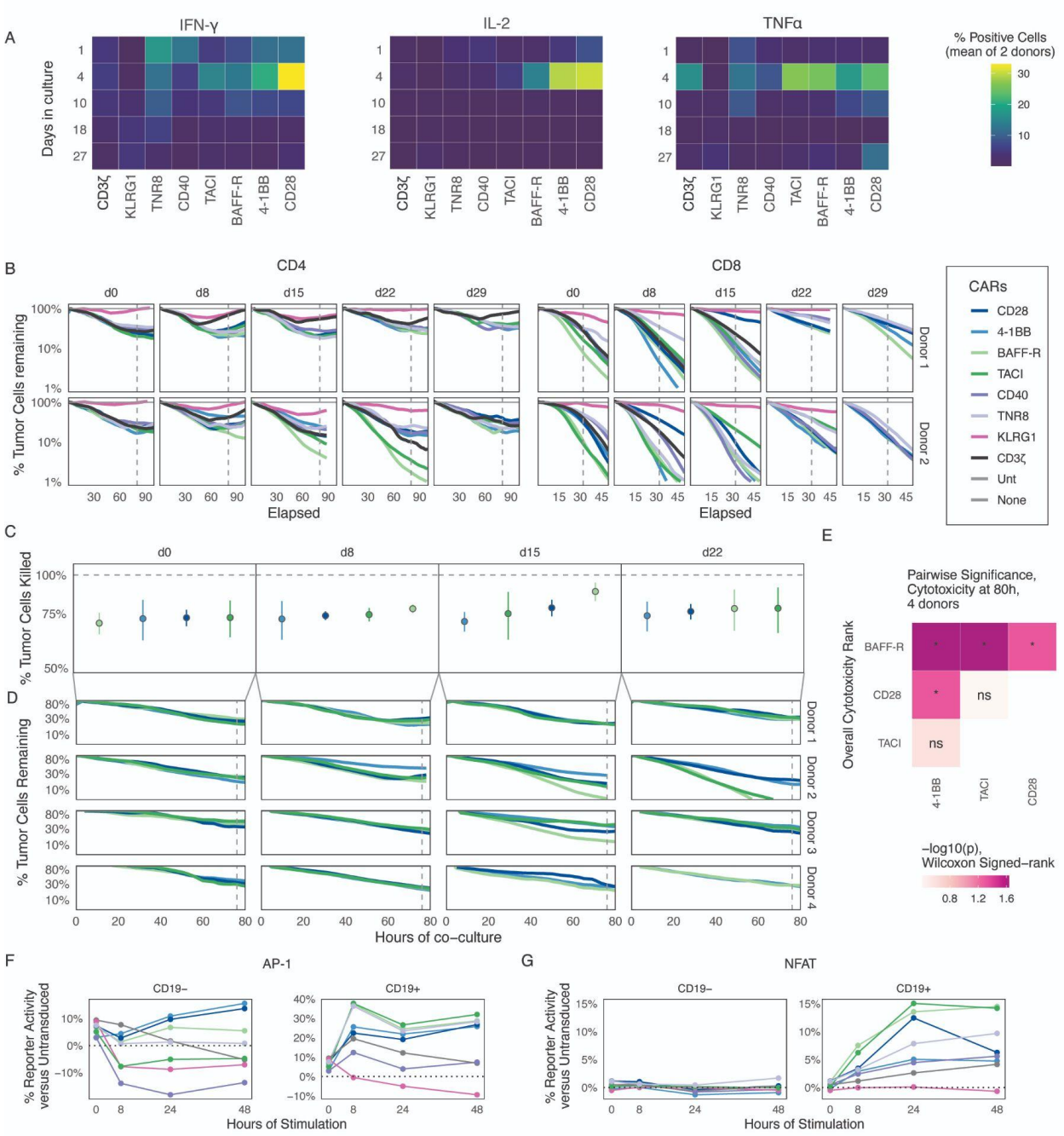
A
IFN-γ
IL-2
TNFα
Days in culture
1
4
10
18
27
CD3ζ
KLRG1
TNR8
CD40
TACI
BAFF-R
4-1BB
CD28
% Positive Cells
(mean of 2 donors)
30
20
10
B
CD4
CD8
d0
d8
d15
d22
d29
% Tumor Cells remaining
100%
10%
1%
Elapsed
Donor 1
Donor 2
CARs
CD28
4-1BB
BAFF-R
TACI
CD40
TNR8
KLRG1
CD3ζ
Unt
None
C
% Tumor Cells Killed
100%
75%
50%
D
% Tumor Cells Remaining
80%
30%
10%
Donor 3
Donor 4
Hours of co–culture
E
Pairwise Significance,
Cytotoxicity at 80h,
4 donors
Overall Cytotoxicity Rank
ns
–log10(p),
Wilcoxon Signed–rank
0.8
1.2
1.6
F
AP-1
CD19–
CD19+
% Reporter Activity
versus Untransduced
Hours of Stimulation
G
NFAT

Fig. 2.12. Time course of cytokine production, cytotoxicity, and transcriptional activity across CARs with chosen costimulatory domains.
(A) Mean cytokine production is shown across all T cells, time points, and CAR T variants, as in Fig. 5B. (B) All cytotoxicity plots across both CD4 and CD8 donors and all measured days are shown as in Fig 5E. (C) Cytotoxicity of CAR T cells were quantified at 80 hours for all four CD4 T cell donors (left) or at 32 hours for all CD8 T cell donors (right) expressing BAFF-R, TACI, CD28, or 4-1BB as in Fig. 5. Colors for each CAR are indicated in the legend. CARs are ranked at each timepoint from least to most cytotoxic (left to right). (D) Representative plots of cytotoxicity of CD4 CAR T cells from all four donors expressing BAFF-R, TACI, CD28, or 4-1BB are shown, with colors labeled as in (B). CARs are ranked at each timepoint from least to most cytotoxic (left to right). Vertical dashed lines indicate the time points analyzed in (C). Error bars indicate the standard error calculated across donors. (E) Table of significant differences in CD4 cytotoxicity shown in (D) using pairwise statistical tests across the chosen 4 donors and 4 CARs. Significance scores are based on a Repeated Measures ANOVA model of percentage of cell killing at 80 hours across different donors and days of repetitive stimulation (FDR < 0.05:*; ns, not significant). (F) Transcriptional activity reporter Jurkat cell lines for activator protein 1 (AP-1) were transduced with each CAR and sorted within one log of GFP expression. The cells were stimulated with either CD19- or CD19+ K562 cells for 0, 8, 24, or 48 hours and then assessed for activity by flow cytometry. Percent transcription factor activity relative to untransduced reporter Jurkat cells is plotted on the y-axis. (G) Transcriptional activity reporter Jurkat cell lines for nuclear factor of activated T-cells (NFAT) as described in (F).

Figure 2.13

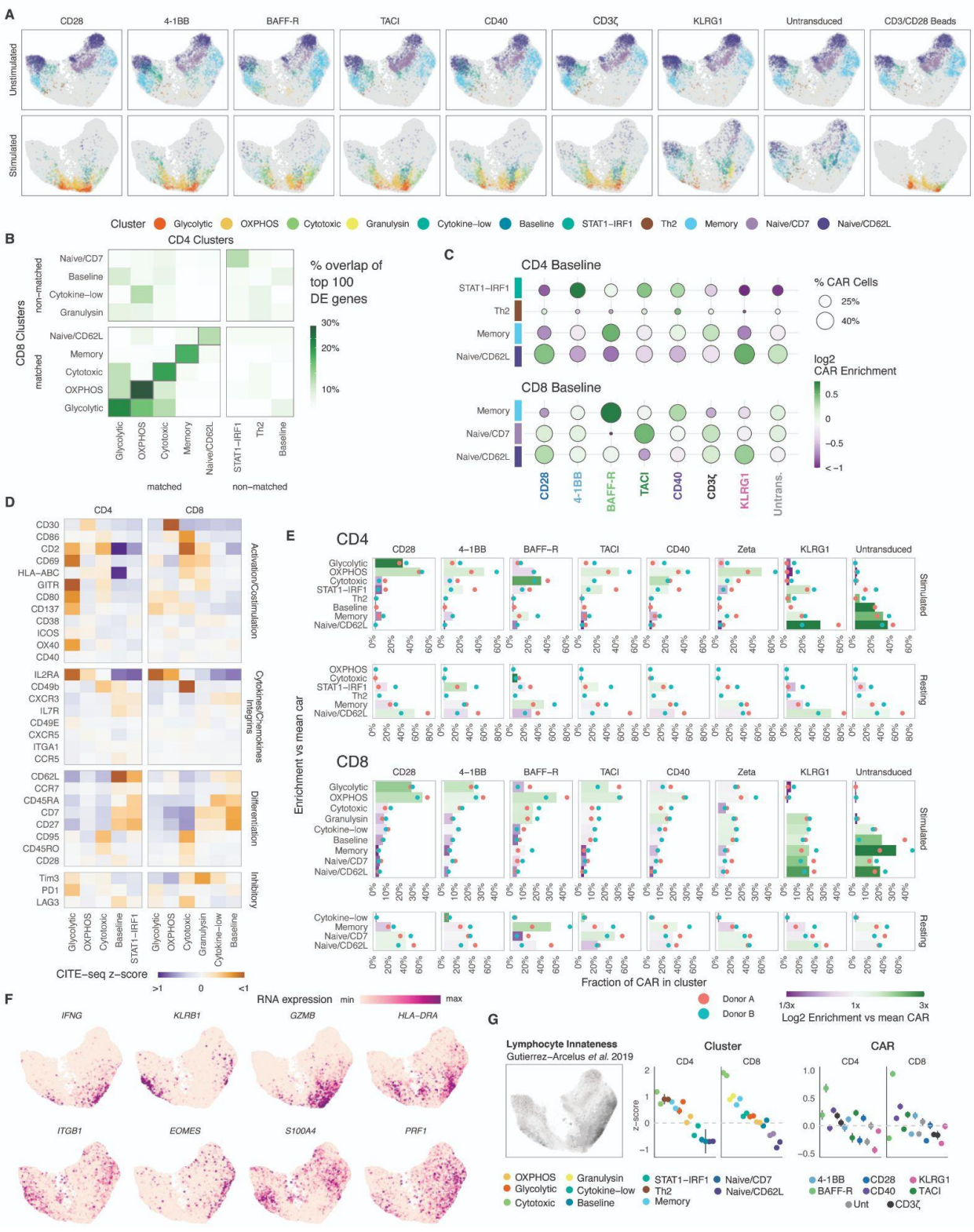
A
CD28
4-1BB
BAFF-R
TACI
CD40
CD3ζ
KLRG1
Untransduced
CD3/CD28 Beads
Unstimulated
Stimulated
Cluster Glycolytic OXPHOS Cytotoxic Granulysin Cytokine–low Baseline STAT1–IRF1 Th2 Memory Naive/CD7 Naive/CD62L
B
CD4 Clusters
CD8 Clusters
non–matched
matched
Naive/CD7
Baseline
Cytokine–low
Granulysin
Naive/CD62L
Memory
Cytotoxic
OXPHOS
Glycolytic
STAT1–IRF1
Th2
% overlap of top 100 DE genes
30%
20%
10%
matched
non–matched
C
CD4 Baseline
CD8 Baseline
% CAR Cells
25%
40%
log2 CAR Enrichment
0.5
0
–0.5
< –1
Untrans.
D
CD4
CD8
CD30
CD86
CD2
CD69
HLA–ABC
GITR
CD80
CD137
CD38
ICOS
OX40
CD40
Activation/Costimulation
IL2RA
CD49b
CXCR3
IL7R
CD49E
CXCR5
ITGA1
CCR5
Cytokines/Chemokines Integrins
CD62L
CCR7
CD45RA
CD7
CD27
CD95
CD45RO
CD28
Differentiation
Tim3
PD1
LAG3
Inhibitory
CITE–seq z–score
>1
0
<1
E
CD4
CD8
CD28
4–1BB
BAFF–R
TACI
CD40
Zeta
KLRG1
Untransduced
Stimulated
Resting
Enrichment vs mean car
Fraction of CAR in cluster
F
RNA expression min max
IFNG
KLRB1
GZMB
HLA–DRA
ITGB1
EOMES
S100A4
PRF1
G
Donor A
Donor B
1/3x
1x
3x
Log2 Enrichment vs mean CAR
Lymphocyte Innateness
Gutierrez–Arcelus et al. 2019
Cluster
CAR
z–score
OXPHOS Granulysin STAT1–IRF1 Naive/CD7
Glycolytic Cytokine–low Th2 Naive/CD62L
Cytotoxic Baseline Memory
4-1BB CD28 KLRG1
BAFF-R CD40 TACI
Unt CD3ζ

Fig. 2.13. Single-cell analysis of CARs with chosen costimulatory domains with and without antigen stimulation.
(A) Uniform manifold approximation and projection (UMAP) plots are faceted separately for each CAR costimulatory domain and stimulation condition. Points are colored the same as Fig. 6A. An additional CD3/CD28 bead stimulation condition is also shown, which was done only in Donor 2. (B) Gene expression overlap is shown across 5 pairs of clusters, which are very similar between CD4 and CD8 T cells (Naive/CD62L, Memory, Cytotoxic, OXPHOS, and Glycolytic). A list of the top 100 differentially expressed genes was calculated for each cluster among all CD4 or CD8 T cells. This plot shows the percentage overlap in these gene lists between clusters, showing a mirroring of gene expression across the CD4-CD8 axis among the 5 matched clusters in the bottom left quadrant. (C) Enrichment of resting CAR T cells containing different signaling domains within each phenotypic cluster, similar to Fig. 6E. The size of each dot corresponds to the percentage of stimulated CAR T cells with a specific costimulatory domain that is assigned to a cluster. The color of each dot corresponds to the log-2 fold enrichment or depletion of that CAR within the cluster. (D) Cellular indexing of transcriptomes and epitopes by sequencing (CITE-seq) z-scores are shown for a variety of surface proteins among T cells in different activated clusters, grouped by their functional classification. Z-scores for CD4 and CD8 T cells were calculated separately. (E) A breakdown of the cluster frequency is shown among all stimulated and resting CAR variants of both donors. The bar length on the x-axis is the percentage of each costimulatory CAR variant (resting and stimulated separately) within that cluster, such that each set of bars within each faceted box sums to 1. The bars represent the mean percentage for both donors, and the blue and red dots represent the individual percentages for each donor. The color of each bar corresponds to the relative log2 enrichment for that CAR variant in that cluster, relative to other CAR variants. (F) UMAP heatmaps display the relative RNA expression of single cells (scaled individually), showing a subset of functionally-important transcripts that are upregulated in the Cytotoxic and Memory subsets. (G) Correlation of T cell gene signatures indicative of lymphocyte innateness, based on Gutierrez-Arcelus et al. (64) (left) with phenotypic clusters in CD4 and CD8 CAR T cells (middle) or with CARs containing different costimulatory domains (right). Cluster and CAR colors match those in Fig. 6F. The two dots per group correspond to donors A and B. Error bars indicate 99% confidence intervals for the z-scores.

Figure 2.14

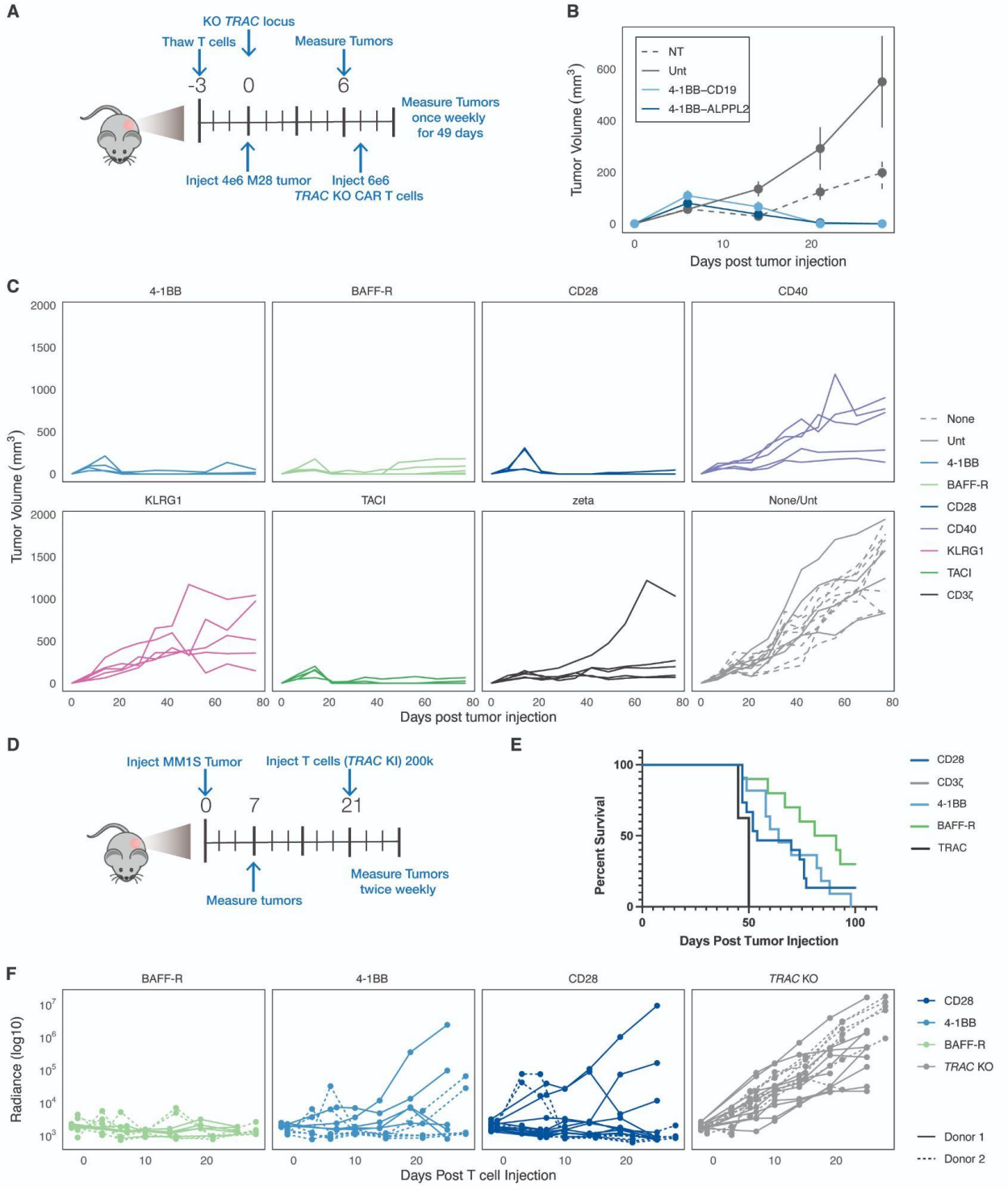
A
KO TRAC locus
Thaw T cells
Measure Tumors
-3
0
6
Measure Tumors once weekly for 49 days
Inject 4e6 M28 tumor
Inject 6e6 TRAC KO CAR T cells
B
NT
Unt
4-1BB–CD19
4-1BB–ALPPL2
Tumor Volume (mm3)
Days post tumor injection
C
4-1BB
BAFF-R
CD28
CD40
KLRG1
TACI
zeta
None/Unt
Tumor Volume (mm3)
Days post tumor injection
None
Unt
4-1BB
BAFF-R
CD28
CD40
KLRG1
TACI
CD3ζ
D
Inject MM1S Tumor
Inject T cells (TRAC KI) 200k
0
7
21
Measure tumors
Measure Tumors twice weekly
E
Percent Survival
Days Post Tumor Injection
CD28
CD3ζ
4-1BB
BAFF-R
TRAC
F
BAFF-R
4-1BB
CD28
TRAC KO
Radiance (log10)
Days Post T cell Injection
CD28
4-1BB
BAFF-R
TRAC KO
Donor 1
Donor 2

Fig 2.14. In vivo efficacy of highlighted signaling domains in the M28 and MM1S cancer models.

(A) Experimental timeline for in vivo M28 mesothelioma tumor model. We injected 4x106 CD19+ M28 mesothelioma tumor cells subcutaneously into the flanks of NOD.Cg-Prkdc scid Il2rg tm1Wjl /SzJ (NSG) mice and, seven days later, transferred 6x106 engineered TRAC knockout (KO) CAR T cells targeting CD19 intravenously into the tail vein. Tumors were measured by caliper every 7 days for a total of 49 days. (B) Tumor burden was measured in mice treated with CAR T cells targeting either ALPPL2 or CD19. Untransduced (Unt) T cells and non-treated (NT) mice were included as controls. Tumors were measured by caliper every 7 days for a total of 30 days. (C) M28 tumor volume was plotted over time for individual mice, corresponding to the mean tumor volumes in Fig. 7A and B. (D) Experimental timeline for in vivo MM1S multiple myeloma tumor model is shown. We injected 1x106 MM1S multiple myeloma tumor cells intravenously into NSG mice and, three weeks later, transferred 200,000 engineered TRAC-knockin CAR T cells targeting B-cell maturation antigen (BCMA) intravenously into the tail vein. (E) Survival curves are shown for mice treated with CAR T cells derived from Donor 1 and Donor 2 in the MM1S tumor model; results were combined for both donors. Mice were monitored over 100 days. (F) MM1S tumor volume is shown plotted over time for individual mice in all treatments, corresponding to Fig. 7C.

2.19 Supplemental Tables

Table 2.1: Expression of individual signaling domains by receptor type.

The table slows a list of all costimulatory domains in our library and whether they are expressed by different immune cell types. Note that some receptors may have low expression or only be expressed under specific circumstances by individual cell types.

Supplemental Table 1. Expression of individual cosignaling receptors by cell type

Cosignaling Receptor	T cell	B cell	NK cell	DC Cell	Macrophages	NKT Cell	Granulocyte	Microglia	Total Cell Types
41BB	X								1
BAFF-R	X	X							2
BCMA		X							1
BTLA	X	X							2
CD2	X		X						2
CD200R	X						X		2
CD244	X		X				X		3
CD28	X	X					X		3
CD300a	X	X	X	X			X		5
CD300f									0
CD40		X			X				2
CD7	X		X						2
CD72		X							1
CD96	X		X						2
CRACC	X	X	X						3
CRTAM	X					X			2
CTLA4	X	X					X		3
CXADR									0
DC-SIGN				X					1
GITR	X		X						2
TIM3	X		X	X					3
ICOS	X								1
ILT2		X	X	X	X				4
ILT3		X	X	X	X				4
ILT4		X	X	X					3
KIR2DL1			X						1
KIR3DL1	X		X						2
KLRG1	X		X						2
LAG3	X		X						2
LAIR1	X	X	X	X					4
NKG2D	X		X	X					3
NKR-P1A	X		X						2
NTB-A	X	X	X	X					4
PD1	X	X	X	X	X			X	6
Siglec-3				X				X	2
TACI	X	X							2
TIGIT	X		X						2
TLT-1									0
CD30	X	X	X		X				4

Table 2.2. List of reagents used in this study.

Reagent	Source	Catalog Number
Antibodies		
Monoclonal anti-human CD197(CCR7)-PE/Cy7 (clone G043H7)	BioLegend	Cat# 353226, RRID: AB_11126145
Monoclonal anti-human CD223(LAG-3)-AF647 (clone 11C3C65)	BioLegend	Cat# 369304, RRID: AB_2566480
Monoclonal anti-human CD27-APC/Cyanine7 (clone M-T271)	BioLegend	Cat# 356424, RRID: AB_2566773
Monoclonal anti-human CD297(PD-1)-BV711 (clone EH12.2H7)	BioLegend	Cat# 329928, RRID: AB_2562911
Monoclonal anti-human CD366(Tim-3)-BV421 (clone F38-2E2)	BioLegend	Cat# 345008, RRID: AB_11218598
Monoclonal anti-human CD39-APC/Cyanine7 (clone A1)	BioLegend	Cat# 328226, RRID: AB_2571981
Monoclonal anti-human CD4-PE (clone OKT4)	BioLegend	Cat# 317410, RRID: AB_571955
Monoclonal anti-human CD4-PE (clone SK3)	BioLegend	Cat# 344606, RRID: AB_1937246

Reagent	**Source**	**Catalog Number**
Monoclonal anti-human CD4-BUV395 (clone SK3)	BD Biosciences	Cat# 563552
Monoclonal anti-human CD4-Pacific Blue (clone SK3)	BioLegend	Cat# 344620, RRID: AB_2228841
Monoclonal anti-human CD45RA-APC (clone HI100)	BioLegend	Cat# 304112, RRID: AB_314416
Monoclonal anti-human CD45RO-BUV395 (clone UCHL1)	BD Biosciences	Cat# 564291
Monoclonal anti-human CD62L-BV785 (clone DREG-56)	BioLegend	Cat# 304830, RRID: AB_2629555
Monoclonal anti-human CD8-PE (clone SK1)	BioLegend	Cat# 344706, RRID: AB_1953244
Monoclonal anti-human CD8-BUV395 (clone RPA-T8)	BD Biosciences	Cat# 563795
Monoclonal anti-human CD8-Pacific Blue (clone SK1)	BioLegend	Cat# 344718, RRID: AB_10551438
Monoclonal anti-human CD95-BV711 (clone DX2)	BioLegend	Cat# 305644, RRID: AB_2632623
Monoclonal anti-human c-Myc-AF594 (clone 9B11)	Cell Signaling Technology	Cat# 9483S

Reagent	**Source**	**Catalog Number**
Monoclonal anti-human IFN-γ-BV786 (clone 4S.B3)	BD Biosciences	Cat# 563731
Monoclonal anti-human IL-2-APC (clone MQ1-17H12)	BD Biosciences	Cat# 554567
Monoclonal anti-human TNF-BUV395 (clone MAb11)	BD Biosciences	Cat# 563996
TotalSeq-A0251 HT1	Biolegend	Cat# 394601
TotalSeq-A0252 HT2	Biolegend	Cat# 394603
TotalSeq-A0253 HT3	Biolegend	Cat# 394605
TotalSeq-A0254 HT4	Biolegend	Cat# 394607
TotalSeq-A0255 HT5	Biolegend	Cat# 394609
TotalSeq-A0256 HT6	Biolegend	Cat# 394611
TotalSeq-A0257 HT7	Biolegend	Cat# 394613
TotalSeq-A0258 HT8	Biolegend	Cat# 394615
TotalSeq-A0259 HT9	Biolegend	Cat# 394617
TotalSeq-A0260 HT10	Biolegend	Cat# 394619

Reagent	**Source**	**Catalog Number**
TotalSeq-A0262 HT12	Biolegend	Cat# 394623
TotalSeq-A0263 HT13	Biolegend	Cat# 394625
ABSeq Oligo Mouse Monoclonal anti-human CD2	BD Biosciences	Cat# 940046
ABSeq Oligo Mouse Monoclonal anti-human CD3	BD Biosciences	Cat# 940000
ABSeq Oligo Mouse Monoclonal anti-human CD183	BD Biosciences	Cat# 940030
ABSeq Oligo Mouse Monoclonal anti-human CD103	BD Biosciences	Cat# 940067
ABSeq Oligo Mouse Monoclonal anti-human CD270	BD Biosciences	Cat# 940097
ABSeq Oligo Mouse Monoclonal anti-human CD54	BD Biosciences	Cat# 940072
ABSeq Oligo Mouse Monoclonal anti-human CD45RA	BD Biosciences	Cat# 940011
ABSeq Oligo Mouse Monoclonal anti-human CD197	BD Biosciences	Cat# 940014
ABSeq Oligo Mouse Monoclonal anti-human CD11a	BD Biosciences	Cat# 940077

Reagent	**Source**	**Catalog Number**
ABSeq Oligo Mouse Monoclonal anti-human CD194	BD Biosciences	Cat# 940047
ABSeq Oligo Mouse Monoclonal anti-human CD336	BD Biosciences	Cat# 940085
ABSeq Oligo Mouse Monoclonal anti-human CD126	BD Biosciences	Cat# 940090
ABSeq Oligo Mouse Monoclonal anti-human CD123	BD Biosciences	Cat# 940020
ABSeq Oligo Mouse Monoclonal anti-human CD5	BD Biosciences	Cat# 940038
ABSeq Oligo Mouse Monoclonal anti-human CD196	BD Biosciences	Cat# 940033
ABSeq Oligo Mouse Monoclonal anti-human CD178	BD Biosciences	Cat# 940089
ABSeq Oligo Mouse Monoclonal anti-human CD24	BD Biosciences	Cat# 940028
ABSeq Oligo Mouse Monoclonal anti-human CD56	BD Biosciences	Cat# 940007
ABSeq Oligo Mouse Monoclonal anti-human CD124	BD Biosciences	Cat# 940092

Reagent	Source	Catalog Number
ABSeq Oligo Mouse Monoclonal anti-human CD185	BD Biosciences	Cat# 940042
ABSeq Oligo Mouse Monoclonal anti-human CD18	BD Biosciences	Cat# 940086
ABSeq Oligo Mouse Monoclonal anti-human IgG	BD Biosciences	Cat# 940027
ABSeq Oligo Mouse Monoclonal anti-human CD127	BD Biosciences	Cat# 940012
ABSeq Oligo Mouse Monoclonal anti-human CD25	BD Biosciences	Cat# 940009
ABSeq Oligo Mouse Monoclonal anti-human CD13	BD Biosciences	Cat# 940044
ABSeq Oligo Mouse Monoclonal anti-human CD1c	BD Biosciences	Cat# 940083
ABSeq Oligo Mouse Monoclonal anti-human CD278	BD Biosciences	Cat# 940043
ABSeq Oligo Mouse Monoclonal anti-human CD274	BD Biosciences	Cat# 940035
ABSeq Oligo Mouse Monoclonal anti-human CD11b	BD Biosciences	Cat# 940008

Reagent	**Source**	**Catalog Number**
ABSeq Oligo Mouse Monoclonal anti-human CD49a	BD Biosciences	Cat# 940094
ABSeq Oligo Mouse Monoclonal anti-human CD11c	BD Biosciences	Cat# 940024
ABSeq Oligo Mouse Monoclonal anti-human CD62L	BD Biosciences	Cat# 940041
ABSeq Oligo Mouse Monoclonal anti-human CD279	BD Biosciences	Cat# 940015
ABSeq Oligo Mouse Monoclonal anti-human CD195	BD Biosciences	Cat# 940050
ABSeq Oligo Mouse Monoclonal anti-human CD69	BD Biosciences	Cat# 940019
ABSeq Oligo Mouse Monoclonal anti-human CD335	BD Biosciences	Cat# 940064
ABSeq Oligo Mouse Monoclonal anti-human CD49b	BD Biosciences	Cat# 940087
ABSeq Oligo Mouse Monoclonal anti-human CD184	BD Biosciences	Cat# 940056
ABSeq Oligo Mouse Monoclonal anti-human CD30	BD Biosciences	Cat# 940103

Reagent	**Source**	**Catalog Number**
ABSeq Oligo Mouse Monoclonal anti-human CD10	BD Biosciences	Cat# 940045
ABSeq Oligo Mouse Monoclonal anti-human CD223	BD Biosciences	Cat# 940080
ABSeq Oligo Mouse Monoclonal anti-human CD61	BD Biosciences	Cat# 940065
ABSeq Oligo Mouse Monoclonal anti-human IL-21R	BD Biosciences	Cat# 940099
ABSeq Oligo Mouse Monoclonal anti-human CD90	BD Biosciences	Cat# 940032
ABSeq Oligo Mouse Monoclonal anti-human CD80	BD Biosciences	Cat# 940036
ABSeq Oligo Mouse Monoclonal anti-human CD94	BD Biosciences	Cat# 940081
ABSeq Oligo Mouse Monoclonal anti-human CD226	BD Biosciences	Cat# 940075
ABSeq Oligo Mouse Monoclonal anti-human HLA-ABC	BD Biosciences	Cat# 940062
ABSeq Oligo Mouse Monoclonal anti-human TCRgd	BD Biosciences	Cat# 940057

Reagent	**Source**	**Catalog Number**
ABSeq Oligo Mouse Monoclonal anti-human CD86	BD Biosciences	Cat# 940025
ABSeq Oligo Mouse Monoclonal anti-human CD155	BD Biosciences	Cat# 940102
ABSeq Oligo Mouse Monoclonal anti-human CD206	BD Biosciences	Cat# 940068
ABSeq Oligo Mouse Monoclonal anti-human CD117	BD Biosciences	Cat# 940051
ABSeq Oligo Mouse Monoclonal anti-human CD95	BD Biosciences	Cat# 940037
ABSeq Oligo Mouse Monoclonal anti-human CD9	BD Biosciences	Cat# 940078
Bacterial and Virus Strains		
Escherichia coli: strain HST08 (Stellar Competent Cells)	Takara Bio	Cat# 636766
NEB 5-alpha Electrocompetent E. coli	New England Biosciences	Cat # C2989
Biological Samples		

Reagent	**Source**	**Catalog Number**
T Cells from Donor D001004304	STEMCELL Technologies	Cat# 70500.2
T Cells from Donor RG1765	STEMCELL Technologies	Cat# 70500.1
T Cells from Donor RV01000251	STEMCELL Technologies	Cat# 70500.1
T Cells from Donor RG1310	STEMCELL Technologies	Cat# 70500.1
T Cells from Donor RG1945	STEMCELL Technologies	Cat# 70500.1
Chemicals, Peptides, and Recombinant Proteins		
Recombinant Human IL-2 Protein	R&D Systems	Cat# 202-IL-500
Acetic acid, glacial	Sigma-Aldrich	Cat# ARK2183-1L
CellTrace Violet	Thermo Fisher	Cat# C34557
eBioscience Brefeldin A Solution (1000X)	Invitrogen	Cat# 00-4506-51
Zombie Yellow Fixable Viability Kit	BioLegend	Cat# 423104

Reagent	**Source**	**Catalog Number**
Dulbecco's Phosphate Buffered Saline	Sigma-Aldrich	Cat# D8537
X-VIVO 15	Lonza Bioscience	Cat# 04-418Q
Human AB Serum Heat Inactivated	Valley Biomedical, Inc	Cat# HP1022HI
N-Acetyl-L-Cysteine	Sigma-Aldrich	Cat# A9165
1.0N NaOH	Sigma-Aldrich	Cat# S2770
2-Mercaptoethanol	Gibco	Cat# 21985-023
RPMI 1640 Medium	Gibco	Cat# 11875-093
Glutamax	Fisher Scientific	Cat# 35050061
Fetal Bovine Serum (Heat Inactivated)	SAFC Biosciences	Cat# 12306C-500ML
Penicillin-Streptomycin (10,000 IU/mL, 10,000 µg/mL)	MP Biomedicals	Cat# 1670249
InFusion	Takara Bio	Cat# 638951

Reagent	**Source**	**Catalog Number**
EasySep Human CD4+ T Cell Isolation Kit	STEMCELL Technologies	Cat# 17952
EasySep Human CD8+ T Cell Isolation Kit	STEMCELL Technologies	Cat# 17953
EasySep Human T Cell Negative Isolation Kit	STEMCELL Technologies	Cat # 17951
Cyto-Last Buffer	BioLegend	Cat# 422501
NucleoSpin Tissue XS	Macherey-Nagel	Cat# 740901.50
NucleoSpin	Macherey-Nagel	Cat# 740952.50S
NucleoSpin 96 Tissue	Macherey-Nagel	Cat# 740741.4
TaKaRa Ex Taq DNA Polymerase	Takara Bio	Cat# RR001B
MiniSeq High Output Reagent Kit (150-cycles)	Illumina	Cat# FC-420-1002
HiSeq 4000 300 Cycle Kit	Illumina	Cat# FC-410-1003
eBioscience Intracellular Fixation & Permeabilization Buffer Set	Invitrogen	Cat# 88-8824-00

Reagent	**Source**	**Catalog Number**
Experimental Models: Cell Lines		
Human: HEK293T	ATCC	
Human: K562 (CD19+mCherry+)	Lim Lab, UCSF	
Human: Nalm6 (CD19+GFP+Luciferase+)	Eyquem Lab, UCSF	
Human: M28	Gerwin Lab, NCI/NIH	
Experimental Models: Organisms/Strains		
Mouse: NOD.Cg-*Prkdc*^{scid} *IL2rg*^{tm1Wjl}/Szj	The Jackson Laboratory	JAX: 005557
Software and Algorithms		
FlowJo version 10	FlowJo, LLC	https://www.flowjo.com
RStudio	RStudio	https://rstudio.com/
IncuCyte Base Software	Essen Bioscience (now part of Sartorius)	https://www.essenbioscience.com/en/

Reagent	**Source**	**Catalog Number**
Living Image	PerkinElmer	https://www.perkinelmer.com
Prism version 9	Graph Pad	https://www.graphpad.com/scientific-software/prism/
Other		
Poly(A), Polyadenylic acid	Roche	Cat# 10108626001
Dynabeads Human T-Activator CD3/CD28	Thermo Fisher	Cat# 11131D
CountBright Absolute Counting Beads	Invitrogen	Cat# C36950
OneComp eBeads Compensation Beads	Invitrogen	Cat# 01-1111-42

2.20 References

1. C. S. Azimi, Q. Tang, K. T. Roybal, J. A. Bluestone, NextGen cell-based immunotherapies in cancer and other immune disorders. Curr. Opin. Immunol. 59, 79–87 (2019).
2. A. Ahmad, S. Uddin, M. Steinhoff, CAR-T Cell Therapies: An Overview of Clinical Studies Supporting Their Approved Use against Acute Lymphoblastic Leukemia and Large B-Cell Lymphomas. Int. J. Mol. Sci. 21 (2020), doi:10.3390/ijms21113906.
3. L. Chen, D. B. Flies, Molecular mechanisms of T cell co-stimulation and co-inhibition. Nat. Rev. Immunol. 13, 227–242 (2013).
4. X. Zhao, J. Yang, X. Zhang, X.-A. Lu, M. Xiong, J. Zhang, X. Zhou, F. Qi, T. He, Y. Ding, X. Hu, F. De Smet, P. Lu, X. Huang, Efficacy and Safety of CD28- or 4-1BB-Based CD19 CAR-T Cells in B Cell Acute Lymphoblastic Leukemia. Mol Ther Oncolytics 18, 272–281 (2020).
5. A. J. Davenport, R. S. Cross, K. A. Watson, Y. Liao, W. Shi, H. M. Prince, P. A. Beavis, J. A. Trapani, M. H. Kershaw, D. S. Ritchie, P. K. Darcy, P. J. Neeson, M. R. Jenkins, Chimeric antigen receptor T cells form nonclassical and potent immune synapses driving rapid cytotoxicity. Proc. Natl. Acad. Sci. U. S. A. 115, E2068–E2076 (2018).
6. O. U. Kawalekar, R. S. O'Connor, J. A. Fraietta, L. Guo, S. E. McGettigan, A. D. Posey Jr, P. R. Patel, S. Guedan, J. Scholler, B. Keith, N. W. Snyder, I. A. Blair, M. C. Milone, C. H. June, Distinct Signaling of Coreceptors Regulates Specific Metabolism Pathways and Impacts Memory Development in CAR T Cells. Immunity 44, 380–390 (2016).

7. R. Weinkove, P. George, N. Dasyam, A. D. McLellan, Selecting costimulatory domains for chimeric antigen receptors: functional and clinical considerations. Clin Transl Immunology 8, e1049 (2019).
8. A. I. Salter, R. G. Ivey, J. J. Kennedy, V. Voillet, A. Rajan, E. J. Alderman, U. J. Voytovich, C. Lin, D. Sommermeyer, L. Liu, J. R. Whiteaker, R. Gottardo, A. G. Paulovich, S. R. Riddell, Phosphoproteomic analysis of chimeric antigen receptor signaling reveals kinetic and quantitative differences that affect cell function. Sci. Signal. 11 (2018), doi:10.1126/scisignal.aat6753.
9. Z. Ying, T. He, X. Wang, W. Zheng, N. Lin, M. Tu, Y. Xie, L. Ping, C. Zhang, W. Liu, L. Deng, F. Qi, Y. Ding, X.-A. Lu, Y. Song, J. Zhu, Parallel Comparison of 4-1BB or CD28 Co-stimulated CD19-Targeted CAR-T Cells for B Cell Non-Hodgkin's Lymphoma. Mol Ther Oncolytics 15, 60–68 (2019).
10. S. L. Maude, T. W. Laetsch, J. Buechner, S. Rives, M. Boyer, H. Bittencourt, P. Bader, M. R. Verneris, H. E. Stefanski, G. D. Myers, M. Qayed, B. De Moerloose, H. Hiramatsu, K. Schlis, K. L. Davis, P. L. Martin, E. R. Nemecek, G. A. Yanik, C. Peters, A. Baruchel, N. Boissel, F. Mechinaud, A. Balduzzi, J. Krueger, C. H. June, B. L. Levine, P. Wood, T. Taran, M. Leung, K. T. Mueller, Y. Zhang, K. Sen, D. Lebwohl, M. A. Pulsipher, S. A. Grupp, Tisagenlecleucel in Children and Young Adults with B-Cell Lymphoblastic Leukemia. N. Engl. J. Med. 378, 439–448 (2018).
11. S. L. Maude, N. Frey, P. A. Shaw, R. Aplenc, D. M. Barrett, N. J. Bunin, A. Chew, V. E. Gonzalez, Z. Zheng, S. F. Lacey, Y. D. Mahnke, J. J. Melenhorst, S. R. Rheingold, A. Shen, D. T. Teachey, B. L. Levine, C. H. June, D. L. Porter, S. A. Grupp, Chimeric

antigen receptor T cells for sustained remissions in leukemia. N. Engl. J. Med. 371, 1507–1517 (2014).

12. J. H. Park, I. Rivière, M. Gonen, X. Wang, B. Sénéchal, K. J. Curran, C. Sauter, Y. Wang, B. Santomasso, E. Mead, M. Roshal, P. Maslak, M. Davila, R. J. Brentjens, M. Sadelain, Long-Term Follow-up of CD19 CAR Therapy in Acute Lymphoblastic Leukemia. N. Engl. J. Med. 378, 449–459 (2018).
13. T. Liu, L. Zhang, D. Joo, S.-C. Sun, NF-κB signaling in inflammation. Signal Transduct. Target. Ther. 2, 17023 (2017).
14. V. Atsaves, V. Leventaki, G. Z. Rassidakis, F. X. Claret, AP-1 Transcription Factors as Regulators of Immune Responses in Cancer. Cancers 11 (2019), doi:10.3390/cancers11071037.
15. Y.-J. Park, S.-A. Yoo, M. Kim, W.-U. Kim, The Role of Calcium–Calcineurin–NFAT Signaling Pathway in Health and Autoimmune Diseases Frontiers in Immunology 11 (2020), doi:10.3389/fimmu.2020.00195.
16. S. Guedan, X. Chen, A. Madar, C. Carpenito, S. E. McGettigan, M. J. Frigault, J. Lee, A. D. Posey Jr, J. Scholler, N. Scholler, R. Bonneau, C. H. June, ICOS-based chimeric antigen receptors program bipolar TH17/TH1 cells. Blood 124, 1070–1080 (2014).
17. S. Guedan, A. D. Posey Jr, C. Shaw, A. Wing, T. Da, P. R. Patel, S. E. McGettigan, V. Casado-Medrano, O. U. Kawalekar, M. Uribe-Herranz, D. Song, J. J. Melenhorst, S. F. Lacey, J. Scholler, B. Keith, R. M. Young, C. H. June, Enhancing CAR T cell persistence through ICOS and 4-1BB costimulation. JCI Insight 3 (2018), doi:10.1172/jci.insight.96976.

18. S. Guedan, A. Madar, V. Casado-Medrano, C. Shaw, A. Wing, F. Liu, R. M. Young, C. H. June, A. D. Posey Jr, Single residue in CD28-costimulated CAR-T cells limits long-term persistence and antitumor durability. J. Clin. Invest. 130, 3087–3097 (2020).

19. Y. Kagoya, S. Tanaka, T. Guo, M. Anczurowski, C.-H. Wang, K. Saso, M. O. Butler, M. D. Minden, N. Hirano, A novel chimeric antigen receptor containing a JAK-STAT signaling domain mediates superior antitumor effects. Nat. Med. 24, 352–359 (2018).

20. N. A. J. Dawson, I. Rosado-Sánchez, G. E. Novakovsky, V. C. W. Fung, Q. Huang, E. McIver, G. Sun, J. Gillies, M. Speck, P. C. Orban, M. Mojibian, M. K. Levings, Functional effects of chimeric antigen receptor co-receptor signaling domains in human regulatory T cells. Sci. Transl. Med. 12 (2020), doi:10.1126/scitranslmed.aaz3866.

21. E. Shifrut, J. Carnevale, V. Tobin, T. L. Roth, J. M. Woo, C. Bui, P. Jonathan Li, M. Diolaiti, A. Ashworth, A. Marson, Genome-wide CRISPR Screens in Primary Human T Cells Reveal Key Regulators of Immune Function, doi:10.1101/384776.

22. T. L. Roth, P. J. Li, F. Blaeschke, J. F. Nies, R. Apathy, C. Mowery, R. Yu, M. L. T. Nguyen, Y. Lee, A. Truong, J. Hiatt, D. Wu, D. N. Nguyen, D. Goodman, J. A. Bluestone, C. J. Ye, K. Roybal, E. Shifrut, A. Marson, Pooled Knockin Targeting for Genome Engineering of Cellular Immunotherapies. Cell 181, 728–744.e21 (2020).

23. F. Diella, N. Haslam, C. Chica, A. Budd, S. Michael, N. P. Brown, G. Trave, T. J. Gibson, Understanding eukaryotic linear motifs and their role in cell signaling and regulation. Front. Biosci. 13, 6580–6603 (2008).

24. S. Kosuri, G. M. Church, Large-scale de novo DNA synthesis: technologies and applications. Nat. Methods 11, 499–507 (2014).

25. M. H. Kershaw, J. A. Westwood, L. L. Parker, G. Wang, Z. Eshhar, S. A. Mavroukakis, D. E. White, J. R. Wunderlich, S. Canevari, L. Rogers-Freezer, C. C. Chen, J. C. Yang, S. A. Rosenberg, P. Hwu, A phase I study on adoptive immunotherapy using gene-modified T cells for ovarian cancer. Clin. Cancer Res. 12, 6106–6115 (2006).

26. J. R. Park, D. L. Digiusto, M. Slovak, C. Wright, A. Naranjo, J. Wagner, H. B. Meechoovet, C. Bautista, W.-C. Chang, J. R. Ostberg, M. C. Jensen, Adoptive transfer of chimeric antigen receptor re-directed cytolytic T lymphocyte clones in patients with neuroblastoma. Mol. Ther. 15, 825–833 (2007).

27. P. J. Teoh, W. J. Chng, CAR T-cell therapy in multiple myeloma: more room for improvement. Blood Cancer J. 11, 84 (2021).

28. A. Sheih, V. Voillet, L.-A. Hanafi, H. A. DeBerg, M. Yajima, R. Hawkins, V. Gersuk, S. R. Riddell, D. G. Maloney, M. E. Wohlfahrt, D. Pande, M. R. Enstrom, H.-P. Kiem, J. E. Adair, R. Gottardo, P. S. Linsley, C. J. Turtle, Clonal kinetics and single-cell transcriptional profiling of CAR-T cells in patients undergoing CD19 CAR-T immunotherapy. Nat. Commun. 11, 219 (2020).

29. B. P. Nicolet, A. Guislain, F. P. J. van Alphen, R. Gomez-Eerland, T. N. M. Schumacher, M. van den Biggelaar, M. C. Wolkers, CD29 identifies IFN-γ–producing human CD8+ T cells with an increased cytotoxic potential. Proc. Natl. Acad. Sci. U. S. A. 117, 6686–6696 (2020).

30. K. J. Lafferty, A. J. Cunningham, A new analysis of allogeneic interactions. Aust. J. Exp. Biol. Med. Sci. 53, 27–42 (1975).

31. J. H. Esensten, Y. A. Helou, G. Chopra, A. Weiss, J. A. Bluestone, CD28 Costimulation: From Mechanism to Therapy. Immunity 44, 973–988 (2016).

32. H. M. Finney, A. D. Lawson, C. R. Bebbington, A. N. Weir, Chimeric receptors providing both primary and costimulatory signaling in T cells from a single gene product. J. Immunol. 161, 2791–2797 (1998).

33. D. B. Goodman, S. Kosuri, G. Cambray, V. K. Mutalik, Y. Gao, A. P. Arkin, D. Endy, G. M. Church, Composability of regulatory sequences controlling transcription and translation in E. coli (2013).

34. L. Jafarzadeh, E. Masoumi, K. Fallah-Mehrjardi, H. R. Mirzaei, J. Hadjati, Prolonged Persistence of Chimeric Antigen Receptor (CAR) T Cell in Adoptive Cancer Immunotherapy: Challenges and Ways Forward. Front. Immunol. 11, 702 (2020).

35. V. D. Fedorov, M. Themeli, PD-1–and CTLA-4–based inhibitory chimeric antigen receptors (iCARs) divert off-target immunotherapy responses. Sci. Transl. Med. (2013) (available at https://stm.sciencemag.org/content/5/215/215ra172.short?casa_token=3XVkIeHcqzcAAAAA:rdIhurVexLs8PILCp5TUzzSwBTXdlV70shQ9Aa4IH5cA50NUs82xYlFOPxz7WbxOulMsnPgDls4lalU).

36. J. Feucht, J. Sun, J. Eyquem, Y.-J. Ho, Z. Zhao, J. Leibold, A. Dobrin, A. Cabriolu, M. Hamieh, M. Sadelain, Calibration of CAR activation potential directs alternative T cell fates and therapeutic potency. Nat. Med. 25, 82–88 (2019).

37. J. R. James, Tuning ITAM multiplicity on T cell receptors can control potency and selectivity to ligand density. Sci. Signal. 11 (2018), doi:10.1126/scisignal.aan1088.

38. C. Xu, E. Gagnon, M. E. Call, J. R. Schnell, C. D. Schwieters, C. V. Carman, J. J. Chou, K. W. Wucherpfennig, Regulation of T Cell Receptor Activation by Dynamic Membrane Binding of the CD3ε Cytoplasmic Tyrosine-Based Motif. Cell 135, 702–713 (2008).

39. J. Holst, H. Wang, K. D. Eder, C. J. Workman, K. L. Boyd, Z. Baquet, H. Singh, K. Forbes, A. Chruscinski, R. Smeyne, N. S. C. van Oers, P. J. Utz, D. A. A. Vignali, Scalable signaling mediated by T cell antigen receptor–CD3 ITAMs ensures effective negative selection and prevents autoimmunity. Nat. Immunol. 9, 658–666 (2008).

40. H. H. Park, Structure of TRAF Family: Current Understanding of Receptor Recognition. Front. Immunol. 9, 1999 (2018).

41. P. V. Hornbeck, B. Zhang, B. Murray, J. M. Kornhauser, V. Latham, E. Skrzypek, PhosphoSitePlus, 2014: mutations, PTMs and recalibrations. Nucleic Acids Res. 43, D512–20 (2015).

42. M. D. Morrison, W. Reiley, M. Zhang, S.-C. Sun, An Atypical Tumor Necrosis Factor (TNF) Receptor-associated Factor-binding Motif of B Cell-activating Factor Belonging to the TNF Family (BAFF) Receptor Mediates Induction of the Noncanonical NF-κB Signaling Pathway*. J. Biol. Chem. 280, 10018–10024 (2005).

43. C.-Z. Ni, G. Oganesyan, K. Welsh, X. Zhu, J. C. Reed, A. C. Satterthwait, G. Cheng, K. R. Ely, Key molecular contacts promote recognition of the BAFF receptor by TNF receptor-associated factor 3: implications for intracellular signaling regulation. J. Immunol. 173, 7394–7400 (2004).

44. J. M. Hildebrand, Z. Luo, M. K. Manske, T. Price-Troska, S. C. Ziesmer, W. Lin, B. S. Hostager, S. L. Slager, T. E. Witzig, S. M. Ansell, J. R. Cerhan, G. A. Bishop, A. J. Novak, A BAFF-R mutation associated with non-Hodgkin lymphoma alters TRAF recruitment and reveals new insights into BAFF-R signaling. J. Exp. Med. 207, 2569–2579 (2010).

45. L.-G. Xu, H.-B. Shu, TNFR-associated factor-3 is associated with BAFF-R and negatively regulates BAFF-R-mediated NF-kappa B activation and IL-10 production. J. Immunol. 169, 6883–6889 (2002).

46. C. Sun, P. Shou, H. Du, K. Hirabayashi, Y. Chen, L. E. Herring, S. Ahn, Y. Xu, K. Suzuki, G. Li, O. Tsahouridis, L. Su, B. Savoldo, G. Dotti, THEMIS-SHP1 Recruitment by 4-1BB Tunes LCK-Mediated Priming of Chimeric Antigen Receptor-Redirected T Cells Cancer Cell 37, 216–225.e6 (2020).

47. R. J. Argüello, A. J. Combes, R. Char, J.-P. Gigan, A. I. Baaziz, E. Bousiquot, V. Camosseto, B. Samad, J. Tsui, P. Yan, S. Boissonneau, D. Figarella-Branger, E. Gatti, E. Tabouret, M. F. Krummel, P. Pierre, SCENITH: A Flow Cytometry-Based Method to Functionally Profile Energy Metabolism with Single-Cell Resolution. Cell Metab. 32, 1063–1075.e7 (2020).

48. J. Hendriks, L. A. Gravestein, K. Tesselaar, R. A. van Lier, T. N. Schumacher, J. Borst, CD27 is required for generation and long-term maintenance of T cell immunity. Nat. Immunol. 1, 433–440 (2000).

49. D. V. Dolfi, A. C. Boesteanu, C. Petrovas, D. Xia, E. A. Butz, P. D. Katsikis, Late signals from CD27 prevent Fas-dependent apoptosis of primary CD8+ T cells. J. Immunol. 180, 2912–2921 (2008).

50. J. Hendriks, Y. Xiao, J. Borst, CD27 promotes survival of activated T cells and complements CD28 in generation and establishment of the effector T cell pool. J. Exp. Med. 198, 1369–1380 (2003).

51. J. M. Carr, M. J. Carrasco, J. E. D. Thaventhiran, P. J. Bambrough, M. Kraman, A. D. Edwards, A. Al-Shamkhani, D. T. Fearon, CD27 mediates interleukin-2-independent

clonal expansion of the CD8+ T cell without effector differentiation. Proc. Natl. Acad. Sci. U. S. A. 103, 19454–19459 (2006).

52. A. Hyrenius-Wittsten, Y. Su, M. Park, J. M. Garcia, N. Perry, G. Montgomery, B. Liu, K. T. Roybal, Enhanced Solid Tumor Recognition and T cell Stemness with SynNotch CAR Circuits. bioRxiv , 2021.01.06.425642 (2021).
53. J.-H. Shi, S.-C. Sun, Tumor Necrosis Factor Receptor-Associated Factor Regulation of Nuclear Factor κB and Mitogen-Activated Protein Kinase Pathways. Front. Immunol. 9, 1849 (2018).
54. X. Z. Xia, J. Treanor, G. Senaldi, S. D. Khare, T. Boone, M. Kelley, L. E. Theill, A. Colombero, I. Solovyev, F. Lee, S. McCabe, R. Elliott, K. Miner, N. Hawkins, J. Guo, M. Stolina, G. Yu, J. Wang, J. Delaney, S. Y. Meng, W. J. Boyle, H. Hsu, TACI is a TRAF-interacting receptor for TALL-1, a tumor necrosis factor family member involved in B cell regulation. J. Exp. Med. 192, 137–143 (2000).
55. A. C. Boroughs, R. C. Larson, N. D. Marjanovic, K. Gosik, A. P. Castano, C. B. M. Porter, S. J. Lorrey, O. Ashenberg, L. Jerby, M. Hofree, G. Smith-Rosario, R. Morris, J. Gould, L. S. Riley, T. R. Berger, S. J. Riesenfeld, O. Rozenblatt-Rosen, B. D. Choi, A. Regev, M. V. Maus, A Distinct Transcriptional Program in Human CAR T Cells Bearing the 4-1BB Signaling Domain Revealed by scRNA-Seq. Mol. Ther. (2020), doi:10.1016/j.ymthe.2020.07.023.
56. M. Stoeckius, C. Hafemeister, W. Stephenson, B. Houck-Loomis, P. K. Chattopadhyay, H. Swerdlow, R. Satija, P. Smibert, Simultaneous epitope and transcriptome measurement in single cells. Nat. Methods 14, 865–868 (2017).

57. Y. Hao, S. Hao, E. Andersen-Nissen, W. M. Mauck 3rd, S. Zheng, A. Butler, M. J. Lee, A. J. Wilk, C. Darby, M. Zager, P. Hoffman, M. Stoeckius, E. Papalexi, E. P. Mimitou, J. Jain, A. Srivastava, T. Stuart, L. M. Fleming, B. Yeung, A. J. Rogers, J. M. McElrath, C. A. Blish, R. Gottardo, P. Smibert, R. Satija, Integrated analysis of multimodal single-cell data. Cell (2021), doi:10.1016/j.cell.2021.04.048.

58. B. P. Nicolet, A. Guislain, M. C. Wolkers, CD29 Enriches for Cytotoxic Human CD4+ T Cells. J. Immunol. (2021), doi:10.4049/jimmunol.2100138.

59. X. Yan, B. D. Johnson, R. J. Orentas, Induction of a VLA-2 (CD49b)-expressing effector T cell population by a cell-based neuroblastoma vaccine expressing CD137L. J. Immunol. 181, 4621–4631 (2008).

60. G. Kassiotis, D. Gray, Z. Kiafard, J. Zwirner, B. Stockinger, Functional specialization of memory Th cells revealed by expression of integrin CD49b. J. Immunol. 177, 968–975 (2006).

61. E. Billerbeck, Y.-H. Kang, L. Walker, H. Lockstone, S. Grafmueller, V. Fleming, J. Flint, C. B. Willberg, B. Bengsch, B. Seigel, N. Ramamurthy, N. Zitzmann, E. J. Barnes, J. Thevanayagam, A. Bhagwanani, A. Leslie, Y. H. Oo, S. Kollnberger, P. Bowness, O. Drognitz, D. H. Adams, H. E. Blum, R. Thimme, P. Klenerman, Analysis of CD161 expression on human CD8+ T cells defines a distinct functional subset with tissue-homing properties. Proc. Natl. Acad. Sci. U. S. A. 107, 3006–3011 (2010).

62. J. R. Fergusson, K. E. Smith, V. M. Fleming, N. Rajoriya, E. W. Newell, R. Simmons, E. Marchi, S. Björkander, Y.-H. Kang, L. Swadling, A. Kurioka, N. Sahgal, H. Lockstone, D. Baban, G. J. Freeman, E. Sverremark-Ekström, M. M. Davis, M. P. Davenport, V. Venturi, J. E. Ussher, C. B. Willberg, P. Klenerman, CD161 defines a transcriptional and

functional phenotype across distinct human T cell lineages. Cell Rep. 9, 1075–1088 (2014).

63. V. Konduri, S. K. Joseph, T. T. Byrd, Z. Nawas, J. Vazquez-Perez, C. J. Hofferek, M. M. Halpert, D. Liu, Z. Liang, Y. Baig, V. S. Salsman, D. Oyewole-Said, A. Tsimelzon, B. A. Burns, C. Chen, J. M. Levitt, Q. Yao, N. M. Ahmed, M. Hegde, W. K. Decker, A subset of cytotoxic effector memory T cells enhances CAR T cell efficacy in a model of pancreatic ductal adenocarcinoma. Sci. Transl. Med. 13 (2021), doi:10.1126/scitranslmed.abc3196.
64. M. Gutierrez-Arcelus, N. Teslovich, A. R. Mola, H. Kim, S. Hannes, K. Slowikowski, G. F. M. Watts, M. Brenner, S. Raychaudhuri, P. J. Brennan, A genome-wide innateness gradient defines the functional state of human innate T cells. bioRxiv , 280370 (2018).
65. B. R. Shy, V. Vykunta, A. Ha, T. L. Roth, A. Talbot, D. N. Nguyen, Y. Y. Chen, F. Blaeschke, S. Vedova, M. R. Mamedov, J.-Y. Chung, H. Li, J. Wolf, T. G. Martin, L. Ye, J. Eyquem, J. H. Esensten, A. Marson, Hybrid ssDNA repair templates enable high yield genome engineering in primary cells for disease modeling and cell therapy manufacturing. bioRxiv , 2021.09.02.458799 (2021).

Chapter 3

Dual CAR Engineering: Testing for additive effects of TNF Receptor Family members on clinical CARs

3.1 Abstract

Costimulatory variations of CARs were previously shown to have modular effects on enhancing CAR T function (Chapter 2). BAFF-R and TACI CARs enhanced cytotoxicity, CD40 CARs enhanced persistence, and KLRG1 CARs seemed to dampen CAR T function. Here, we interrogate the potential for multiplexing the modular functions of each of these domains into combinatorial therapeutics. While additional engineering is likely required, we found no in vivo enhanced efficacy of either differential CARs in CD4s and CD8s or dual CAR systems combining a clinical CAR (CD28 or 41BB) with one of our TNFRF CARs (BAFF-R, TACI, or CD40).

3.2 Introduction

Costimulatory receptor signaling has previously been investigated in groupings of protein families or pathways of activation such as PI3K and TRAF signaling in CD28 and 41BB respectively. However, while phenotypically different, each of the hits we identified in our previous screen (Chapter 2) were all members of the TNF Receptor Family and utilized TRAF signaling, similar to 41BB, indicating that the downstream effects of costimulation are dictated by more than those two paradigms. Previous studies have introduced multiple costimulatory domains into the CAR architecture to varying degrees of success including CARs with multiple full length costimulatory domains N-terminal to the CD3-zeta domain as well as CARs containing multiple signaling motifs

originating from different domains (1, 2, 3). However, most have delved primarily into the signaling of CD28 and 4-1BB as they have been more thoroughly investigated in the literature. Here we investigate the potential for BAFF-R, TACI, and CD40 to have an additive effect on the clinical CAR T cells in vivo.

3.3 T cell specific CAR T treatments

As our previous results indicated distinct advantages for our library hits within CD4 T cells, we decided to test whether combining CAR T cell treatments utilizing differential CARs with CD4 and CD8 T cells would enhance in vivo efficacy as compared to the clinical CAR treatments. To do so we transduced bulk CD3 CAR T cells as previously described and, 3 days post virus removal, we performed a negative selection CD4 or CD8 pulldown on the bulk, CD3+ fraction to isolate pure, untouched CAR T cells that were either CD4 or CD8 positive. We subsequently measured the purity using flow cytometry and performed additional purification via FACS to all samples. The CAR T cells were then rested overnight and mixed 50:50 CAR positive CD4 and CD8 T cells injected intravenously into the tail vein (Fig. 3.1A to B). We then proceeded to measure tumors once weekly for over 3 weeks. Through these comparisons, we determined no detectable increase in CD28 CAR T cell anti-tumor cytotoxicity with any combinatorial CD4 CD8 treatment (Fig. 3.1C). Additionally, we observed that the CD4 fraction seemed to have a greater effect on tumor clearance than the CD8 fraction, with CD28 CD4 + BAFF-R CD8 performing similarly to CD28 CAR T cells whereas BAFF-R CD4 + CD28 CD8 treatment performed poorly. This CD4 CAR T cell potency in vivo has previously been documented (4, 5), and is potentially dependent on cytokine production as NSG mice are missing a majority of their paracrine cytokines from other

immune populations (6). This result repeated within the 41BB combinatorial treatment as well (Fig. 3.1D).

3.4 Dual CAR Treatment

To further investigate the potential for combinatorial CAR treatments, we performed dual CAR T cell treatments within the M28 model where we cotransduced bulk CD3 T cells with two CAR T vectors. Based on our previous work, we were especially interested in potential proliferative capabilities of adding CD40 to the clinical CARs. To distinguish cotransduced cells we cloned a flag tag onto 41BB and CD28 for surface staining in comparison with the myc tag and T2A GFP expressed on the library hits. All CAR variants targeted CD19 utilizing the same scFv. We thawed, stimulated, and transduced as described (Chapter 2 methods), with an additional FACS sorting for flag positive myc positive cotransduced cells on a Fortessa 2 machine 8 days post T cell thaw (Fig. 3.2A). We then injected mice intravenously via the tail vein 7 days post M28 injection and monitored weekly for 30+ days. We saw no significant differences between CD28-only CAR T cells and CD28-CD40 or CD28-41BB CAR T cells (Fig. 3.2B). As the tumor clearance dynamics were all quite similar, we decided to repeat this experiment with ¼ the original dose to determine if we were able to distinguish a beneficial effect (Fig. 3.2C). After monitoring for 40 days, we determined there was no significant effect (Fig. 3.2D).

To further investigate the capacity for a dual CAR T cell treatment, we tested the BAFF-R, CD20, and TACI CARs against 4-1BB to determine if they had any additive anti-tumor effect within the M28 model. As described in Fig 3.2A, all CD19 CAR variants were selected via FACS sorting for flag positive myc positive cotransduced cells on a Fortessa 2 machine 8 days post T cell thaw and were injected via tail vein two days later (Fig. 3.3A). After monitoring for over 30 days we noted no significant improvement in cotransduced cells as compared to 4-1BB only T cell treatments

(Fig 3.3B). However, 3/5 4-1BB-TACI treated mice cleared their tumors (not shown). We therefore repeated the 4-1BB and TACI groups with two additional human donors at 1/2 of the original dose (now 1e6) and found no effect on tumor burden (Fig. 3.3C and D).

3.5 Discussion

Here we tested the capacity to utilize either T cell specific CAR expression or dual CAR expression as additive components of T cell therapeutics. Although we have not found additional additive effects within our systems, there are still potential benefits to be unveiled with additional engineering. Due to the dual CARs both being anti-CD19, there are potential complications due a limited amount of antigen available. If both CARs are not fully bound to antigen then you can potentially get insufficient signaling from both and mixed effects resulting in no additive benefit. Additionally, both CARs within the dual CAR system had the CD8 hinge domain which can heterodimerize and potentially result in dampened signaling from about 50% of the complexes which will contain heterodimers of each costimulatory domain. Further engineering is required to truly test this system including an additional scFv, and swapping which CAR has each scFv in each pairing, alongside inclusion of another hinge domain to prevent heterodimers.

3.6 Materials and Methods

Lentivirus Production/Concentration and Cell Lines

To produce lentivirus, Lenti-X 293T cells (Takara Bio) were transfected with a transgene expression vector and the viral packaging plasmids pCMVdR8.91 and pMD2.G using TransIT-Lenti Transfection Reagent (Mirus Bio LLC). Lentiviral concentration was performed 72 hours

after Lenti-X 293T cell transfection through collection and filtration of the viral supernatant. Per 20mL of viral supernatant we added 4.58mL 50% PEG 8000 (final concentration 8%) and 2mL of 4M NaCl (final concentration 0.3M) for 6-8 hours. We pelleted the virus by spinning down cells at 3500rpm for 20 minutes at 4C, decanted, and resuspended the pellet in 200uL PBS. We then snap froze aliquots on dry ice for storage in a -80C freezer.

M28 in vivo experiments:

M28 tumor cells were originally obtained from B. Gerwin's laboratory at the National Cancer Institute. M28 cells were transduced to exogenously express CD19 using lentiviral transduction and flow cytometry sorting to obtain a pure population with CD19 expression within a one log maximum width. All FACS was performed on a Fortessa-2 staining 1:200 for CD19-PE and FACS Diva software.

Tumor growth and injections: Four days prior to tumor injection, M28 CD19+ tumor cells were split and 0.75x106 cells were plated in one T182 flask for every 2.5 mice for propagation. On day 0, M28 CD19+ cells were trypsinized, counted, and resuspended in RPMI-1640 at 40x106 cells/mL. We injected NOD-scid IL2Rgammanull (NSG) mice with 4x106 M28 cells subcutaneously on the right flank and measured the initial tumor growth by caliper 6 days later. Groups were split up so that they have even tumor volume variance. A dose of 1-2x106 GFP positive anti-CD19 CAR T cells were injected on the 7th day post tumor injection intravenously by tail vein. Tumors were measured by caliper every 3 to 7 days for a total of 30 to 50 days.

T cell generation: We produced T cells as described above in Chapter 2 using 30μL concentrated virus per 1x106 T cells to reach a transduction rate between 65 and 90% as assessed by flow cytometry. T cells were injected as described above 10 days after initial thaw.

3.7 Figures

Figure 3.1

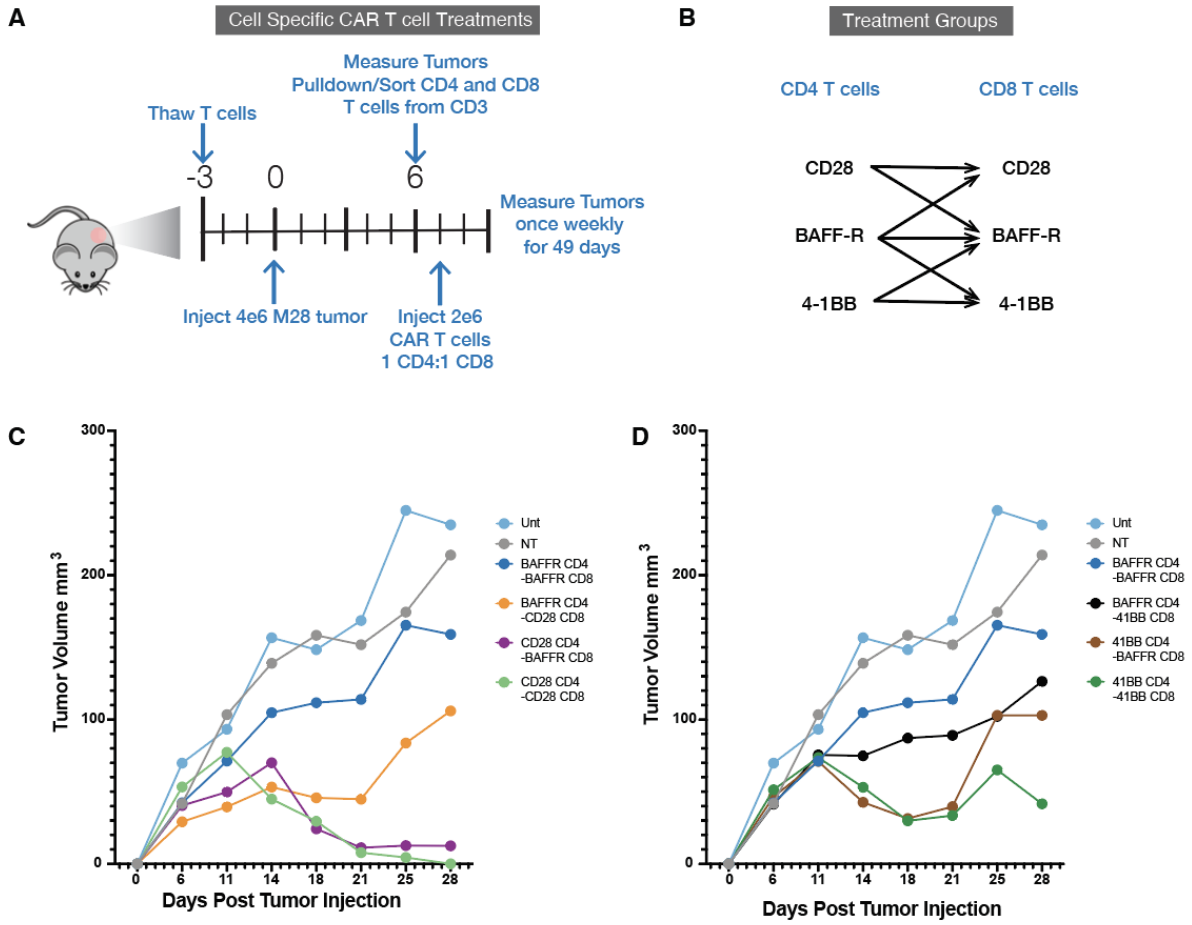

Fig 3.1. In vivo efficacy of T cell specific CAR T mesothelioma treatments.
(A) Experimental timeline for in vivo M28 mesothelioma tumor model. We injected 4x106 CD19+ M28 mesothelioma tumor cells subcutaneously into the flanks of NOD.Cg-Prkdc scid Il2rg tm1Wjl /SzJ (NSG) mice and, seven days later, transferred 2x106 engineered CAR T cells targeting CD19 intravenously into the tail vein. CAR T cells were sorted based on cell type and combined 1:1 CD4s: CD8s on injection day. Tumors were measured by caliper every 7 days for a total of 49 days. (B) Experimental outline indicating the treatment groups tested below. (C) Tumor burden was measured in mice treated with CD28 or CD28 mixed with other CAR T cells targeting CD19. Untransduced (Unt) T cells and non-treated (NT) mice were included as controls. Tumors were measured by caliper every 7 days for a total of 30 days. (D) Tumor burden was measured in mice treated with 4-1BB or 4-1BB mixed with other CAR T cells as indicated in (C).

Figure 3.2

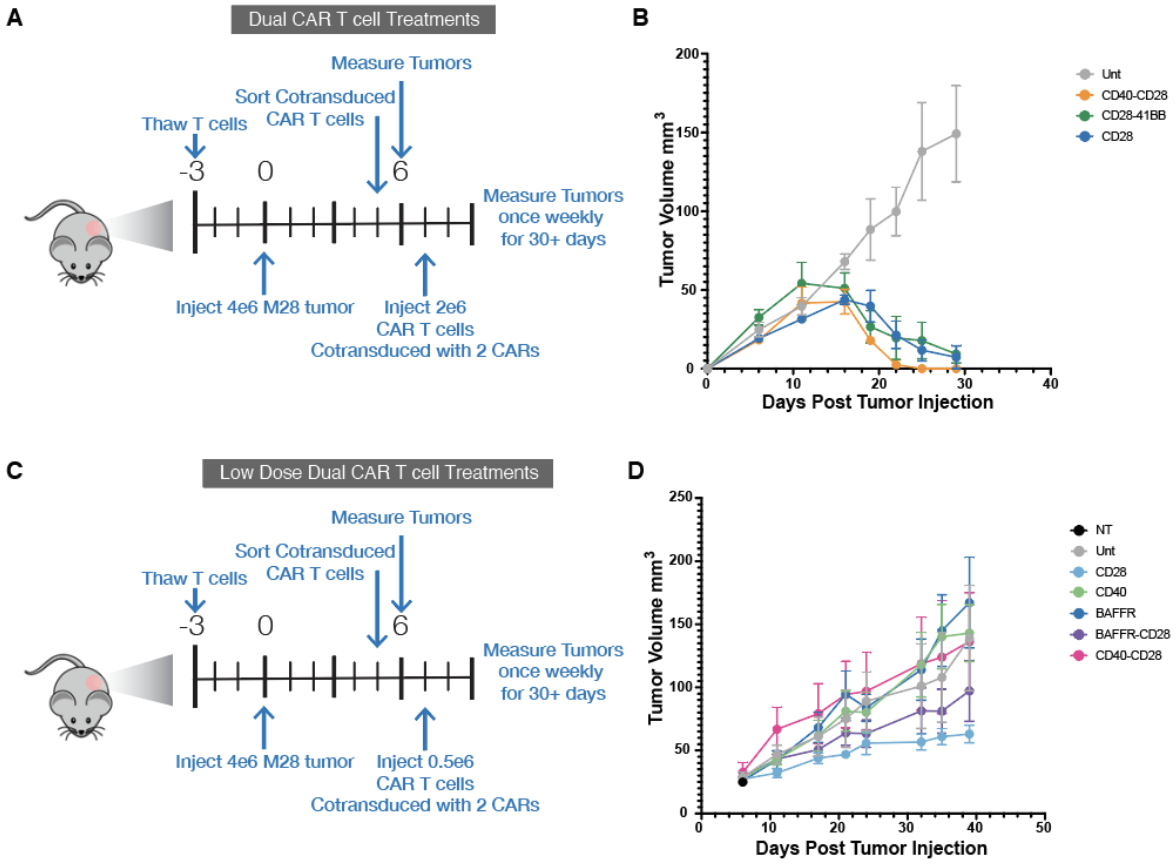

Fig 3.2. In vivo efficacy of CD28 Dual CAR T mesothelioma treatments.
(A) Experimental timeline for in vivo M28 mesothelioma tumor model. We injected 4x106 CD19+ M28 mesothelioma tumor cells subcutaneously into the flanks of NOD.Cg-Prkdc scid Il2rg tm1Wjl /SzJ (NSG) mice and, seven days later, transferred 2x106 engineered CAR T cells targeting CD19 intravenously into the tail vein. CAR T cells were sorted based on cotransduction of CD28 and either CD40 or 4-1BB. Tumors were measured by caliper every 7 days for a total of 30 days. (B) Tumor burden was measured in mice treated with CD28 or CD28 cotransduced with anti-CD19 CD40 or 4-1BB CARs. Mice treated with untransduced (Unt) T cells were included as controls. Tumors were measured by caliper every 3-4 days for a total of 30 days. (C) Experimental timeline as indicated in (A) of a low dose dual CAR T cell treatment. After M28 tumors have been in mice for 7 days they were injected with 0.5x106 CAR T cells of each indicated treatment and monitored for over 40 days. (D) Tumor burden was measured in mice by caliper every 3-4 days for a total of 40 days. Tumor volume was calculated by length x width x width x 0.5.

Figure 3.3

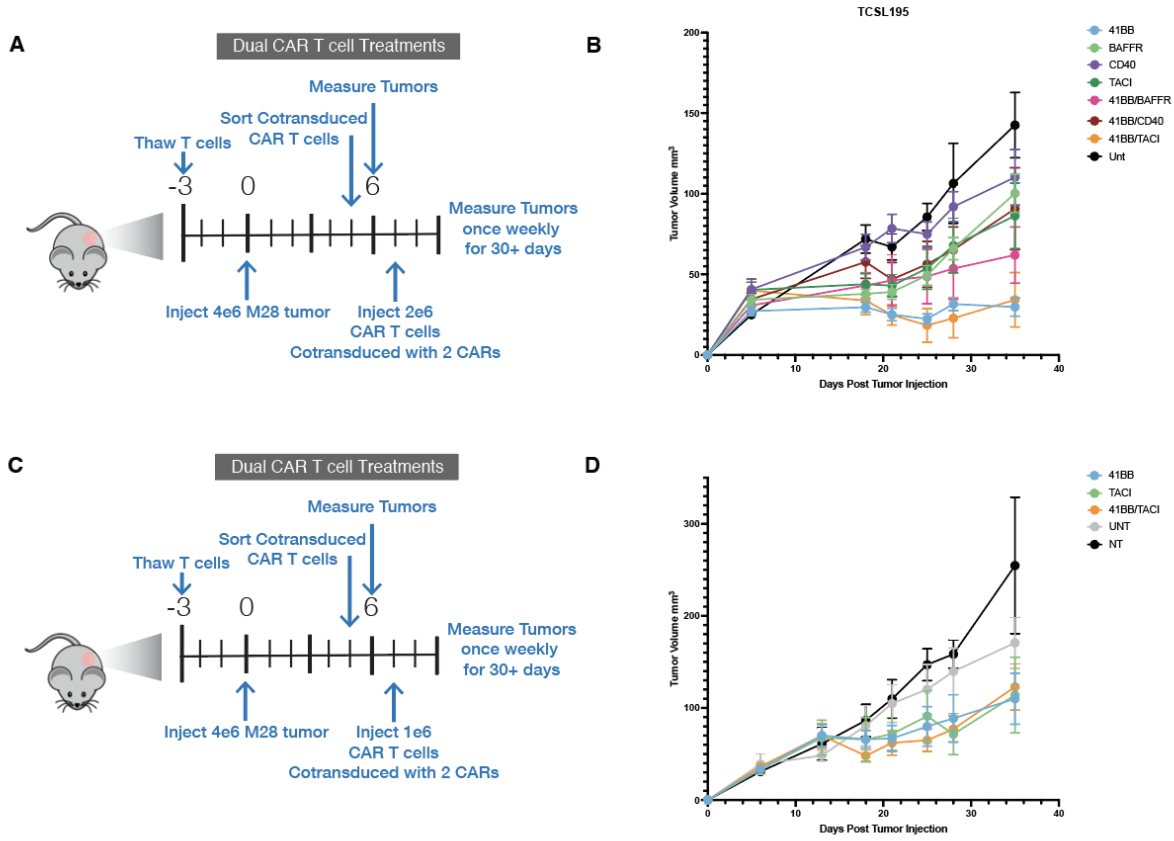

Fig 3.3. In vivo efficacy of 4-1BB Dual CAR T mesothelioma treatments.
(A) Experimental timeline for in vivo M28 mesothelioma tumor model. We injected 4x106 CD19+ M28 mesothelioma tumor cells subcutaneously into the flanks of NOD.Cg-Prkdc scid Il2rg tm1Wjl /SzJ (NSG) mice and, seven days later, transferred 2x106 engineered CAR T cells targeting CD19 intravenously into the tail vein. CAR T cells were sorted based on cotransduction of 4-1BB and either CD40, BAFF-R, or TACI. Tumors were measured by caliper every 7 days for a total of 30 days. (B) Tumor burden was measured in mice treated with 4-1BB or 4-1BB cotransduced with anti-CD19 CD40, BAFF-R, or TACI CARs. Mice treated with untransduced (Unt) T cells were included as controls. Tumors were measured by caliper every 3-4 days for over 30 days. (C) Experimental timeline as indicated in (A) of a low dose dual CAR T cell treatment. After M28 tumors have been in mice for 7 days they were injected with 1x106 CAR T cells of each indicated treatment and monitored for over 30 days. (D) Tumor burden was measured in mice by caliper every 3-4 days for over 30 days. Tumor volume was calculated by length x width x width x 0.5.

3.8 References

1. Guedan S, Posey AD Jr, Shaw C, Wing A, Da T, Patel PR, McGettigan SE, Casado-Medrano V, Kawalekar OU, Uribe-Herranz M, Song D, Melenhorst JJ, Lacey SF, Scholler J, Keith B, Young RM, June CH. Enhancing CAR T cell persistence through ICOS and 4-1BB costimulation. JCI Insight. 2018 Jan 11;3(1):e96976. doi: 10.1172/jci.insight.96976. PMID: 29321369; PMCID: PMC5821198.
2. Dai Q, Han P, Qi X, Li F, Li M, Fan L, Zhang H, Zhang X, Yang X. 4-1BB Signaling Boosts the Anti-Tumor Activity of CD28-Incorporated 2nd Generation Chimeric Antigen Receptor-Modified T Cells. Front Immunol. 2020 Nov 13;11:539654. doi: 10.3389/fimmu.2020.539654. PMID: 33281809; PMCID: PMC7691374.
3. Roselli E, Boucher JC, Li G, Kotani H, Spitler K, Reid K, Cervantes EV, Bulliard Y, Tu N, Lee SB, Yu B, Locke FL, Davila ML. 4-1BB and optimized CD28 co-stimulation enhances function of human mono-specific and bi-specific third-generation CAR T cells. J Immunother Cancer. 2021 Oct;9(10):e003354. doi: 10.1136/jitc-2021-003354. PMID: 34706886; PMCID: PMC8552146.
4. Agarwal S, Hanauer JDS, Frank AM, Riechert V, Thalheimer FB, Buchholz CJ. In Vivo Generation of CAR T Cells Selectively in Human CD4+ Lymphocytes. Mol Ther. 2020 Aug 5;28(8):1783-1794. doi: 10.1016/j.ymthe.2020.05.005. Epub 2020 May 16. PMID: 32485137; PMCID: PMC7403353.
5. Wang D, Aguilar B, Starr R, Alizadeh D, Brito A, Sarkissian A, Ostberg JR, Forman SJ, Brown CE. Glioblastoma-targeted CD4+ CAR T cells mediate superior antitumor activity. JCI Insight. 2018 May 17;3(10):e99048. doi: 10.1172/jci.insight.99048. PMID: 29769444; PMCID: PMC6012522.
6. Shultz LD, Brehm MA, Garcia-Martinez JV, Greiner DL. Humanized mice for immune system investigation: progress, promise and challenges. Nat Rev Immunol. 2012 Nov;12(11):786-98. doi: 10.1038/nri3311. Epub 2012 Oct 12. PMID: 23059428; PMCID: PMC3749872.

Chapter 4

Conclusion

The field of synthetic immunology is often most liberated and limited by the creativity and bandwidth of the scientists performing the work. While the impact of cancer immunotherapeutics and CAR T cell treatments cannot be underestimated, engineering novel receptors through arrayed cloning and screening can be restricting due to its labor intensive nature and the in vivo validation required. As the explored arena of what types of domains can be utilized within a CAR expands, so must our capacity for screening potential receptor designs. My work on CAR Pooling, as described in this dissertation, represents an important advance in our capacity to iteratively engineer novel receptors within the CAR architecture.

Through this work, I have demonstrated how to build pooled libraries, how to push them to their limits within an exhaustive environment, and the power to design novel receptors to enhance CAR T cell function. Most notably, our discovery of the anti-exhaustion functionality of many members within the TNF Receptor family, despite their classical expression within B cells, is an exemplar of the power of CAR Pooling to reduce the bandwidth and allow for this exploration of non-T cell signaling domains from across immune proteome. Furthermore, within this work I have shown the BAFF-R CAR's specialized capacity for enhanced cytotoxicity and in vivo tumor clearance as well as its overlapping transcriptional signature with patient studies assessing CAR T cell engraftment and patient survival. This work has resulted in two licensed patents, an accepted manuscript at Science Translational Medicine, and additional testing of the BAFF-R CAR by our collaborators for inclusion within a multiple myeloma clinical trial starting at UCSF. In addition to those more quantifiable metrics, the discovery of the BAFF-R CAR has illuminated the flexible

capacity of T cell signaling to incorporate non-native domains and is the first step toward determining what can truly compose a T cell costimulatory domain and how to synthetically build and enhance them in the future. Lastly, while not included within this thesis, I have helped expand our capacity for library screening from the modest 40 member library described above to new 10,000 member in vivo screens, exponentially expanding the depth of questions we can ask via CAR Pooling.

As I continue onward in my scientific career, I cannot help but be enamored by the potential of synthetic immunology, not only within cancer immunotherapeutics but autoimmunity, neurodegeneration, and more. The more I learn about the role the immune system plays within different disease states, the more I see their interconnection and the shifting of scales within the regulation of inflammation and immunosuppression and the potential for novel receptor designs to impact these systems in clinically translatable ways.

Publishing Agreement

It is the policy of the University to encourage open access and broad distribution of all theses, dissertations, and manuscripts. The Graduate Division will facilitate the distribution of UCSF theses, dissertations, and manuscripts to the UCSF Library for open access and distribution. UCSF will make such theses, dissertations, and manuscripts accessible to the public and will take reasonable steps to preserve these works in perpetuity.

I hereby grant the non-exclusive, perpetual right to The Regents of the University of California to reproduce, publicly display, distribute, preserve, and publish copies of my thesis, dissertation, or manuscript in any form or media, now existing or later derived, including access online for teaching, research, and public service purposes.

DocuSigned by:
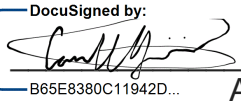
B65E8380C11942D...

Author Signature

12/14/2022

Date